Dissertations, Theses, and Masters Projects   Theses, Dissertations, & Master Projects

2008

Acoustic measurements of cohesive sediment transport: Suspension to consolidation

Ho Kyung Ha

College of William and Mary - Virginia Institute of Marine Science

Follow this and additional works at: https://scholarworks.wm.edu/etd

Part of the Oceanography Commons

ACOUSTIC MEASUREMENTS OF COHESIVE SEDIMENT TRANSPORT:
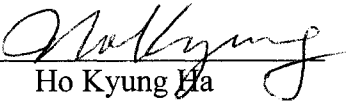
SUSPENSION TO CONSOLIDATION

_____

A Dissertation

Presented to

The Faculty of the School of Marine Science

The College of William and Mary in Virginia

In Partial Fulfillment

Of the Requirements for the Degree of

Doctor of Philosophy

_____

by

Ho Kyung Ha

2008
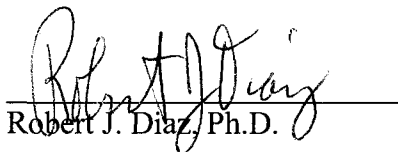
APPROVAL SHEET

This dissertation is submitted in partial fulfillment of

the requirements for the degree of

Doctor of Philosophy

Ho Kyung Ha

Approved by the Committee, April 2008

Jerome P.-Y. Maa, Ph.D.
Committee Chairman/Advisor

Robert J. Diaz, Ph.D.

Carl T. Friedrichs, Ph.D.

Jesse E. McNinch, Ph.D.

Charles W. Holland, Ph.D.
Pennsylvania State University
University Park, Pennsylvania

TABLE OF CONTENTS

ACKNOWLEDGMENTS

LIST OF TABLES

LIST OF FIGURES

Chapter V

ABSTRACT

This dissertation aims at utilizing the acoustic approach to measure cohesive sediment behaviors including (1) suspension, (2) settling, (3) deposition and (4) consolidation. The first two processes were attempted to interpret by means of backscattered signal analysis, while the last two processes were done by echo signal 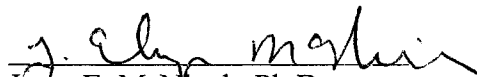analysis. The acoustic instruments used in this study include Acoustic Doppler Velocimeter (ADV), Pulse Coherent Acoustic Doppler Profiler (PC-ADP) and Micro-Chirp system. Used sediments are pure kaolinite and in-situ sediments collected from Mai Po and Clay Bank.

5-MHz ADV was used to estimate the suspended sediment concentration (SSC) and settling velocity (w_s). For a limited range of SSC, the time-averaged backscatter wave strength can be well correlated with the SSC. Backscattered signals would be sometimes too noisy due to high amplification ratio, high sampling rate, and small sampling volume, and thus, a moving average was used to yield the instantaneous changes of SSC. The measurement of w_s with Clay Bank sediment showed that turbulence can increase w_s, up to one order larger than that for calm water. When turbulence is stronger than a limit, however, it contributes to the decrease in w_s.

For the measurement of SSC profile, the performance of 1.5 MHz PC-ADP was evaluated. Clay Bank sediment showed a higher correlation coefficient between range-corrected volume scattering (SSC_v) and backscattered signal within a limited SSC range (ca. < 10 g/L). On the other hand, kaolinite showed a much smaller range of SSC for linear correlation. This different response might be attributed to the fact that the acoustic response is primarily controlled by the SSC and particle size in suspension at a given frequency. This study suggests that PC-ADP is a potential instrument to reveal the high-resolution (about 1.6 cm) SSC profiles near the bed, if the sediment is sufficiently large.

Annular flume experiments with Mai Po sediment were conducted to address a debatable issue regarding the critical shear stress for deposition (τ_{cd}). The direct observation from the flume bottom suggests that τ_{cd} does exist, and that the deposition only occurs when the local bed shear stress (τ_b) is less than τ_{cd}. The changes of deposit length and SSC under the simulated tidal cycles demonstrate that deposition can happen only at tidal decelerating phases with a recognizable τ_{cd}. This study further proves that both τ_b (a hydrodynamic parameter) and τ_{cd} (a sediment parameter) are the main controlling parameters for determining cohesive sediment deposition.

A non-intrusive acoustic technique and a signal-processing protocol were developed to estimate the bulk density at consolidating sediment interface. Using high-frequency (300-700 KHz) Chirp acoustic waves, laboratory measurements were carried out in a consolidation tank filled with clay-water mixtures. Because the acoustic echo strength is proportional to the difference in acoustic impedance, and the sound speed in water is close to that in clay, the approximation of bulk density could be successfully presented. The acoustic wave reflectivity increased with increasing the bulk density at the water-sediment interface, which are well correlated with the consolidation status.

ACOUSTIC MEASUREMENTS OF COHESIVE SEDIMENT TRANSPORT: SUSPENSION TO CONSOLIDATION

CHAPTER I. INTRODUCTION

1. Rationale

Cohesive sediment, or mud, is ubiquitously found in most aqueous environments. It has been historically used as a valuable resource for construction, agriculture soil enrichment and ecosystem restoration. In nature, mud usually exists as a mixture of clay (< 4 μm), silt (< 63 μm), water, organic and inorganic matters. Compared with non-cohesive sediment, cohesive sediment is controlled by the competition between the attractive and repulsive force acting on its surface and within its mass. When the attractive force exceeds the repulsive one, the particles stick together to form flocs. This cohesion becomes more important as grain size decreases, and it would increase with the electrical conductivity (particularly, salinity) of ambient water and the proximity of particles or flocs. It was found that medium to coarse silts with a diameters greater than 40 μm are practically cohesionless in fresh water, whereas they shows the cohesive behavior in salty water (McAnally, 1999). Therefore, the study of cohesive sediment requires the synchronous description of mutual interactions of grains (e.g., flocculation), their physical properties (e.g., grain size and mineral composition) and the ambient water conditions.

Leaving aside the forces of nature, it is obvious that human activities such as structure construction and dredging that involve cohesive sediments may result in adverse economic and ecological effects on human society. For instance, severe erosion results in the wetland loss and river profile degradation. The increased turbidity by such an erosion can endanger the health of eco-system by limiting the light penetration and the primary production. In particular, the resuspension of contaminated cohesive sediment leads to the high concentration of pollutant in water, as many pollutants tend to preferentially

absorb to the cohesive sediment due to its chemical properties (Winterwerp and van Kesteren, 2004). On the other hand, deposition can obstruct the navigation channel, contribute to flooding, clog water intakes, smother the valuable aquatic organisms, and create other problematic conditions. Especially, fine-grained sediment tends to accumulate in sheltered water areas such as harbors and channels, which requests a high dredging cost for maintenance. Even though the siltation may not seriously hinder the navigation, a regular dredging is necessary to keep the quality of water and sediment bed (Bruens, 2003).

In general, sediment transport is primarily controlled by the important tripartite components: (1) turbulence, (2) suspended sediment and (3) bed morphology (Leeder, 1999). These components are mutually interactive for feedback, as illustrated in Fig. 1-1. When the bed shear stress is applied to sediment bed, for instance, erosion or dispersion process may occur near the bed. The amount of erodible sediments can be determined by the competition between applied bed shear stress and bed resistance. The bed roughness and morphology contribute to the overall flow resistance and turbulence structure near the bottom boundary layer (Leeder, 1999). Once the bottom sediments are agitated to erode, the turbulent diffusion and advection may deliver them to the upper or adjacent water column, which results in increasing suspended sediment concentration (SSC). The stratification caused by this sediment suspension would dampen the turbulence. Also, turbulence plays an important role in determining the floc size and its distribution. It can increase the floc size by increasing the collision frequency of primary particles, whereas it can also break up the floc under highly turbulent conditions. The flocs with higher settling velocities will settle toward the bed faster, compared with individual particles.

Biological processes often influence on cohesive sediment behaviors with two opposite functional groups: (1) bio-stabilizer and (2) bio-destabilizer (Widdows and Brinsley, 2002). For example, the bio-stabilizers (e.g., submerged aquatic vegetation (SAV)) may protect the bed from erosion and resuspension by reducing the turbulence near the bed. Biological glues such as extracellular polymeric substrates (EPS) and mucus excreted by organism smooth cohesive sediment surface and strength the bonding structure between particles, so that they may increase the erosion threshold and the flocs in suspension might be rapidly settled from the water column. In contrast, the bio-destabilizers (i.e., biotubators) can increase the sediment erodibility, sediment water content, resuspension rate, and bed roughness. Despite these important roles of biology, it is practically difficult to address its quantitative contribution to cohesive sediment behaviors due to highly spatial and temporal variations. Most sediment models, therefore, would modify input parameters (e.g., settling velocity and critical shear stress for erosion) on the basis of the in-situ or laboratory measurement in order to account for complex biological parameters (Winterwerp and van Kesteren, 2004).

For the purpose of understanding the physical and non-physical processes described above (see Fig. 1-1), many works have been attempted by means of a variety of measuring instruments with different energy sources (e.g., sound, light, laser, electric and nuclear). Each one has its own characteristic advantages as well as disadvantages in the system operation, data acquisition and interpretation. It is generally acknowledged that none of available instruments and methods is completely free from measuring error and limitation. At present, both optical and acoustic instruments are most commonly found everywhere in the commercial market as well as scientific communities for cohesive

sediment (Thorne and Hanes, 2002). The problematic issues related to the measurements of cohesive sediment can be summarized as follows.

The first is regarding the measurement method of SSC. It can be simply classified into three major categories: direct sampling, optical and acoustic instruments. The operation principle, advantages and disadvantages of individual method were compared in Table 1-1. Direct manual sampling is the most straightforward method to get the true SSC. Also, optical method such as an optical backscattering sensor (OBS) is a good device to measure the time series of SSC at a fixed elevation. Its response output was well studied in both low and high concentration ranges (for review, see Downing, 2006). However, one of noticeable drawbacks of optical method and manual sampling is that a probe or sampler itself could disturb the turbulence structure and the distribution of suspended solids, when deployed to the area of interest. Such an intrusion feature might prevent from measuring the SSC near the bed where the gradient is usually the largest. Also, the spatial and temporal resolution is too poor to provide continuous profiles. In order to overcome these shortcomings, acoustic probes such as an Acoustic Backscattering Sensor (ABS) are widely being used to get the time series of SSC profiles. However, the acoustic backscattering theory and empirical relationship among complex variables had been mainly formulated for non-cohesive sediments so far. This is because non-cohesive sediments have a clear interface between sediment and water, and the granular sediments are less influenced by underlying processes such as biological effects. However, cohesive sediments tend to continuously alternate flocculation and breakup by the interactions of hydrodynamic, electrochemical and biological forces. Therefore, the scattering properties of cohesive sediments cannot be predicted to be the same as non-

cohesive sediments. It is also noticed that the sound attenuation caused by clay sediment is more affected by the viscosity absorption component than by the sound scattering component (Richards et al., 1996). In these aspects, a robust framework of acoustic backscattering theory for cohesive sediments is a challenging issue to be resolved.

Secondly, various instruments have been developed and deployed for in-situ settling velocity measurement (for review, see Eisma et al., 1997; Mantovanelli and Ridd, 2006), since the Owen Tube method (Owen, 1976) was firstly released. There is still, however, no consensus in both measuring technique and data interpretation protocol due to inherent complexities in flocculation. With a simplified assumption, recently, Fugate and Friedrichs (2002) used an Acoustic Doppler Velocimeter (ADV) to estimate the settling velocity of aggregated estuarine particles, which is a promising approach but has rooms to be improved in both in-situ measurement and data interpretation (Maa and Kwon, 2007).

Third, after cohesive sediment flocs settle toward the bed, they tend to experience further processes of deposition and self-weight consolidation in a static condition. One of debatable issues related to cohesive sediment deposition is the existence of a critical shear stress for deposition because there is a salient conflict between the laboratory and in-situ measurement of SSC under the cyclic tidal forces (Krone, 1962; Sanford and Halka, 1993; Winterwerp and van Kesteren, 2004). To date, two opposite paradigms – "exclusive" or "simultaneous" erosion and deposition – have been used to describe the exchange of cohesive sediments at the sediment-water interface. Hence, the direct observation on when deposition actually occurs is necessary as an evidence to resolve the dispute of these two paradigms.

Finally, the consolidating or consolidated bed generally exhibits the largest gradient in sedimentary properties near the sediment-water interface (Mehta and Dyer, 1990; Winterwerp and van Kesteren, 2004; Holland et al., 2005). This gradient may be induced by the complexity of near-bed processes (e.g., erosion, deposition, consolidation and bioturbation) as a result of redistribution of near-bed sediments. If it is possible to measure the uppermost layer of sediment bed without any structure destruction, this may provide the important clues for revealing sedimentary history and predicting future sediment behaviors. In this aspect, the acoustic approach can be one of candidates for measuring near-bed properties (e.g., bulk density) without the bed destruction.

In the context of "acoustics-sediment", the acoustic return signal can be simply categorized into two signal types: (1) backscattered signal and (2) echo signal. As the transmitted source signal propagates along the pathway, the suspended sediment may backscatter a portion of source energy. Because the amount of scatterers is directly related to the SSC in water, the former signal intensity can be used as a proxy for SSC (Thorne et al., 1991; Holdaway et al., 1999; Admiraal and Garcia, 2000). It can be converted to the real SSC through a proper signal calibration against ground truth data. On the other hand, when the source energy is strong enough to come to and penetrate into the sediment bed, the sediment-water interface generally generates a relatively stronger intensity of return signals. Also, echo signals returned from the sediment bed can provide the information on bed location and internal acoustic interface within sediment bed, if exists. In particular, if a high-concentration fluffy layer (e.g., fluid mud) may exist near the cohesive bed, the spikes detected in the return acoustic wave near the bed might be

8

indicative of the upper or lower boundary of this suspension layer, as the gradient of acoustic impedance is very high at those boundaries.

As a summary, acoustics is a promising approach for synchronously estimating all tripartite components in cohesive sediment dynamics owing to recent advances in high-frequency acoustic technology (e.g., Thorne et al., 1991; Vincent et al., 1991; Hamilton et al., 1998; Holdaway et al., 1999; Smerdon, 1998; Shi et al., 1999; Admiraal and Garcia, 2000; Wren, 2000; Thorne and Hanes, 2002). It also has a capability to measure non-intrusively the physical properties of sediment with a high resolution in time and space, because the transducer is located relatively far from the target layer to be investigated. At the developing stage, acoustics is currently opening a new dimension to measure various parameters involved with cohesive sediment dynamics. Furthermore, the more accurate measurement with acoustics can enhance the capability to predict the sediment transport and its fate and the reliability of a sediment model.

2. Scope and objectives

With the rationale mentioned above, this dissertation aims at utilizing the acoustic approach to measure cohesive sediment behaviors including (1) suspension, (2) settling, (3) deposition and (4) consolidation. In the view of acoustic signal, the first two processes were attempted to interpret by means of backscattered signal analysis, while the last two processes were done by echo signal analysis.

The acoustic instruments used in this study range from commercially available devices such as ADV and Pulse Coherent Acoustic Doppler Profiler (PC-ADP) to in-house-developed acoustic device (Micro-Chirp System) by assembling pre-existing

acoustic transducers and electric parts. Depending on a required resolution of sediment properties to be measured, an appropriate frequency was selected to optimize the sensitivity. For instance, 5-MHz ADV was used to estimate SSC and settling velocity, and Micro-Chirp System employed the frequency ranges of 300-700 KHz to measure the bulk density of consolidating bed.

With the acoustic approach used in this study, it is practically hard to quantitatively address biological effects on four sedimentary processes mentioned above. In the laboratory measurement, the used sediments had relatively weak or no biological activities, so that biological processes were not discussed hereafter. Instead, this study emphasizes on physical processes of cohesive sediment in the water column, sediment-water interface and top (uppermost several centimeters) sediment layer.

The specific objectives can be summarized as follows: (1) To understand ADV responses in a wide range of SSC on the basis of acoustic backscattering theory and reveal the effects of turbulence and SSC on the settling velocity, (2) To measure the SSC profile using acoustic inversion algorithm for PC-ADP, (3) To estimate a critical shear stress for cohesive sediment deposition and to evaluate two opposite paradigms for cohesive sediment dynamics using the annular flume experiments, and (4) To develop a non-intrusive acoustic method and a data-processing protocol for measuring bulk density of consolidating clay bed.

3. Outline of dissertation

Each chapter is related to an individual sedimentary process, and stands alone as a separate piece of work with its own introduction, methods, results, discussion and conclusions.

Chapter II includes the estimation of SSC and settling velocity using an ADV. Two kinds of sediments were compared in terms of acoustic responses. Especially, the reverse relationship between signal strength and SSC was found in the high concentration range. The effects of turbulence and SSC on settling velocity were studied using ADV. The limitation of ADV approach and possible improvement were discussed.

Chapter III deals with the measurement of SSC profile using PC-ADP. The practical operation range and measuring requirement for guaranteeing a successful performance were investigated. The detail description of calibration was given and the uncertainty associated with measurement and signal converting process was discussed.

Chapter IV presents the laboratory flume experiment to reveal depositional behaviors. The debatable concept of "a critical shear stress for deposition" was dealt with to understand the cohesive sediment dynamics under the tidal forces. The acoustic technique had been tried to detect any change of bed thickness during the deposition, which might provide the direct evidence on when the deposition actually occurs. Unfortunately, it was concluded that the mounted contact-type transducer do not have the sufficient resolution to identify the small change of sediment-water interface during the flume experiments. Alternatively, the lateral growth of deposit and OBS readings were used as indicators for determining the change of depositional rate and SSC.

Chapter V contains the development of an acoustic measuring device to estimate the bulk density for consolidating clay bed. The detail protocol for acoustic signal processing was given. Using acoustic responses such as wave reflectivity near the sediment-water interface, the maturity of consolidation status was determined.

4. Definitions

The definitions of cohesive sediment processes were given below to clarify the meaning and importance, and to avoid any confusion when compared with other studies.

- *Erosion*: The process by which the bed loses the pre-achieved resistance, and thus, the sediment particles (flocs) or masses are stripped from the bed, when an applied shear stress exceeds a critical value (McAnally, 1999).

- *Dispersion* (or *re-dispersion*): When tide changes from slack to flood or ebb, the newly deposited material can be immediately suspended because the time for consolidation is practically negligible and critical shear stress for erosion is practically zero (Maa and Kim, 2002).

- *Downward flux*: The gravity-induced net downward movement of sediment particles or flocs (McAnally, 1999).

- *Settling*: The gravity-induced downward movement of a particle or floc.

- *Settling velocity*: The velocity at which particles or flocs settle through a static fluid when the resistance of the fluid exactly equals the downward force of gravity acting on the particles or flocs (Mantovanelli and Ridd, 2006).

- *Deposition*: Settling particles (or flocs) come to the bed and then stick to it. The most important process is to become a part of sediment bed (Krone, 1993; Ha and

Maa, in prep.). In this aspect, the deposition is different with the downward settling.

- *Flocculation*: The process by which colliding particles bind together to form a floc, also known as aggregation.

- *Deflocculation*: The process by which a floc are broken up, resulting in decreasing the floc size, also known as disaggregation.

- *Fluid mud*: A high concentration aqueous suspension of fine-grained sediment in which settling is substantially hindered by the proximity of sediment grains and flocs, but which has not formed an interconnected matrix of bonds strong enough to eliminate the potential for mobility (McAnally et al., 2007). Its concentration is on the order of several 10 to 100 g/L (Whitehouse et al., 2000).

- *Consolidation* (particularly, self-weight consolidation): The process that the porosity would decrease but the bulk density would increase, as the pore water is squeezed out of bed.

The processes dealt in this dissertation are schematically shown in Fig. 1-2. The existence of high-concentration layer (or fluid mud) was assumed, because this layer can be easily formed with the thickness of several millimeters to meters during the stagnant conditions such as a slack tide. Some previous works (e.g., Ross and Mehta, 1989) used four-layer concept which divided the high-concentration layer (or fluid mud) into two more sublayers (i.e., mobile and stationary fluid mud layer), but this study considered these two layers as one single layer, because of the difficulty in practically differentiating the boundary between two layers.

It is noted that there is a difference in definition compared with other authors. For instance, Bruens (2003) defined the process crossing down the interface [1-2] as "deposition", but this study referred to this process as "settling" because the layer 2 is assumed to be still in suspension (Fig. 1-2). Chapter IV has been devoted to further discuss the difference between these two terms.

References

Admiraal, D.M., Garcia, M.H., 2000. Laboratory measurement of suspended sediment concentration using an Acoustic Concentration Profiler (ACP). Experiments in fluids, 116-127.

Bruens, A., 2003. Entraining mud suspensions. Ph.D. Thesis, Technique University of Delft, 137 pp.

Downing, J., 2006. Twenty-five years with OBS sensors: the good, the bad, and the ugly. Continental Shelf Research 26, 2299-2318.

Eisma, D., Dyer, K.R., van Leussen, W., 1997. The in-situ determination of the settling velocities of suspended fine-grained sediment- a review. In: N. Burt, R. Parker and J. Watts (Editors), Cohesive Sediment. John Wiley and Sons, pp. 17-44.

Fugate, D.C., Friedrichs, C.T., 2002. Determining concentration and fall velocity of estuarine particle populations using ADV, OBS and LISST. Continental Shelf Research 22, 1867-1886.

Ha, H.K., Maa, J.P.-Y., in prep. Evaluation of cohesive sediment paradigm for deposition.

Hamilton, E.L., 1998. Calibration and interpretation of acoustic backscatter measurements of suspended sediment concentration profiles in Sydney Harbour. Acoustics Australia 3, 87-93.

Holdaway, G.P., Thorne, P.D., Flatt, D., Jones, S.E., Prandle, D., 1999. Comparison between ADCP and transmissometer measurements of suspended sediment concentration. Continental Shelf Research 19, 421-441.

Holland, C.W., Dettmer, J., Dosso, S.E., 2005. Remote sensing of sediment density and velocity gradients. J, of Acoust. Soc. Am. 118(1), 163-177.

Krone, R.B., 1962. Flume studies of the transport of sediment in estuarial shoaling processes, University of California, Berkeley. 110 pp.

Krone, R.B., 1993. Sedimentation revisited. In: Mehta, A.J. (Ed.), Nearshore and Estuarine Cohesive Sediment Transport. AGU, Washington D.C., pp. 108-125.

Leeder, M.R., 1999. Sedimentology and Sedimentary Basins. Blackwell Science Ltd., 608 pp.

Maa, J. P.-Y., Kwon, J.-I., 2007. Using ADV for cohesive sediment settling velocity measurements. Estuarine, Coastal and Shelf Science 73, 351-354.

Maa, J.P.-Y., Kim, S.-C., 2002. A constant erosion rate model for fine sediment in the York River, Virginia. Environmental Fluid Mechanics 1, 345-360.

Mantovanelli, A., Ridd, P.V., 2006. Devices to measure settling velocities of cohesive sediment aggregates: a review of the in situ technology. J. of Sea Research 56(3) 199-226.

McAnally, W.H., 1999. Aggregation and deposition of estuarial fine sediment. Ph.D. Thesis, Univ. of Florida, 366 pp.

McAnally, W.H., Friedrichs, C.T., Hamilton, D., Hayter, E., Shrestha, P., Rodriguez, H., Sheremet, A., Teeter, A., 2007. Management of fluid mud in estuaries, bays, and lakes. I: present state of understanding on character and behavior. J. of Hydraulic Engineering 1333(1), 9-22.

Mehta, A.J., Dyer, K.R., 1990. Cohesive sediment transport in estuarine and coastal waters. The Seas. Ocean Engineering Science.

Owen, M.W., 1976. Determination of the settling velocities of cohesive muds. IT161, Hydraulic Research Station.

Richards, S.D., Heathershaw, A.D., Thorne, P.D., 1996. The effect of suspended particulate matter on sound attenuation in seawater. J, of Acoust. Soc. Am. 100(3) 1447-1450.

Ross, M.A., Mehta, A.J., 1989. On the mechanics of lucoclines and fluid mud. J. of Coastal Research (Spec. Issue 5), 51-61.

Sanford, L.P., Halka, J.P., 1993. Assessing the paradigm of mutually exclusive erosion and deposition of mud with examples from upper Chesapeake Bay. Marine Geology 114, 37-57.

Shi, Z., Ren, L.F., Hamilton, L.J., 1999. Acoustic profiling of fine suspension concentration in the Changjiang Estuary. Estuaries 22(3A) 648-656.

Smerdon, A.M., Rees, J.M., Vincent, C.E., 1998. An acoustic backscatter instrument to measure near-bed sediment processes, Aquatec Electronic Ltd. 18 pp.

Thorne, P.D., Vincent, C.E., Hardcastle, P.J., Rehman, S., Pearson, N., 1991. Measuring suspended sediment concentrations using acoustic backscatter devices. Marine Geology 98(1), 7-16.

Thorne, P.D., Hanes, D.M., 2002. A review of acoustic measurement of small-scale sediment processes. Continental Shelf Research 22(4), 603-632.

Vincent, C.E., Hanes, D.M., Bowen, A.J., 1991. Acoustic measurements of suspended sand on the shoreface and the control of concentration by bed roughness. Marine Geology 96(1-2), 1-18.

Whitehouse, R., Soulsby, R.L., Roberts, W., Mitchener, H., 2000. Dynamics of estuarine muds; a manual for practical applications. Thomas Telford, 232 pp.

Widdows, J., Brinsley, M., 2002. Impact of biotic and abiotic processes on sediment dynamics and the consequences to the structure and functioning of the intertidal zone. J. of Sea Research 48, 143-156.

Winterwerp, J.C., van Kesteren, W.G.M., 2004. Introduction to the physics of cohesive sediment in the marine environment. Elsevier, Amsterdam, 466 pp.

Wren, D.G., 2000. Studies in suspended sediment and turbulence in open channel flows, Ph.D. Thesis, Univ. of Mississippi, 136 pp.

Table 1-1. Comparison of direct sampling, optical and acoustic method for measuring suspended sediment concentration.

Characteristics	Direct sampling	Optical	Acoustic
Operation principle	Sediment-water mixture is taken and filtered to measure concentration	Backscatter or transmission of light within sampling volume by suspended particles is measured.	Sound backscatter by suspended particles is used to determine size and concentration
Intrusiveness	Intrusive	Intrusive	Non-intrusive
Energy source	n/a	Infrared or visible	Acoustic wave
Calibration requirement	No	Yes	Yes
Measurement type	Point measurement	Point measurement	Entire profile
Sensitivity	n/a	Better for finer sediment	Better for coarser sediment
Sampling rate	n/a	Programmable	Programmable
Advantages	- No calibration required - Cost effective - Ground truth for other methods	- Good temporal resolution - Relatively inexpensive - Remote deployment possible	- Good temporal and spatial resolution - Non-intrusive - Determination of particle size is possible, because signal intensity depends on it
Disadvantages	- Poor temporal and spatial resolution - Time-consuming laboratory analysis - Disturb flow and distribution of particles - Require on-site personnel	- Signal attenuation at high concentration - Calibration necessary with in-situ sediment - Response depending on the particle size - Only fixed point measurement	- Signal attenuation at high concentration - Calibration necessary with in-situ sediment
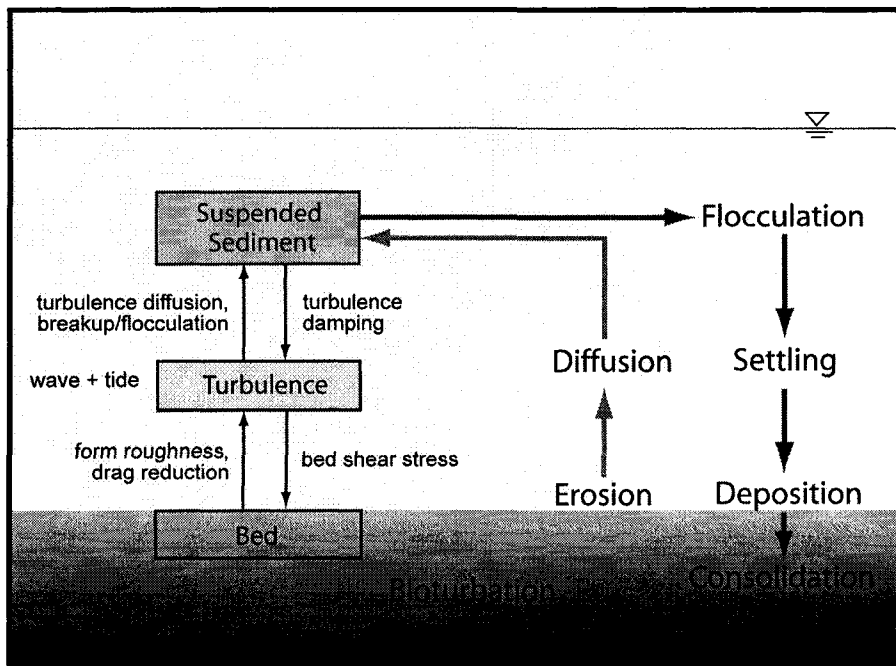
Fig. 1-1. Outline of cohesive sediment processes in natural waters. To study the
suspension, diffusion, settling, deposition and consolidation of cohesive
sediment, ADV, PC-ADP, OBS, annular flume and Micro-Chirp System were
used in this study.
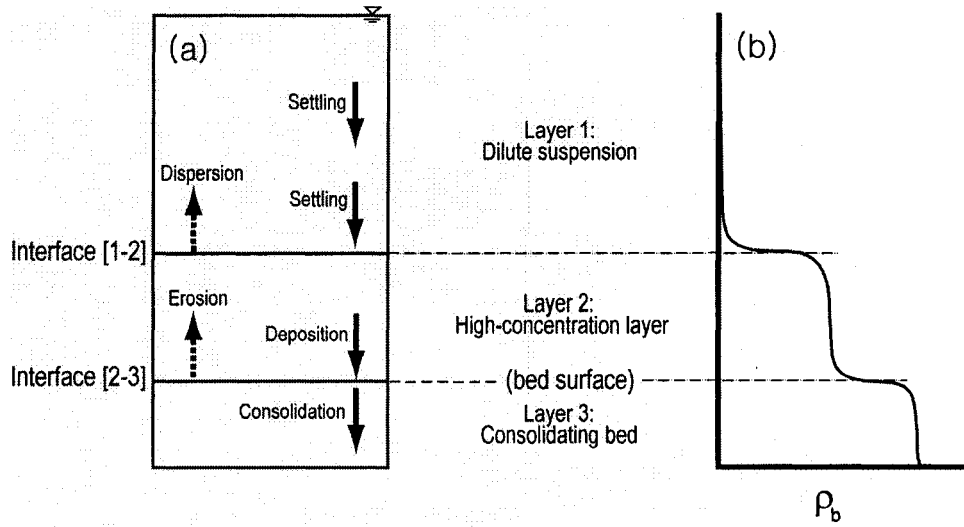
Fig. 1-2. (a) Schematic processes of cohesive sediment in water column and near-bed
layer (after Bruens, 2003); (b) Conceptual profile of bulk density.

CHAPTER II. USING AN ACOUSTIC DOPPLER VELOCIMETER (ADV) FOR MEASURING CONCENTRATION AND SETTLING VELOCITY OF COHESIVE SEDIMENTS

Abstract

Using an Acoustic Doppler Velocimeter (ADV), the laboratory experiments were carried out to estimate the suspended sediment concentration (SSC) and investigate the effect of SSC and turbulence on the settling velocity (w_s) of cohesive sediment. Within the limited ranges of SSC, ADV backscatter strength can be used as a proxy to convert into the SSC. The 5-MHz ADVOcean has an operational range up to 1 and 4 g/L for Clay Bank sediment and kaolinite, respectively. For the higher SSC, ADV output was saturated or decrease with increasing SSC. Backscattered signals would be sometimes too noisy due to high amplification ratio, high sampling rate (e.g., > 10 Hz) and small sampling volume, and thus, a moving average was used to yield the instantaneous changes of SSC. The measurement of w_s with Clay Bank sediment showed that turbulence can increase w_s, up to one order larger than that for calm water. When turbulence is stronger than a limit, however, it contributes to the decrease of w_s. Results suggest that ADV is a potential tool to simultaneously estimate SSC and w_s in turbulent dominant environment without interfering with ambient flows.

Keywords: ADV; suspended sediment concentration; settling velocity; cohesive sediment; turbulence

1. Introduction

Acoustic Doppler Velocimeter (ADV) is a powerful tool to measure all three components of flow velocities in laboratory and field environments. Salient advantages of ADV are that no calibration is required for velocity measurements and it can measure the velocities without interfering with the flow because the sampling volume is approximately 5-18 cm (depends on a model) away from the transducer (SonTek, 2006). Beyond this primary function for measuring velocities, ADV can potentially estimate Suspended Sediment Concentration (SSC) and settling velocity (w_s) through a proper signal processing (e.g., Kawanisi and Yokosi, 1997; Gratiot et al., 2000; Fugate and Friedrichs, 2002). Both SSC and w_s are key factors to determine the deposition rate and the mass fluxes in sediment dynamics. Therefore, the accurate estimation of both parameters is essential to understand the suspended sediment behavior in water column and to enhance the capability for better predicting the sediment transport and its fate.

The backscattered signal strength has been used to determine SSC, and the acoustic scattering theories have been developed to reveal the relationship between scattering wave strength and SSC (e.g., Vincent et al., 1991; Lee and Hanes, 1995; Thosteson and Hanes, 1998; Merckelbach and Ridderinkhof, 2006). To date, the successful use of sound to measure the SSC has been mostly confined to the suspension of granular sediment with a limited range of SSC before multiple scattering and attenuation by suspended sediments become significant (for review, see Thorne and Hanes, 2002). The acoustic application to cohesive sediments, however, has not been clearly proven because cohesive sediments rarely exist as

24

primary particles in natural environments. Much large and loosely structured flocs are easily formed and commonly exist. Furthermore, few attempts have been made to check the performance of acoustic device for fine and fluffy cohesive sediments (e.g., Shi et al., 1997). In these aspects, the possible acoustic scattering responses for cohesive sediments remain to be verified.

For the measurement of w_s of cohesive sediments, many measuring instruments and techniques have been developed (for review, see Mantovanelli and Ridd, 2006). At present, however, there is still no consensus in both measuring technique and data interpretation due to inherent complexities in cohesive sediment settling. Even at the same site, the estimated w_s can be very different depending on the type of instrument or the analytical method (Eisma et al., 1997). Among the myriad approaches for w_s, most recently, ADV has emerged as a novel device capable of simultaneously estimating the SSC and w_s (e.g., Fugate and Friedrichs, 2002, 2003; Voulgaris and Meyers, 2004; Scully, 2005; Maa and Kwon, 2007; Kawanisi and Shiozaki, 2008). Nonetheless, the presented data are somehow noisy and the correlation coefficient is sometimes low, presumably due to the simplified analytical assumption. To verify the hidden factors related to these scattered data, laboratory experiments that most conditions are controllable are necessary.

With the rationale mentioned above, using ADV, this paper prompts (1) the investigation for possible relationship between backscatter strength and suspended cohesive sediment concentration and (2) the measurement of w_s in a range of turbulence and SSC and its dependence on these two parameters. Moreover, the

limitation of ADV approach for measuring SSC and w_s and the possible improvement were discussed.

2. Materials and methods

2.1. Experimental apparatus

A 5-MHz ADVOcean manufactured by SonTek was used to measure the time series of acoustic backscattered strength as well as turbulence. Based on the operational principle, the signal amplitude (or count) obtained by ADV is proportional to the logarithm of acoustic strength (1 count=0.43 dB; SonTek, 2006). Because this scattering strength is a function of the amount and the type of suspended sediment in the sampling volume (ca. 2 cm^3) located at 18 cm from the transmitter, ADV can be used to measure SSC when the acoustic response of sediment is known.

More than that, scattering theory indicates that the range of particle size that can be detected by acoustic waves depends on the parameter of ka where k (=$2\pi/\lambda$, λ is the acoustic wavelength) is the acoustic wave number, and a is the particle radius (Thorne and Hanes, 2002). The backscattering strength is the maximum when ka=1, and it is more or less constant when ka>1 (Thorne and Hanes, 2002). For the 5-MHz ADV employed here, a corresponding particle radius for peak strength is approximately 50 μm (SonTek, 2006).

Two bilge pumps with different pumping rates (i.e., 1900 and 5700 L/hr) were used to stir up the sediment. The output vent was connected with different adaptors (straight, L- and T-shape) to generate the artificial turbulence with different intensities (Table 2-1; Fig. 2-1).

2.2. Sediments

Two different types of sediments (commercially available kaolinite and sediment sample collected from Clay Bank of the York River) were used to check the acoustic responses with sediment properties. Clay Bank sediment shows a bimodal distribution (Fig. 2-2a). The first (ca. 1 μm) and the second mode (ca. 88 μm) are found in the clay and very fine sand range, respectively. Organic content is about 6.1%. The clay minerals are composed of mainly Illite (75%) and the rest is rather uniformly distributed as Kaolinite, Chlorite and Smectite (ca. 8% each) (Maa and Kim, 2002). In contrast, kaolinite shows a unimodal distribution (Fig. 2-2b) that major components are less than 10ϕ. The mode is about 1 μm. For the measurement of w_s, only Clay Bank sediment was used because of its higher acoustic response (see Fig. 2-3).

2.3. Experimental method

Prior to the ADV measurement, a sediment-water mixture was placed in a cylindrical tank (diameter: 0.75 m; height: 1.5 m), and then diluted with tap water until the pre-determined SSC was attained. In particular, the kaolinite-water mixture lasted more than 30 days to reach a fully water-saturated condition. At the beginning of each experiment, pumps were operated to fully mix the sediment slurry and keep the sediment in suspension for 24 hrs. The same conditions for pumping rate, adaptor type and vent direction were applied during the entire time of an individual measurement. In order to verify ADV responses and record the time series of SSC, as

27

another reference, an Optical Backscattering Sensor (OBS) was also installed at the same sampling level of the ADVOcean. The location of OBS was horizontally off the sound propagation path of the ADVOcean because the backscattered signal measured by both optic and acoustic sensors can be contaminated if any foreign object exists in the sensing range. The sampling levels for ADV, OBS and a corresponding port for water sampling were all located at 0.9 m above the tank bottom. Withdrawn water samples were filtered through a 0.7-μm glass fiber filters. The residue left on the filter was oven dried at 103-105°C for 24 hrs, and then weighted for determining the SSC. Calculated mass concentrations were used to calibrate the signal strength of ADV and OBS.

2.4. Data analysis

In the sediment mass conservation equation, by neglecting across (y) channel and vertical (z) advection, the balance along channel direction (x) can be expressed as

$$\frac{\partial C}{\partial t} + \frac{\partial(uC)}{\partial x} + w_s \frac{\partial C}{\partial z} - \frac{\partial}{\partial z}\left(K \frac{\partial C}{\partial z} \right) = 0 \qquad (2\text{-}1)$$

where C is the sediment concentration, and K is the eddy diffusivity. As the first order approximation, the local concentration changes, $\frac{\partial C}{\partial t}$, and the advection term, $\frac{\partial(uC)}{\partial x}$, were assumed to be negligibly small in order to analytically estimate w_s of aggregated particles (Fugate and Friedrichs, 2002). As a result, the SSC at a given height above bed can be simply represented by a balance between upward turbulent diffusive flux and downward settling flux,

$$K\frac{\partial C}{\partial z} = w_s C \qquad (2\text{-}2)$$

Using a Reynolds flux, the turbulent diffusion term can be alternatively expressed as

$$K\frac{\partial C}{\partial z} = -\langle w'C' \rangle \qquad (2\text{-}3)$$

By substituting Eq. 2-3 into Eq. 2-2, Reynolds concentration flux is balanced by the settling flux,

$$-\langle w'C' \rangle = w_s \langle C \rangle \qquad (2\text{-}4)$$

where w is the vertical velocity, C is the SSC derived from the ADV backscatter, the prime denotes the fluctuations from the mean value, and the angular bracket means the time average. In the plot of $\langle C \rangle$ versus $\langle w'C' \rangle$, the slope of a linear regression equation yields a constant w_s. An x-axis intercept of regression equation is interpreted as "background concentration" which represents the non-settling components. Due to the linear relationship between $\langle w'C' \rangle$ and $\langle C \rangle$, this approach provides a single value of w_s regardless of SSC, and thus, it is impossible to address the relationship between w_s and SSC.

In order to overcome this issue, as an extension of the above approach, Maa and Kwon (2007) proposed to use an exponential relationship between two parameters, instead of the linear regression,

$$-\langle w'C' \rangle = m\langle C \rangle^n \qquad (2\text{-}5)$$

where m and n are empirical constants derived by a non-linear least-squares fit. Consequently, w_s can be expressed as a function of SSC.

$$w_s = m\langle C \rangle^{n-1} \qquad (2\text{-}6)$$

29

By changing the location of pump, adaptor type and vent direction, several

turbulent conditions were artificially made (Table 2-1; Fig. 2-1). The effect of

turbulence on w_s was obtained from the concurrent measurement of SSC and

turbulence. To represent the turbulence in the water tank, turbulent kinetic energy

(TKE) was used.

$$TKE = \frac{1}{2} \rho_w \left(\overline{u'^2} + \overline{v'^2} + \overline{w'^2} \right) \qquad (2\text{-}7)$$

where ρ_w is the water density, u', v' and w' are three turbulent fluctuating

components.

3. Results and discussions

3.1. SSC measurement by ADV

In calibration, 2-min average of backscattered signal strength, S, was

compared with the sample-derived SSC. Both kaolinite and Clay Bank sediments

commonly showed that S increased with increasing SSC, reached a maximum

strength when the SSC surpassed an upper limit, and then decreased even though SSC

was still increasing (Fig. 2-4). Overall, a good correlation was shown, and the

regression coefficients (r^2) of kaolinite and Clay Bank sediment were 0.91 and 0.96,

respectively. However, it was found that there are different responses to SSC in

terms of the maximum level and the increasing (or decreasing) rate of S. In case of

kaolinite, S increased gently in the lower SSC ranges (< 4 g/L), and then, decreased

also gently when the SSC was larger than 4 g/L. On the other hand, Clay Bank

sediment caused more rapid increase of S when the SSC was less than 1 g/L, and

exhibited a flat region with a constant maximum output while SSC was changing between 1 and 10 g/L. S rapidly decreased after 10 g/L. The peaks of S for kaolinite and Clay Bank sediment were approximately 61 and 72 dB, respectively. These differences in ADV responses might be associated with the fact that the acoustic signal response mainly depends on the sediment grain size and the reflectivity of particles (or flocs) at a given frequency (Thorne and Hanes, 2002). Assuming that the sound speed in water is approximately 1500 m/s, the values of "ka" for kaolinite and dominant sand portion (a=44 μm) of Clay Bank sediment with 5-MHz ADV are about 0.01 and 0.9, respectively. Based on the scattering theory, the acoustic backscattered signal amplitude is proportional to $(ka)^2$ within the Rayleigh scattering regime (ka<<1) where the circumference of scatterer is much smaller than acoustic wavelength (SonTek, 1997). Also, the acoustic intensity is proportional to the signal amplitude squared. Hence, it is expected that the acoustic intensity generated from Clay Bank sediment is much higher than that from kaolinite (Fig. 2-3), assuming that (1) the suspended particle is a sphere, (2) no flocculation occurs, and (3) the same amplification ratio is applied. Due to the higher acoustic response, therefore, Clay Bank sediment has relatively high r^2 (see Fig. 2-4). Although S of kaolinite should be always lower than that of Clay Bank sediment, it is noticeable that kaolinite has higher signal strength than Clay Bank sediment when SSC is lower than 0.5 g/L. This is probably caused by the automatic gain control of ADV for conditioning return signal. ADV might apply a higher gain setting for kaolinite because its return signal is too weak, whereas it used a lower gain for Clay Bank sediment. Due to the variable amplification ratio depending on the amplitude of backscattering signal, it is

31

hard to compare two sediments only in view of signal strength. Unfortunately, the gain settings employed during the measurement cannot be archived at this time and the manufacturer insisted that the amplification ratio should be fixed for all types of sediments (SonTek, personal communication). Therefore, further works are needed to confirm gain control in the firmware of ADV.

The decreasing trend of S in the high concentration ranges (> 4 g/L for kaolinite; >10 g/L for Clay Bank sediment) may be attributed to other reasons: (1) increase of sound absorption with increasing SSC; and (2) multiple scatter becomes important because more sound waves off the suspended materials are redirected to ambient particles in high SSC, so that more sound attenuation might occur along the multiple propagation path. This kind of response is common for all instruments using the backscatter waves to measure the SSC. For example, Kineke and Sternberg (1992) found that OBS output had an exponentially decreasing trend with increasing SSC in high SSC range.

Although S shows a good correlation with SSC for low SSC, the instantaneous SSC derived from the ADVOcean's backscatter strength (C_{ADV}) was highly fluctuated. For instance, the fluctuation range measured by the ADVOcean for Clay Bank sediment was approximately $\pm$ 40-80 mg/L over the entire measurement period (Fig. 2-5a). When compared with the SSC observed from the OBS (C_{OBS}) at the same time and location, C_{OBS} showed a much smoother response than C_{ADV} (Fig. 2-5b). The high fluctuations in C_{ADV} may be attributed to a high amplification ratio required for detecting the backscatter waves. In principle, an average of certain numbers of pings, around 20 to 30 pings, should be included in data processing (SonTek, personal

communication). For processing ADV signals for velocity, a process that systematically averages a certain number of pings, depending on the sampling rate, is included. This implies that using ADV signals for SSC measurements should also include an averaging process to increase signal-to-noise ratio (SNR). This process should be done while collecting data during experiment. Unfortunately, this was not recognized at that time, and thus, a post-processing technique was suggested as a remedy to effectively reduce the noise level from original ADV data acquired at 10 Hz. After taking a 40-point moving average with equal weight, the abnormal fluctuations induced by noises were significantly dampened (see the black line in Fig. 2-5a). Depending on the sampling rate and amount of noises, the adjustment of data points for averaging is needed to produce the reliable instantaneous variation of SSC.

As might be expected, OBS showed relatively smooth responses because it senses the total light backscatter within a sampling domain around 20 cm^3 close to the sensor (Fig. 2-6; Downing, 2006). Since this domain is much larger than that used in ADV (ca. 2 cm^3), OBS responses represent the average of a spatial domain. This averaging process, although on spatial domain, can also smooth the data. Therefore, there is no need to do moving average again for the OBS signals. To summarize, the OBS responses may be too smooth to represent the true fluctuation of SSC at a local point. In the other extreme, the ADV responses at the high sampling rate (e.g., > 10 Hz) would be too rough due to low SNR.

3.2. w_s measurement by ADV

Fig. 2-7 shows an example of settling measurements under a moderate (TKE=

0.69 kg m^{-1}s^{-2}) turbulent conditions. The 5-min average of ADV-derived SSC

($<C_{ADV}>$) and $\frac{\partial C}{\partial t}$ decreased with a settling time. The initial $<C_{ADV}>$ was about 680

mg/L when fully mixed by the simultaneous operation of two pumps. With only

pumping capacity of 1900 L/hr after stopping another pump, $<C_{ADV}>$ gradually

decreased and then reached approximately 320 mg/L at the elapsed time of 8 hr. The

turbulent diffusive flux, $\langle w'C' \rangle$, was calculated by the average of products of two

components (i.e., w' and C') during every 5-min time window. Overall, $\langle w'C' \rangle$ also

gradually decreased with time (Fig. 2-7b). It is noticed that most data of $\langle w'C' \rangle$ were

positive, but some occasionally became negative. Due to a random chance, the

instantaneous product of w' and C' before time averaging can be instantaneously

positive or negative. Either (1) $-w'$ and $+C'$ or (2) $+w'$ and $-C'$ can create the

negative sign of product. This is exactly the same as the Reynolds averaging

approach used to calculate a momentum flux, $\langle u'w' \rangle$. Both u' and w' can

instantaneously be positive and negative, but the time average of the product of these

two terms will have a consistent sign indicating the direction of flux. In the ideal

settling condition, therefore, the time-averaged value (i.e., $\langle w'C' \rangle$) should be positive

in order to represent the upward flux direction. Depending on the applied turbulent

conditions, however, about 10-30% of total flux data were negative. By increasing

the time span for averaging, the number of negative signs can be reduced to a certain

degree, but not totally eliminated. Although the negative data are included in data

34

processing, their absolute values are much smaller than positive data (see Fig. 2-7b), and thus, ADV-derived w_s ($w_{s\text{-ADV}}$) might not be significantly influenced by the negative sign of $\langle w'C' \rangle$.

Among several settling experiments conducted in this study (see Table 2-1), the selected plots of $\langle C \rangle$ versus $\langle w'C' \rangle$ were given for Clay Bank sediment (Fig. 2-8). Owing to the non-linear regression (Maa and Kwon, 2007), w_s can be expressed as a function of SSC. All data sets showed the increase in w_s with increasing SSC. It was commonly found that the data are quite noisy. Main reason of data scattering might be due to the simplified analytical assumptions (i.e., steady state and no horizontal gradient of SSC) in Eq. 2-1. Another possible reason is associated with the dependence of backscattered signal on the particle size. Provided that the suspended sediment is composed of multi-class particles and their size distribution significantly changes with time, ADV mainly detect the coarser and denser component of insonified materials. Even though the backscattered signals can be produced by the fine-grained component in suspension, their contribution is relatively small in the total scattered amount (see Fig. 2-3). This different response can influence on the accuracy of C' and $\langle C \rangle$ by overestimation or underestimation. Therefore, it is feasible that ADV approach may yield the noisy data, in the condition that SSC and grain size is highly changing during the measurement.

In order to enhance the correlation coefficient, Scully (2005) only selected the positive $\langle w'C' \rangle$ for analysis. He further grouped the noisy ADV data into several bins with an equal increment of $\langle C \rangle$, and then, the median of each bin was used to

determine w_s. It was revealed that w_s estimated from binned data is nearly close to w_s derived from non-binned data, and that the correlation was highly improved. Hence, this approach might be one of alternatives to partially solve the scatterance of data.

To reveal the effect of SSC on w_s, the regression equations for $w_{s\text{-ADV}}$ were compared with other studies (Fig. 2-9). Because the tested SSC was in the range of about 200-700 mg/L, the estimated equations for $w_{s\text{-ADV}}$ were only valid in this range. For the given range of SSC, $w_{s\text{-ADV}}$ is approximately 1-3 orders larger than w_s measured by the Owen Tube (Kwon, 2005). This higher w_s is due to the effect of ambient turbulence which was blocked in Owen Tube (Maa and Kwon, 2007). It is noted that sediments used in Owen Tube method is not exactly same with that used in ADV method due to the different sediment preparation, even though they were collected at the same site. If the equations for $w_{s\text{-ADV}}$ were extended to the much lower SSC (see Fig. 2-9), the expected $w_{s\text{-ADV}}$ is roughly on the same order of earlier measured w_s in Clay Bank area (w_s= 0.7-1.6 mm/s; Scully, 2005).

It was found that turbulence would contribute to the increase of w_s within a limited range, whereas w_s would decrease if it exceeded this range. With the available data, w_s was the highest when TKE is 0.69 kg m^{-1}s^{-2} except for SSC < 240 mg/L. It is noticeable that the w_s measured at the still water condition is about 10 times smaller than the w_s measured at the turbulent condition, even under the same SSC (see two solid lines in Fig. 2-9). This difference is primarily related to the more frequent collision of suspended particles which results in forming larger flocs. The number of collision is governed mainly by the turbulent shear (Winterwerp, 2002). Therefore, it is the turbulence that primarily controls the formation of flocs and their

properties (e.g., size and density). Turbulence plays two opposite roles in promoting

the growth of flocs and limiting their size (Whitehouse et al., 2000). At low

turbulences, the floc size may be in a growth phase, i.e., the floc size increases with

turbulence intensity, due to the increased frequency of collision between the particles

(Fennessy et al., 1994). However, as the turbulence intensity reaches an upper limit

when the length scale of the smallest turbulent eddies (i.e., Kolmogorov microscale)

is roughly on the same order of the floc diameter, the flocs will be broken, so that

turbulence can limit the floc size and the corresponding w_s (van Leussen, 1997).

In high SSCs, w_s is mostly higher than 10 mm/s (see Fig. 2-9). In particular,

w_s increased up to approximately 60 mm/s, when SSC is 0.7 g/L and TKE is 0.69 kg

$m^{-1}s^{-2}$. These values are is too high for w_s of mud flocs, considering the previous

works (Kwon, 2005; Scully, 2005). It is the coarser and denser components (i.e.,

sand) of Clay Bank sediment (see Fig. 2-2a), therefore, that caused w_s to increase at

high SSC. At the beginning of measurement, the grain size distribution in water

column is almost uniform due to a fully mixing condition. Since the coarser and

denser particles settled rapidly settled, the size of particles (or flocs) became smaller

as time elapsed. Also, the stronger signal by sand is dominant at high SSC, because

ADV with a single frequency is more sensitive to the coarser materials than fine-

grained particles. As a result, the larger size and strong acoustic response might

cause a fast w_s in high SSC range.

Following the approach given in Fugate and Friedrichs (2002), the relative

importance of local concentration change term ($\frac{\partial C}{\partial t}$) and settling term ($w_s \frac{\partial C}{\partial z}$) in

sediment continuity equation was evaluated (Fig. 2-10). $\frac{\partial C}{\partial t}$ was estimated by the difference in C_{ADV} at every 5 min interval. Instead of using a constant value of w_s as in Fugate and Friedrichs (2002), the w_s that is a function of $<C_{ADV}>$ was used here. The vertical gradient of SSC, $\frac{\partial C}{\partial z}$, was determined with the discrete data of water sample-derived SSCs at 10 and 110 cm above the tank bottom. Because the water samples were not taken at every 5 minute, the interpolated data of $\frac{\partial C}{\partial z}$ with 5-min interval were used for comparison. Fig. 2-10 reflects that the settling term was 2-3 orders of magnitude larger than the local concentration change. The change of SSC and velocity in the lateral direction is negligibly small due to the limited lateral dimension of tank. Also, since only one point ADV data is available, the lateral advection cannot be computed. In this study, therefore, the advection term (i.e., $\frac{\partial(uC)}{\partial x}$) in Eq. 2-1 was not compared with settling term. Based on the above results and previous works, the w_s at a given height above bed, as the first order, can be approximated by a balance between upward turbulent diffusive flux and downward settling flux.

4. Conclusions

ADV backscatter strength can be used as a proxy to convert into the SSC within limited ranges of SSC if the suspicious gain setting problem can be confirmed. The 5-MHz ADVOcean has an operational range up to 1 and 4 g/L for Clay Bank sediment and kaolinite, respectively. For the higher SSC, ADV signals were

saturated or decrease with increasing SSC. This response should be noticed when measuring the high-concentration suspension near the bed. Backscattered signals would be sometimes too noisy to address the instantaneous changes of SSC due to high amplification setting, high sampling rate (e.g., > 10 Hz), and small sampling volume. A moving averaging was used to effectively reduce the undesirable noises. For the better response to cohesive sediments, furthermore, one has to select an ADV with an optimal frequency depending on in-situ sediment properties. Precaution should be taken when a measuring site has a significant change of grain size distribution with time. This is because the backscattered signal strength is primarily controlled by both the acoustic wavelength (i.e., frequency) and the sediment properties (i.e., particle size, flocculation status and floc structure).

Using a balance between the turbulent diffusion flux and settling flux, ADV can reveal the effect of SSC and turbulence on w_s. Compared with a still condition, the measurement of w_s with Clay Bank sediment showed that turbulence can increase w_s, up to one order larger when it is lower than a limit (TKE=0.69 kg m^{-1}s^{-2}). When the turbulence is higher than this limit, however, w_s becomes decreasing with the further increase of TKE. In conclusion, ADV is a potential tool to simultaneously estimate SSC and w_s in turbulent dominant environment without interfering with ambient flows.

References

D&A Instrument Inc., 2001. OBS-3A manual, 37 pp.

Deines, K.L., 1999. Backscatter estimation using broadband acoustic Doppler current
profilers, IEEE 6th Working Conference on Current Measurement, San Diego,
pp. 249-253.

Downing, J., 2006. Twenty-five years with OBS sensors: the good, the bad, and the
ugly. Continental Shelf Research 26, 2299-2318.

Eisma, D., Dyer, K.R., van Leussen, W., 1997. The in-situ determination of the
settling velocities of suspended fine-grained sediment- a review. In: N. Burt,
R. Parker and J. Watts (Editors), Cohesive Sediment. John Wiley and Sons, pp.
17-44.

Fennessy, M.J., Dyer, K.R., Huntley, D.A., 1994. INNSEV: An instrument to
measure the size and settling velocity of flocs in situ. Marine Geology 117,
107-117.

Fugate, D.C., Friedrichs, C.T., 2002. Determining concentration and fall velocity of
estuarine particle populations using ADV, OBS and LISST. Continental Shelf
Research 22, 1867-1886.

Fugate, D.C., Friedrichs, C.T., 2003. Controls on suspended aggregate size in
partially mixed estuaries. Estuarine, Coastal and Shelf Science 58, 389-404.

Gratiot, N., Mory, M., Auchere, D., 2000. An acoustic Doppler velocimeter (ADV)
for the characterisation of turbulence in concentrated fluid mud. Continental
Shelf Research 20, 1551-1567.

Kawanisi, K., Shiozaki, R., 2008. Turbulence effects on settling veolcity of

suspended sediment. J. Hydraulic Engineering 134(2), 261-266.

Kawanisi, K., Yokosi, S., 1997. Characteristics of suspended sediment and turbulence

in a tidal boundary layer. Continental Shelf Research 17(8), 859-875.

Kineke, G.C., Sternberg, R.W., 1992. Measurements of high concentration suspended

sediments using the optical backscatterance sensor. Marine Geology 108, 253-

258.

Kwon, J.-I., 2005. Simulation of turbidity maximums in the York River, Virginia,

Ph.D. Thesis, College of William and Mary, 127 pp.

Lee, T.H., Hanes, D.H., 1995. Direct inversion method to measure the concentration

profile of suspended particles using backscattered sound. J. of Geophysical

Research 100(C2), 2649-2657.

Maa, J.P.-Y., Kwon, J.-I., 2007. Using ADV for cohesive sediment settling velocity

measurements. Estuarine, Coastal and Shelf Science 73, 351-354.

Maa, J.P.-Y., Kim, S.-C., 2002. A constant erosion rate model for fine sediment in the

York River, Virginia. Environmental Fluid Mechanics 1, 345-360.

Mantovanelli, A., Ridd, P.V., 2006. Devices to measure settling velocities of cohesive

sediment aggregates: a review of the in situ technology. J. of Sea Research

56(3), 199-226.

Merckelbach, L.M., Ridderinkhof, H., 2006. Estimating suspended sediment

concentration using backscatterance from an acoustic Doppler profiling

current meter at a site with strong tidal currents. Ocean Dynamics 56, 153-168.

Scully, M.E., 2005. The interaction between stratification, circulation, and sediment transport in a partially-mixed estuary. Ph.D. Thesis, College of William and Mary, 148 pp.

Shi, Z., Ren, L.F., Zhang, S.Y., Chen, J.Y., 1997. Acoustic imaging of cohesive sediment resuspension and re-entrainment in the Changjiang Estuary, East China Sea. Geo-Marine Letter 17, 162-168.

SonTek, 1997. SonTek Doppler current meters-using signal strength data to monitor suspended sediment concentration, SonTek/YSI Inc., 7 pp.

SonTek, 2006. ADVField Acoustic Doppler Velocimeter-technical documentation, SonTek/YSI Inc.

Thorne, P.D., Hanes, D.M., 2002. A review of acoustic measurement of small-scale sediment processes. Continental Shelf Research 22(4), 603-632.

Thosteson, E.D., Hanes, D.H., 1998. A simplified method for determining sediment size and concentration from multiple frequency acoustic backscatter measurements. J, of Acoust. Soc. Am. 104(2), 820-830.

van Leussen, W., 1997. The Kolmogorov microscale as a limiting value for the floc sizes of suspended fine-grained sediments in estuaries, In: N. Burt, R. Parker and J. Watts (Editors), Cohesive Sediment. John Wiley and Sons, pp. 45-62.

Vincent, C.E., Hanes, D.M., Bowen, A.J., 1991. Acoustic measurements of suspended sand on the shoreface and the control of concentration by bed roughness. Marine Geology 96(1-2), 1-18.

Voulgaris, G., Meyers, S.T., 2004. Temporal variability of hydrodynamics, sediment

concentration and sediment settling velocity in a tidal creek. Continental Shelf

Research 24, 1659-1683.

Whitehouse, R., Soulsby, R.L., Roberts, W., Mitchener, H., 2000. Dynamics of

estuarine muds: a manual for practical applications. Thomas Telford, 232 pp.

Winterwerp, J.C., 2002. On the flocculation and settling velocity of estuary mud.

Continental Shelf Research 22, 1339-1360.

Table 2-1. Experimental conditions for measuring settling velocity.

Experiment	Pump rate* (L hr^{-1})	Adaptor type	Pump level (above bottom)	Pumping direction (toward)	Temperature ($^\circ$C)	Mean TKE (kg m^{-1}s^{-2})
CB1121	0	n/a	n/a	n/a	21.4	0.002
CB0727	0	n/a	n/a	n/a	26.7	0.004
CB1129	1900	L-shape	5 cm	Bottom	23.2	0.69
CB1128	1900	T-shape	5 cm	Sidewall	23.5	0.76
CB0831	1900	L-shape	30 cm	Bottom	24.8	0.98
CB0830	1900	T-shape	30 cm	Sidewall	25.1	1.31
CB0809	5700	Straight	0 cm	Sidewall	27.0	1.48

*provided by manufacturer
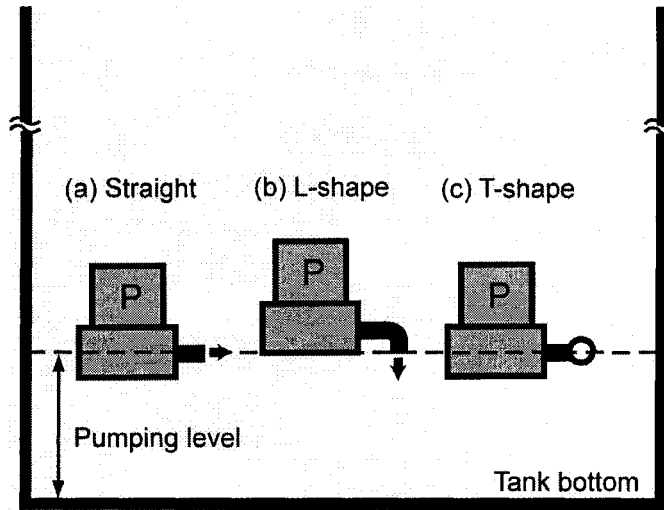
Fig. 2-1. Pumping conditions with a different adaptor. The arrow indicates the pumping direction. The pumping direction of T-shape is perpendicular to this paper.
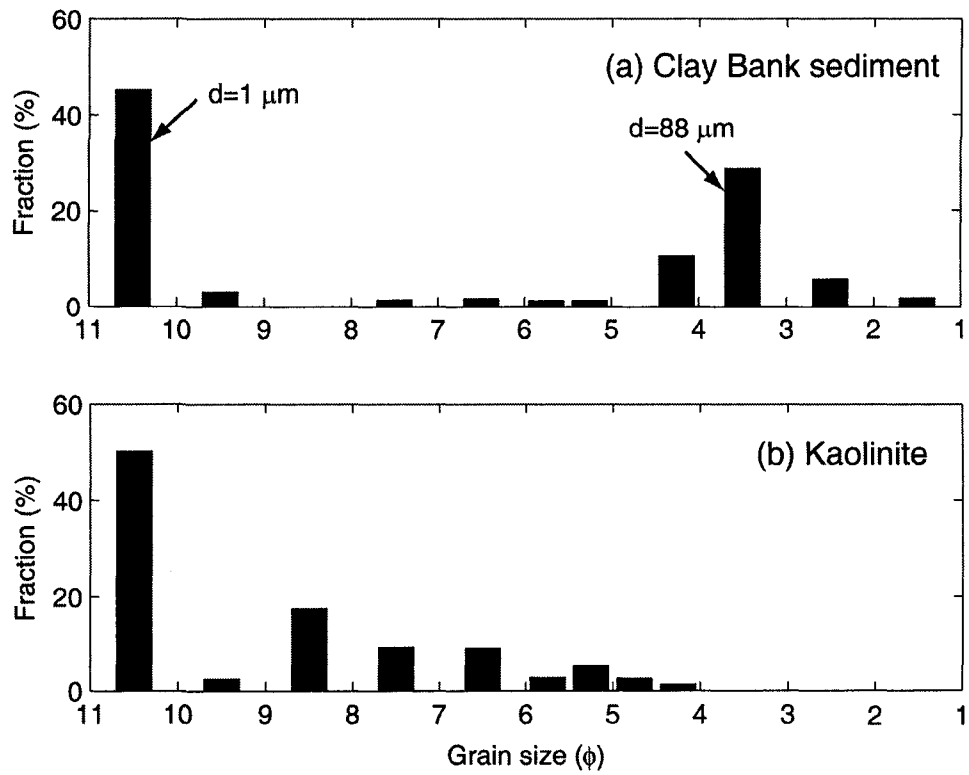
Fig. 2-2. Grain size distribution of used sediments: (a) Clay Bank sediment and (b) kaolinite.
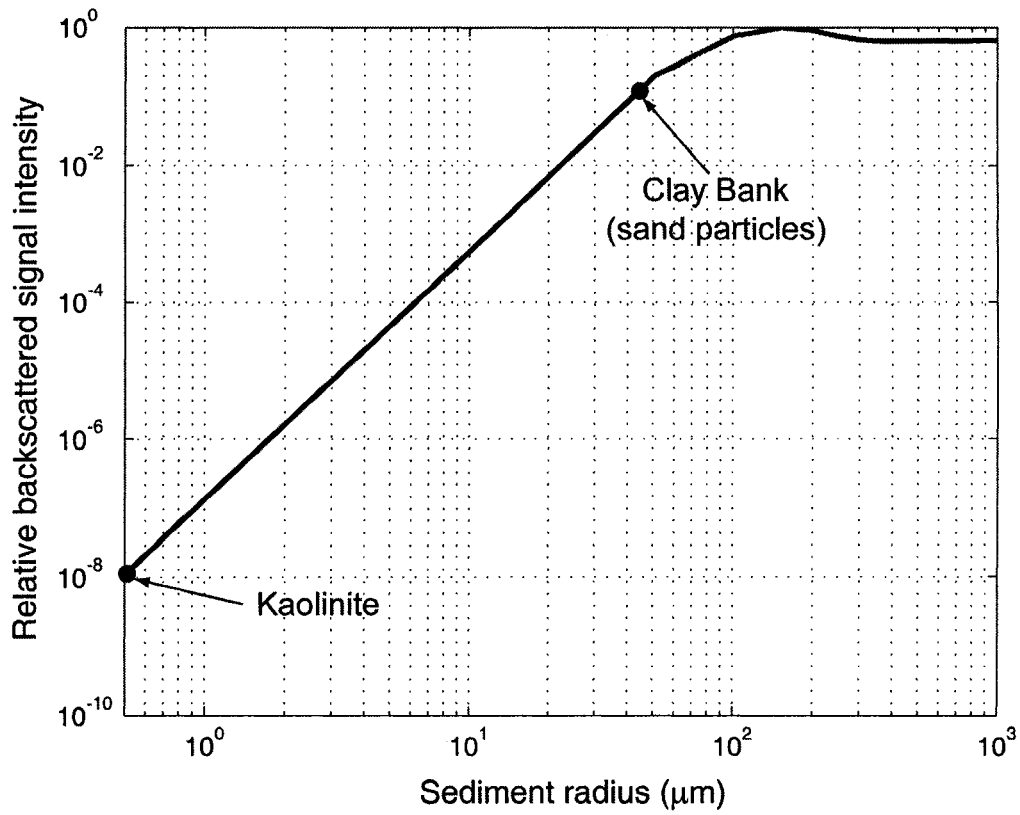
Fig. 2-3. Relative backscattered acoustic intensity expected at the frequency of 5
MHz, assuming that the particle is a rigid sphere.
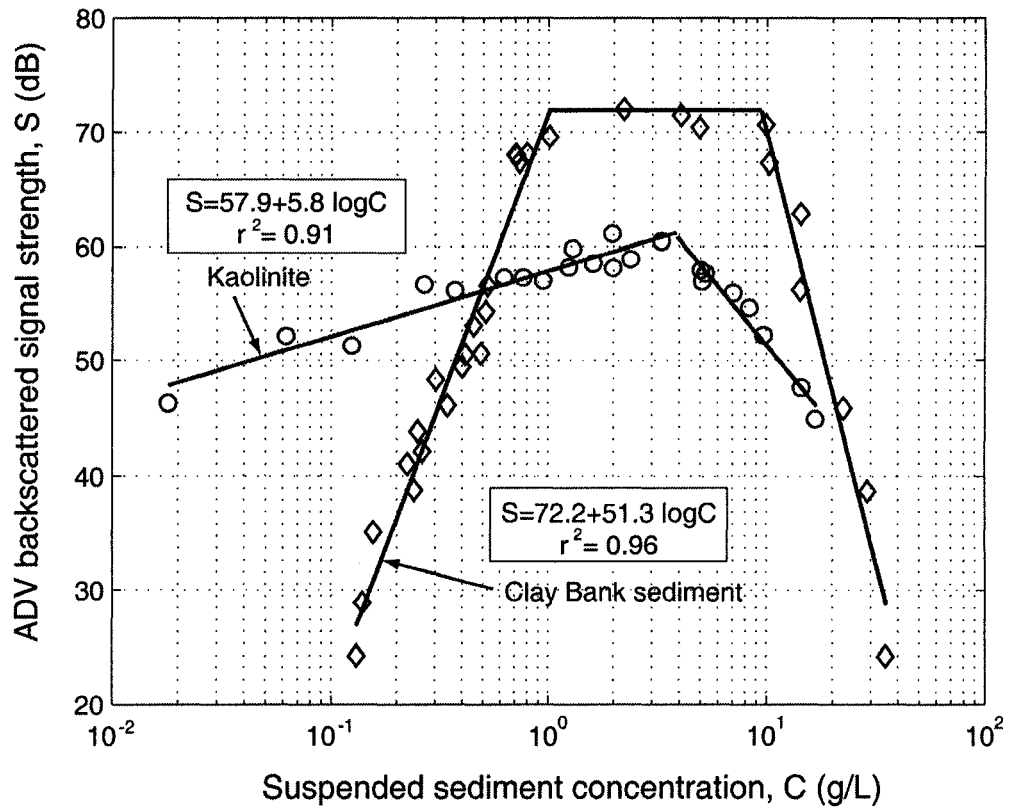
Fig. 2-4. Averaged backscatter strength of the 5-MHz ADVOcean for suspended
kaolinite and Clay Bank sediment in tap water. The regression equations for
the low suspended sediment concentration are marked with r^2 values.
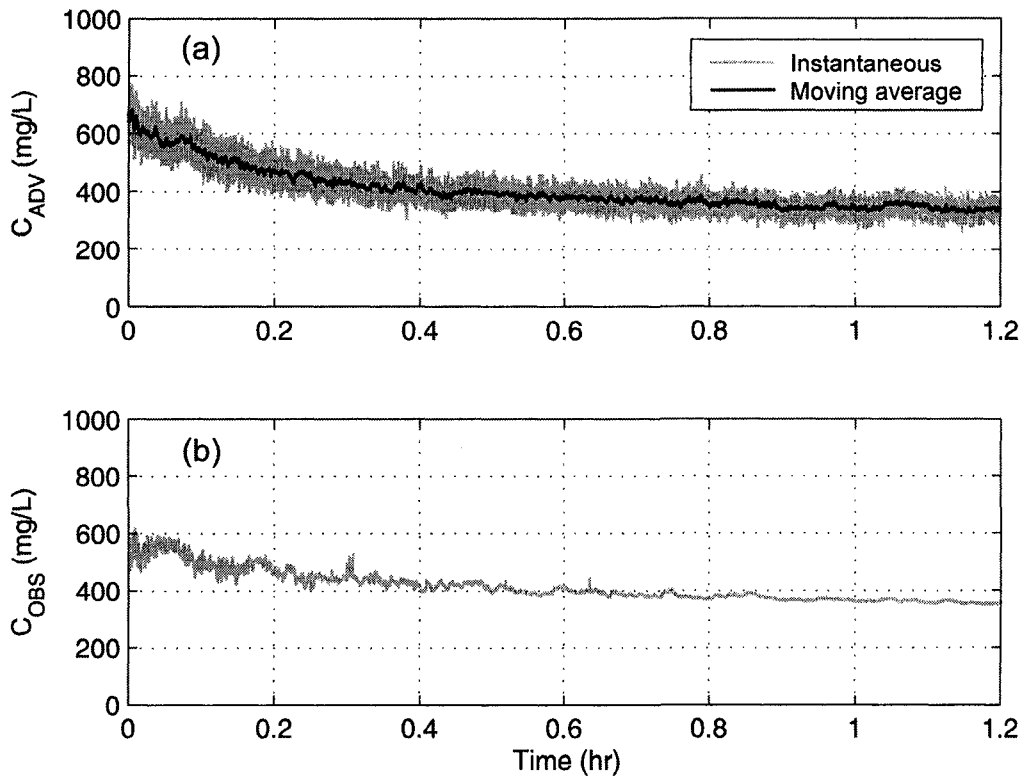
Fig. 2-5. SSC changes of Clay Bank sediment during the settling measurement: (a) ADV-derived SSC and (b) OBS-derived SSC. The gray line is the change of instantaneous SSC at the sampling rate of 10 Hz. The black line represents the moving average of adjacent 40 data points.
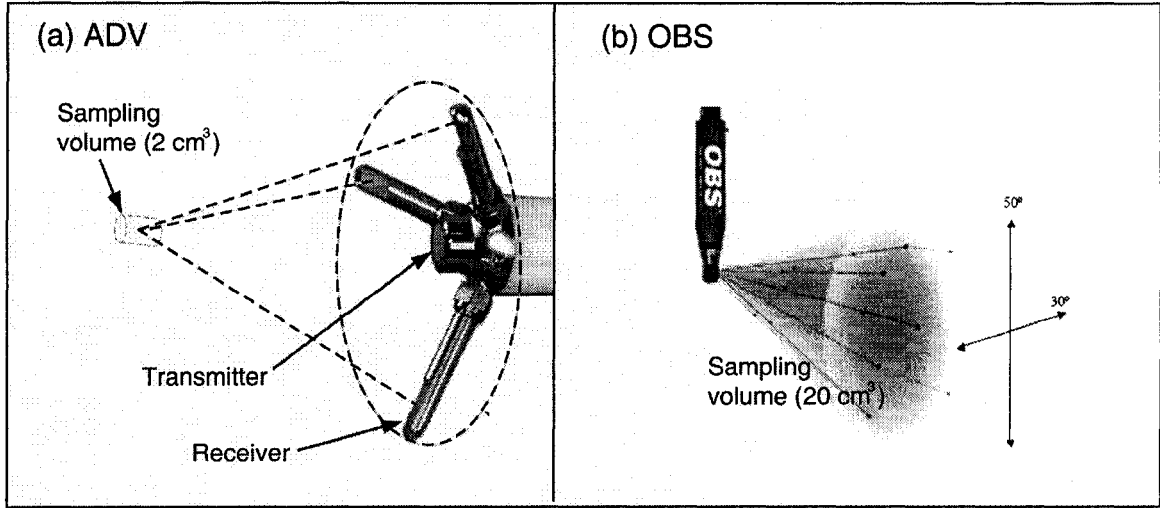
Fig. 2-6. Difference in sampling volume of ADV and OBS (SonTek, 2006; D&A
Instrument, 2001).
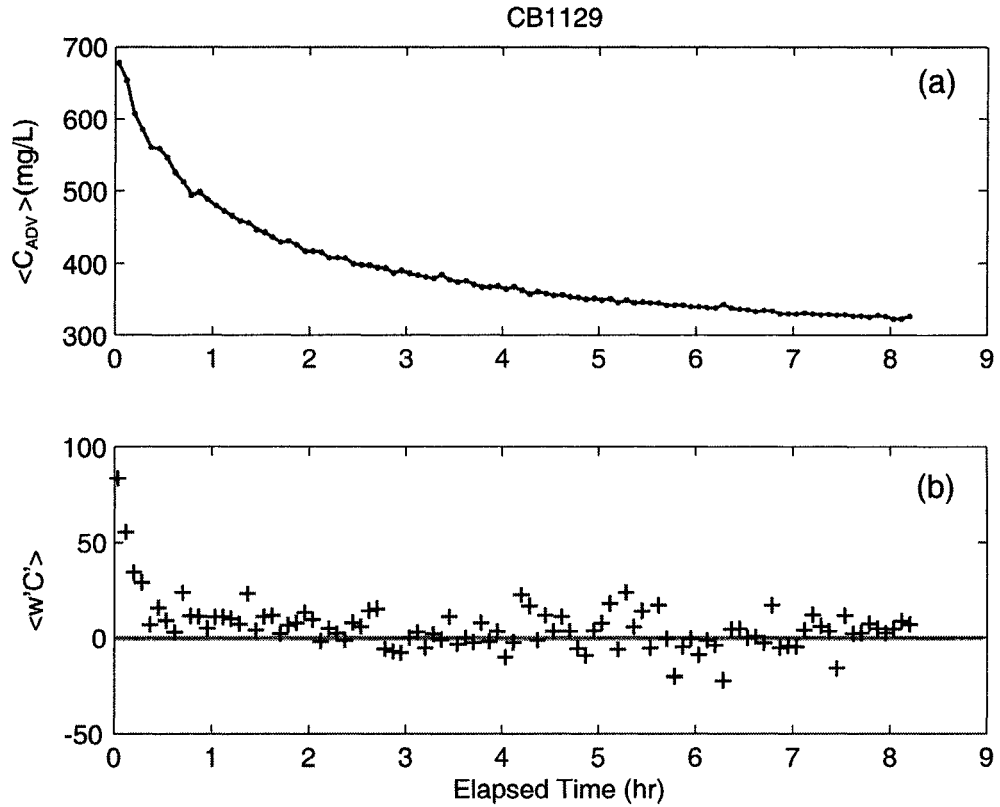
Fig. 2-7. Variations of 5-min averaged suspended sediment concentration ($<C_{ADV}>$) and the turbulent diffusive flux ($\langle w'C' \rangle$). For detail experimental conditions, see CB1129 in Table 2-1.
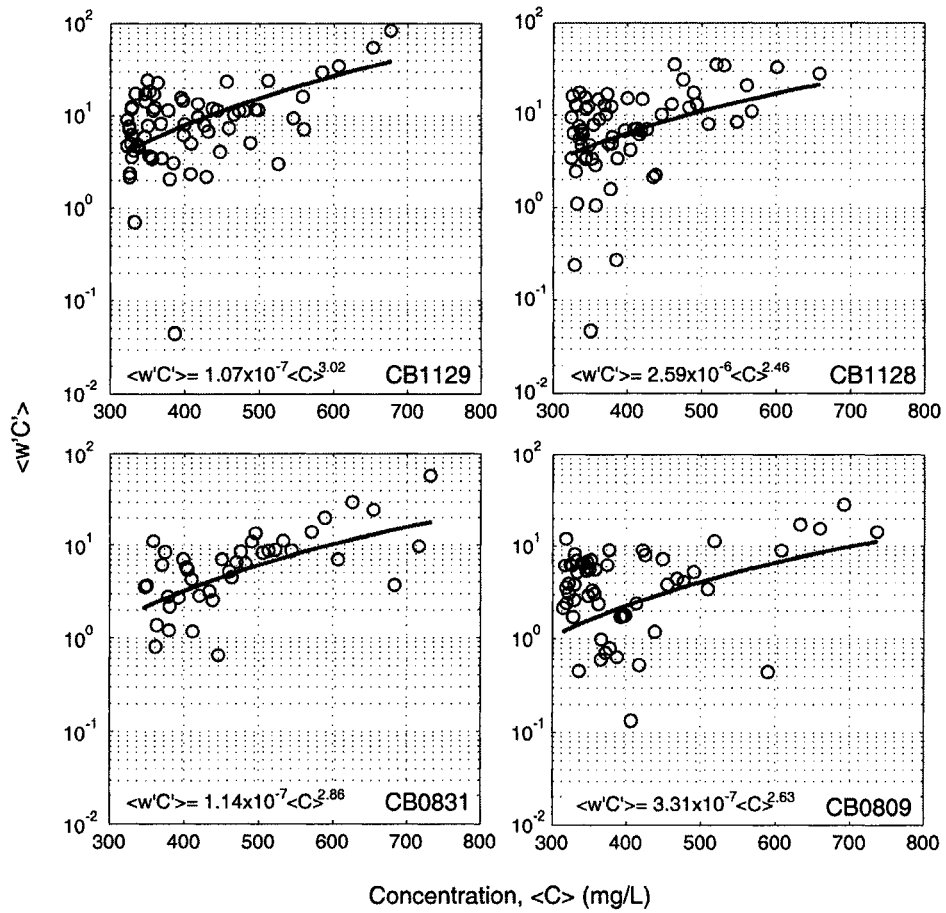
Fig. 2-8. Non-linear relationship between $\langle w'C' \rangle$ and $\langle C \rangle$ for estimating settling velocity. The solid lines indicate the best-fit regression equations. Detail experimental conditions were given in Table 2-1.
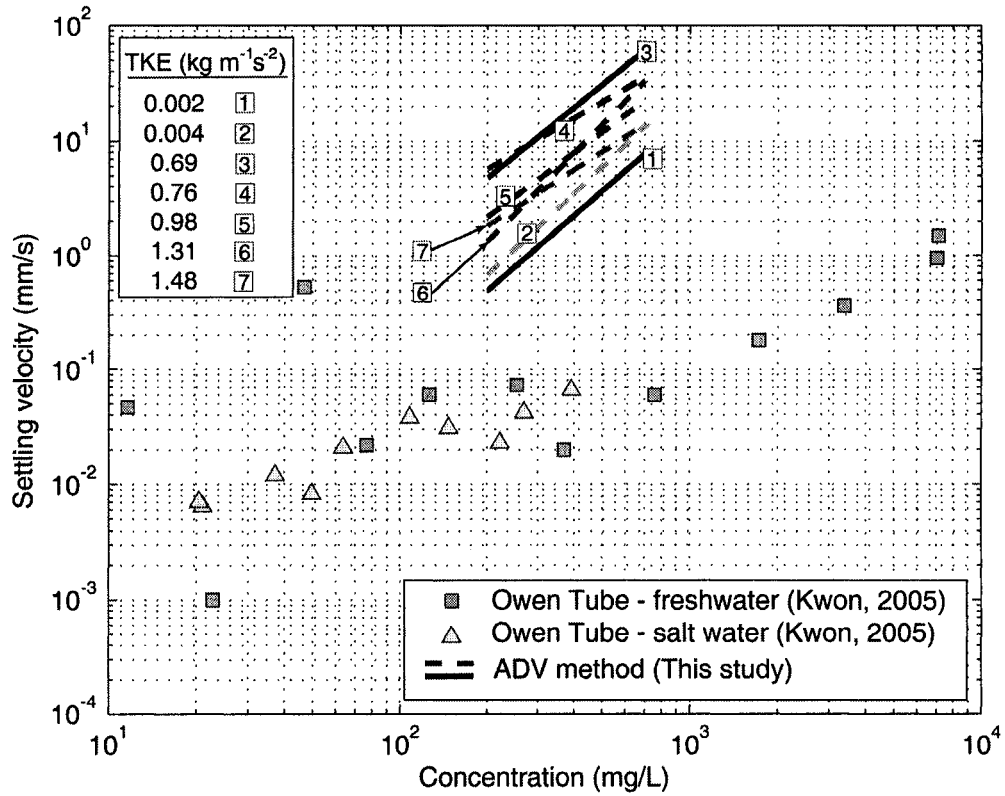
Fig. 2-9. Effects of SSC and turbulence on settling velocity of Clay Bank sediment. Two solid lines represent the maximum and minimum settling velocities.
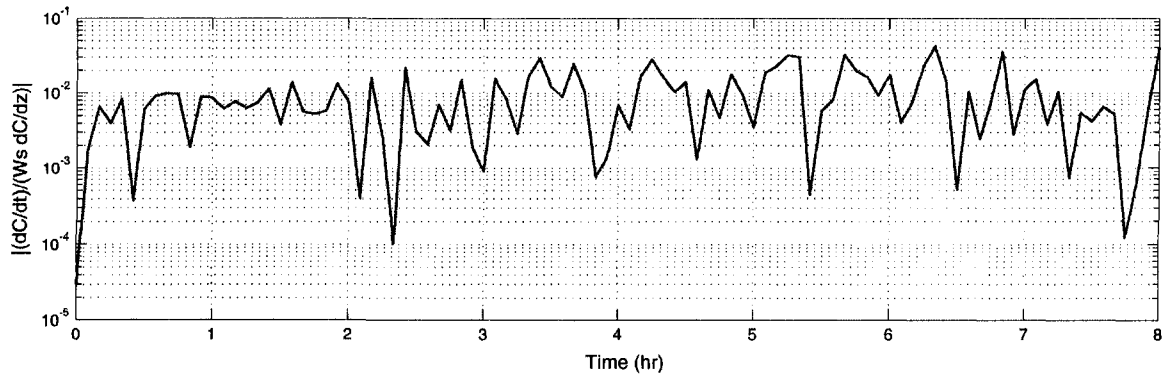
Fig. 2-10. Comparison between local concentration change term and downward settling term.

**CHAPTER III. MEASUREMENT OF SUSPENDED SEDIMENT
CONCENTRATION PROFILE USING A PULSE COHERENT
ACOUSTIC DOPPLER PROFILER (PC-ADP)**

Abstract

Pulse Coherent Acoustic Doppler Profiler (PC-ADP) was originally developed to measure the near-bed velocity profiles with high spatial resolution, but it also records the profile of backscattered signal. This study investigated the capability of using a PC-ADP to estimate the Suspended Sediment Concentration (SSC) profiles. The sound attenuation by sediment was included in the signal inversion algorithm because of its significance in the near-bed layer. Two sediments used in the experiment showed quite different responses. Clay Bank sediment with mixture of clay and very fine sand has a higher correlation coefficient (r^2=0.92) between range-corrected volume scattering (SSC_v) and PC-ADP signal level within a limited SSC range (ca. <10 g/L). On the other hand, pure kaolinite clay has a much smaller range of SSC for linear correlation. This different response might be attributed to the fact that the acoustic response is primarily controlled by the SSC and particle size in suspension at a given frequency. The laboratory measurements for Clay Bank sediment showed that the SSC profile derived from PC-ADP has a good agreement with sample- and OBS-derived outcomes. Therefore, PC-ADP might be a potential instrument to reveal the high-resolution (about 1.6 cm) SSC profiles near the bed, if the sediment is sufficiently large.

Keywords: PC-ADP, acoustic, backscatter, cohesive sediment, suspended sediment concentration

1. Introduction

Accurate measurement of Suspended Sediment Concentration (SSC) is an important task in understanding sediment dynamics in the coastal and estuarine environments. During last few decades, considerable efforts have been dedicated to develop the measuring techniques and increase the data accuracy (see Wren et al., 2000 for review). As a representative method, the optical measurement has been evolved and widely used to estimate the SSC (e.g., Sternberg et al., 1986; Downing and Beach, 1989; Kineke and Sternberg, 1992; Sutherland et al., 2000; Downing, 2006). Even though the optical method can be easily calibrated and widely acceptable, its measurement is restricted to a fixed single point. Deployment of multi-sensors can enhance the spatial resolution of profile. Too many probes, however, may disturb the structure of turbulent flow as well as the distribution of suspended solids, when applied to the vicinity of sediment bed. These drawbacks consistently shed new light on the acoustic measuring system as an alternative method for estimating SSC profile in various studies (e.g., Vincent et al., 1991; Holdaway et al., 1999; Shi et al., 1999; Thorne and Hanes, 2002).

Recent advances in high-frequency acoustic technology opened a new dimension to understand the suspended sediment transport processes by overcoming the shortcomings of other conventional measurement methods. As a non-intrusive method, the acoustic instruments have been used as a reliable tool for obtaining the SSC for the laboratory and field measurements (e.g., Hanes et al., 1988; Lee and Hanes, 1995; Admiraal and Garcia, 2000; Thorne and Hanes, 2002; Mouraenko, 2004; Betteridge et al., 2008). In the commercial market, the Acoustic Backscatter Sensor (ABS) with multi-frequency transducers is available for measurement of SSC profile and particle size (Smerdon,

1996). When one needs the turbulence information, however, an extra current profiler should be deployed within the measuring range. In order to meet the demand on the concurrent measurement of SSC and flow velocity, conventional acoustic Doppler current profilers (ADCPs) with pulse-to-pulse incoherent mode have been widely used (e.g., Land et al., 1997; Gartner and Cheng, 2001; Hill et al., 2003). However, the previous works with ADCPs were not able to accurately address the near-bed SSC profile because the incoherent single pulse profilers were generally used to measure the changes within the entire water column (10-100 m) with a low spatial resolution. In signal analysis, the sound attenuation by suspended matters was not generally taken into account because it is negligibly small in the upper water column where SSC is relatively low (ca. < 0.1 g/L). As a complementary for measuring near-bed sediment behaviors, Pulse Coherent Acoustic Doppler Profiler (PC-ADP) has emerged with the high-resolution profiling capability. Even though its primary function is to provide a time series of velocity profiles, the strength of acoustic backscattered signals might be a proxy to address the SSC profiles near the sediment bed. In this aspect, PC-ADP has a merit to simultaneously monitor the turbulent processes and suspended sediment behaviors without disturbance of flow and sediment distribution. Despite these prospective features, few studies have reported the performance of PC-ADP for measurement of SSC (e.g., SonTek, 1997).

In this study, therefore, the capability of using a 1.5-MHz PC-ADP for the above mentioned objective was investigated with two different types of sediments. The detail calibration procedure in the laboratory was described, and the uncertainties embedded in the measurement and the signal processing were discussed.

2. Acoustic inversion

Since the acoustic technique is an indirect method, the measured backscattered signals should be calibrated to convert into SSC. To correctly compensate the range- and SSC-dependent acoustic signal strength, one of the important tasks in calibration is to consider the sound attenuation by water-sediment mixture along the insonified path. Thus, the following sections describe the determination of sound attenuation coefficient and the basis of acoustic inversion algorithm for estimating SSC profiles.

2.1. Sound attenuation coefficient

Sound intensity would be attenuated exponentially with distance from the source transducer. The attenuation coefficient is a function of many parameters such as temperature, pressure, salinity, frequency and the concentration, mineralogy and shape of suspended sediments as well as the presence of air bubbles (Richards et al., 1996). The total attenuation coefficient (α_t) is considered as a sum of the attenuation by water (α_w) and by suspended sediments (α_s).

$$\alpha_t = \alpha_w + \alpha_s \qquad (3\text{-}1)$$

Firstly, α_w was expressed by Fisher and Simmons (1977) as

$$\alpha_w = \left(10\log e^2\right)\left(\frac{A_1 P_1 f_1 f^2}{f_1^2 + f^2} + \frac{A_2 P_2 f_2 f^2}{f_2^2 + f^2} + A_3 P_3 f^2\right) \qquad (3\text{-}2)$$

where $10\log e^2$ transfers [Neper/m] to [dB/m], f is the frequency (Hz), the subscripts 1 and 2 represent boric acid and magnesium sulfate relaxation process, respectively. The subscript 3 represents the absorption from pure water.

Boric acid component in sea water:

$$A_1 = \frac{8.68}{c}10^{(0.78pH-5)}$$

$$P_1 = 1 \qquad\qquad (3\text{-}2a)$$

$$f_1 = 2.8\sqrt{\frac{S}{35}}10^{[4-1245/(273+T)]}$$

Magnesium sulfate component in sea water:

$$A_2 = 21.44\frac{S}{c}(1+0.025T)$$

$$P_2 = 1 - 1.37\times10^{-4}z + 6.2\times10^{-9}z^2 \qquad\qquad (3\text{-}2b)$$

$$f_2 = \frac{8.17\times10^{[8-1990/(273+T)]}}{1+0.0018(S-35)}$$

Pure water component:

$$A_3 = 4.937\times10^{-4} - 2.59\times10^{-5}T + 9.11\times10^{-7}T^2 - 1.50\times10^{-8}T^3 \qquad \text{for } T \le 20°C$$

$$A_3 = 3.964\times10^{-4} - 1.146\times10^{-5}T + 1.45\times10^{-7}T^2 - 6.5\times10^{-10}T^3 \qquad \text{for } T > 20°C \qquad (3\text{-}2c)$$

$$P_3 = 1 - 3.83\times10 - 5z + 4.9\times10^{-10}z^2$$

where pH is alkalinity of seawater, T is temperature (°C), S is salinity (psu), z is depth (m), and c is sound speed (m/s). Fig. 3-1 shows the variation of sound attenuation by water in a wide range of frequency. As the frequency increases, α_w would accordingly increase, and its gap between the sea water and fresh water would decrease. At 1.5 MHz which is the operational frequency of the PC-ADP, in particular, α_w in sea water is very close to that in fresh water if the contribution by salinity is negligible.

Secondly, α_s can be determined by the SSC in the range (R) between the sensor and sensing area as well as two absorption components: scattering (ξ_s) and viscous absorption (ξ_v) (Richards et al., 1996).

60

$$\alpha_s = \frac{1}{R} \int_0^R (\xi_v + \xi_s) SSC(r) \, dr \qquad (3\text{-}3)$$

where $\xi_v = \left(10 \log e^2\right)\left(\dfrac{k(\sigma-1)^2}{2}\left[\dfrac{s}{s^2+(\sigma+\delta)^2}\right]\right)$,

$$\xi_s = \frac{3}{4\langle a_s \rangle \rho_s} \langle \chi \rangle,$$

$$\delta = \frac{1}{2}\left[1 + \frac{9}{2\beta \langle a_s \rangle}\right],$$

$$s = \frac{9}{4\beta \langle a_s \rangle}\left[1 + \frac{1}{\beta \langle a_s \rangle}\right],$$

$$\sigma = \frac{\rho_s}{\rho_0},$$

$$\beta = \left(\frac{\pi f}{\nu}\right)^{1/2},$$

$$\langle \chi \rangle = \frac{4 k_\alpha x^4}{3\left[1 + x^2 + \dfrac{4}{3} k_\alpha x^4\right]},$$

$\langle a_s \rangle$ is mean radius of sediment particles, ρ_s is sediment density, ρ_0 is water density, f is

frequency of acoustic waves, ν is kinematic viscosity of water, $\langle \chi \rangle$ is the normalized

total scattering cross-section, $x = k a_s$, and k_α is a constant (~0.18) (Thorne et al., 1991).

The sediment scattering portion is dominant for larger particles, while the viscous

absorption becomes important for fine-grained (< 90 μm) sediment particles (Fig. 3-2b).

The peak of α_s occurs at around 2 μm when the frequency is set to 1.5 MHz. When

calculating the total sound attenuation for 1.5 MHz acoustic waves, α_s becomes larger

than α_w if the median grain size (d_{50}) is about 2 μm and the SSC is higher than about 0.2

g/L (Fig. 3-2c). When the SSC is higher than 1 g/L, α_s is about 5.4 times greater than

α_w.

2.2. Acoustic backscattering theory

The backscattered signal strength is mainly dependent on the setups of selected

acoustic system and the conditions of suspended sediment. The former includes the

acoustic wave frequency, transmit power, sensor sensitivity and other system settings.

They are usually known by a manufacture or can be fixed during the measurement. On

the other hand, the latter is mainly associated with the concentration, size and type of

suspended sediment particles. The physical parameters of water such as temperature and

salinity also have some secondary effects. Although it is theoretically possible to

determine the system-related parameters through a laboratory calibration or manufacture'

specification, it is still questionable whether all of them might be still applied for any

measuring condition where sediment-related variables are different. Also, the absolute

calibration of system parameters is a difficult task requiring the specific instruments and

facility. It is generally acknowledged, therefore, that the SSC can be obtained by

calibrating the relative acoustic signal intensity using sample sediments from a

deployment site (Thorne and Hanes, 2002).

For the practical application of acoustic Doppler velocity profiler (ADCP), Deines

(1999) simplified the sonar equation to estimate the SSC profile,

$$S_v = K_c(E - E_r) + 20\log(R) + 2\alpha_w R - 10\log(PL) - 10\log(P) + C \qquad (3\text{-}4)$$

where $S_v = 10\log(SSC)$ is volume scattering strength (dB), E is echo level (count), E_r is received noise level (count), R is range (m) between transducer and measurement volume, α_w is sound attenuation coefficient by water (dB/m), PL is transmit pulse length (m), P is transmit power (watt), K_c and C are calibration constants.

In Eq. 3-4, it is noted that only contribution by water is considered for sound attenuation. For low SSC (ca. < 0.01 g/L), the sound attenuation by suspended particles can be negligibly small compared with that by water (see Fig. 3-2c), such that this equation can be used for signal conversion to SSC. However, biased results can be introduced when SSC is high (ca. > 0.5 g/L) enough to significantly attenuate the signal strength along the sound pathway. For that reason, the contribution of sound attenuation by suspended sediments is included to yield more realistic SSC profile, especially when SSC is high, as follows:

$$S_v = K_c(E - E_r) + 20\log(R) + 2(\alpha_w + \alpha_s)R - 10\log(PL) - 10\log(P) + C \qquad (3\text{-}5)$$

Because E_r, PL, P and C are fixed during the experiment, a new calibration coefficient (C') can be made by combining all of them, and Eq. 3-5 is more simplified as given below

$$SSC_v = K_c E + C' \qquad (3\text{-}6)$$

where $SSC_v = 10\log(SSC) - 20\log(R) - 2(\alpha_w + \alpha_s)R$, the net volume scattering corrected by subtracting the sound spreading and attenuation in the sensing range.

If the SSCs at several levels were measured simultaneously with acoustic profiling, two calibration constants (i.e., K_c and C') can be determined by linear regression (Deines, 1999; Kim and Voulgaris, 2003; Traykovski et al., 2007). For the calibration in laboratory, using the mixing chamber which can generate a homogeneous suspension is a

common approach (e.g., Thorne et al., 1991; Mouraenko, 2004). In the plot of E versus

SSC_v, the slope of a linear regression equation is K_c, and y-intercept is C'. By

rearranging Eq. 3-6, the SSC at i-th cell can be expressed by

$$SSC_{[i]} = 10^{\left[\frac{K_c E_{[i]} + C' + 20\log(R_{[i]}) + 2(\alpha_{w_{[i]}} + \alpha_{s_{[i]}})R_{[i]}}{10}\right]} \qquad (3-7)$$

The main problem in this equation is that $\alpha_{s_{[i]}}$ is also a function of $SSC_{[i]}$, such that it is

impossible to directly estimate the entire profile. To solve this problem, $\alpha_{s_{[i]}} R_{[i]}$ in the

right hand side of Eq. 3-7 can be expressed as the following form (see Fig. 3-3),

$$\alpha_{s_{[i]}} R_{[i]} = \alpha_{s_{[i-1]}} R_{[i-1]} + \xi_{[i-1]} \frac{R_{[i]} - R_{[i-1]}}{2} SSC_{[i-1]} + \xi_{[i]} \frac{R_{[i]} - R_{[i-1]}}{2} SSC_{[i]} \qquad (3-8)$$

where ξ_i is a sum of scattering and viscous absorption at i-th cell (see Eq. 3-3). By

assuming that the gradient of SSC between $R_{[i-1]}$ and $R_{[i]}$ is not significant, $SSC_{[i]}$ can be

replaced with $SSC_{[i-1]}$. Since the cell size of PC-ADP is on the order of several

centimeters, this assumption is acceptable for a practical application. Thus, Eq. 3-8 is

simplified as

$$\alpha_{s_{[i]}} R_{[i]} = \alpha_{s_{[i-1]}} R_{[i-1]} + \xi_{[i-1]} \left(R_{[i]} - R_{[i-1]}\right) SSC_{[i-1]} \qquad (3-9)$$

The calculation of SSC commences in the first cell by assuming $\alpha_s = 0$. Using the

iterative calculation with known calibration coefficients, $SSC_{[i]}$ and $\alpha_{s_{[i]}}$ can be

sequentially calculated by moving to the next cells (Lee and Hanes, 1995; Thorne and

Hanes, 2002).

3. Materials and methods

3.1. Instrumentation

A 1.5-MHz PC-ADP produced by SonTek was used to measure the SSC profiles using acoustic backscattered signals. Three transducers with a diameter of 2 cm are equally spaced at 120° relative azimuth angles, and each one is a monostatic system that the same transducer acts as transmitter and receiver. The slant angle of transducer is about 15° off the vertical axis and the beam spreading angle is around 1.85° between -3 dB points. The minimum cell height is about 1.6 cm, and an optimal sensing range is around 1-2 m which is proper for the measurement of bottom boundary layer. The ping rate is governed by the size and number of cells. For example, under the calibration setup in this study that the size and number of cells are 1.6 cm and 40 cells, respectively, the ping rate is about 15 pings per second (SonTek, 2001). In the pulse-coherent mode, two pulses are transmitted with a time lag. Instead of using the Doppler shift of return signal under the pulse-incoherent mode, the phase change between a pair of pulses was used to measure the velocity (SonTek, 2001). This operation mechanism makes it possible to provide the profiles with much higher accuracy.

For the calibration of backscattered signals, a mixing chamber (Fig. 3-4) housed in the VIMS was used. It is made of Plexiglas and the bottom part is designed as a funnel shape for preventing the sediment from settling on the bottom. A circulation pump in the outside of chamber is connected to the end of funnel, and pumps the water-sediment mixture through four PVC pipes (I.D.= 1.9 cm) back to the upper level of the chamber in order to accomplish a fully mixed suspension with nearly constant SSC and grain size distribution. Six sampling ports (see Fig. 3-4) exist with the interval of 10 cm to

65

withdraw water samples for calculating the ground truth SSC for signal calibration. For the purpose of checking the homogeneity of the mixture in the calibration chamber, the sample-derived SSCs (SSC_{SAM}) at different ranges were compared. Fig. 3-5 shows the ratio of individual SSC_{SAM} to range-averaged SSC (between 0.16 and 18.89 g/L). Because most individual samples were generally within about ±5-15% of mean SSC, it was concluded that the suspension in the chamber is nearly homogenous within the measurement errors.

3.2. Calibration procedures

Before starting the measurement, the mixing chamber was filled with tap water and left for 1 day to be stabilized in the room temperature, allowing air bubble to escape from the chamber. While a circulation pump was continuously running to make a homogenous suspension, sediment slurry was added to the chamber until a predetermined SSC is reached. To correct the slant angle (15°) of transducer, the mount frame was purposely tilted to make the beam axis normal to the chamber base. Thus, only a single transducer beam can be calibrated at every measurement. This artificial tilting caused the beams transmitted by the other two transducers to hit the sidewall of chamber, which may contaminate return signals of calibrated transducer. By checking the values of signal array after blocking the unused transducers, it was confirmed that their effects were not significant to disturb the true data. The mean acoustic profile was produced by ensemble-averaging a number of pings recorded for 2-min measurement. After finishing an acoustic profiling and sampling at the pre-determined SSC, the additional water-sediment mixture was added for next measurements.

For different SSCs, several samples were taken by protruding the PVC tube connected to a sampling port into the interior of chamber (see Fig. 3-4). The withdrawn samples were vacuum filtered through pre-weighted glass fiber filters with a pore size of 0.7 μm, if the SSC of a sample is low (ca. < 1 g/L). If the SSC is high (ca. > 1 g/L), then a pre-weighted aluminum pan was used to avoid a clogging problem in filtration. The residue on filter (or the sample in aluminum pan) was oven dried at 103-105 °C for 24 hrs, and then weighted for determining the SSC.

3.3. Sediments

Two types of sediments were used: (1) bottom sediment collected in Clay Bank area, the York River, and (2) commercially available kaolinite. Clay Bank sediment shows a bimodal distribution. The first (ca. 1 μm) and the second mode (ca. 88 μm) are found in the clay and very find sand range, respectively (Fig. 3-6a). Organic content is about 6.1%. The clay minerals are composed of mainly Illite (75%) and the rest is rather uniformly distributed as Kaolinite, Chlorite and Smectite (ca. 8% each) (Maa and Kim, 2002). In contrast, kaolinite shows a unimodal distribution (Fig. 3-6b) that major component is less than 10ϕ. The mode is about 1 μm.

4. Results and discussions

4.1. Calibration of PC-ADP

For the calibration, the SSC in the mixing chamber varied in the range of 0.16-18.89 g/L for Clay Bank sediment and 0.07-34.63 g/L for kaolinite. Fig. 3-7 shows the PC-ADP responses with Clay Bank sediment. The presented data were calculated from

the SSCs measured at the second (R=19 cm) to the sixth (R=59 cm) sampling port and echo levels in their corresponding cells. It is noted that y-axis value of SSC_v is the corrected volume scattering strength (see Eq. 3-6) by subtracting the spreading loss and the sound attenuation by sediment and water. The acoustic responses of Clay Bank sediment can be divided into two groups based on SSC. The first group (0.16-9.43 g/L) showed a good linear relationship between SSC_v and echo level (r^2= 0.92). Using a linear regression, the slope (K_c) and y-intercept (C') are determined as 0.70 and -70.83, respectively. When SSC was about 9.43 g/L, the echo level reached the signal saturation level of 142 counts, which represents the maximum output for selected sediment. On the other hand, the second group (12.68-18.89 g/L, see the filled circles in Fig. 3-7) showed a much smaller range of SSC for linear response. In the individual regression equation, the highest echo level corresponds to the measurement at the closest sampling port (R=19 cm) from the transducer, whereas the lowest echo level represents the measurement at R=59 cm. In this group, the echo level at a fixed range decreased with increasing SSC due to more sound attenuation by suspended particles. Also, it was observed that SSC_v increased but K_c slightly decreased with the increase of SSC (see the dashed lines in Fig. 3-7). This indicates that the volume scattering term (i.e., S_v=10log(SSC)) is larger than the sum of spreading loss and sound attenuation term (see Eq. 3-6), but the increment of S_v becomes smaller than that of total sound loss while SSC was increasing.

Kaolinite showed a quite different response (Fig. 3-8). The responses indicate a very small range of SSC within which the echo level is linearly proportional to SSC_v. It is not possible to define a unified calibration equation. SSC_v gradually increased with the increase of SSC. The signal saturation level was observed around 105 counts, which is

68

much lower than that of Clay Bank sediment. Due to this earlier saturation, the increment of echo level was not as much as Clay Bank sediment while SSC was increasing. For kaolinite, as a result, PC-ADP is not a good device for measuring SSC profile.

The salient difference in acoustic responses of two sediments might be explained by the concept of form factor describing the scattering properties of the insonified particle (Thorne and Hanes, 2002). This is primarily determined by the value of "ka" where k ($=2\pi f/c$, where f is acoustic wave frequency and c is sound speed in water) is the wave number and a is the particle radius. The peak of acoustic response occurs when the circumference of particle (assuming a spherical shape) is equal to the acoustic wavelength (i.e., $ka=1$), and the backscattering signal amplitude is proportional to $(ka)^2$ in Rayleigh scattering regime ($ka<<1$) where the grain size is much smaller than the sound wavelength. Also, the acoustic intensity is proportional to $(ka)^2$. The values of ka for kaolinite and very fine sand portion of Clay Bank sediment are approximately 0.003 and 0.3, respectively, assuming that c is about 1500 m/s. As a result, the PC-ADP's signal intensity of kaolinite (a=0.5 μm) is expected to be about eight orders of magnitude less than that of very fine sand (a=44 μm) of Clay Bank sediment (Fig. 3-9). This implies that the size of kaolinite is too small to be effectively detected by the system, and thus the performance of PC-ADP with kaolinite is not warranted. If the operational frequency is doubled, the detectable particle radius can be half of that at 1.5 MHz. However, the tradeoff between the frequency and SSC-dependent sound attenuation should be considered to get an optimal output.

4.2. Profiling experiment

Based on the calibration results for Clay Bank sediment (see Fig. 3-7), the capability of PC-ADP to estimate the SSC profile was tested in another settling tank (diameter: 0.75 m, height: 1.5 m). After stirring up the water-sediment mixture, the pumps stopped to allow suspended sediments to settle. The tilted PC-ADP pointing downward recorded the profile of backscattered signals at every 10 sec. The cell thickness was set to 4.7 cm. Fig. 3-10a demonstrates the time series of SSC profiles calculated by the inversion algorithm described in Section 2.2. Discrete data in each profile were interpolated to smooth data. As the time elapsed, the suspended sediments were settled downward, and thus, the SSC gradually decreased. Due to the blanking zone, the first cell starts at the range of 15 cm. The strongest echo near the range of 120 cm was generated by the tank bottom. In the field measurement, the maximum level of echo signal can be interpreted as the echo from the sediment bed. For instance, the footprint radius of PC-ADP's main lobe will be about 3.2 cm (=2 m*tan(1.85°/2)), if the deployed elevation is 2 m. Therefore, it is also possible to address the temporal changes of local bed level induced by erosion and deposition of bottom sediments with the resolution of cell size.

To verify the PC-ADP-derived SSC (SSC_{PC-ADP}) profile, the SSC_{SAM} outcomes at the selected times were also marked in Fig. 3-10b. While the coarser and denser materials were suspended, the good correlation between SSC_{PC-ADP} and SSC_{SAM} was found. As they rapidly settle, however, the calibration became worse. This is because the signal strength is more affected by coarser material rather than fine particle when the multi-class sediments are mixed.

For another comparison, Optical Backscattering Sensor (OBS) was installed at the range of 38.5 cm which corresponds to the 5th cell of deployed PC-ADP. 2-min averaged data were shown in Fig. 3-11. In general, the SSC_{PC-ADP} has a reasonable correlation with OBS-derived SSC (SSC_{OBS}) (r^2=0.90). When the SSC is higher than about 0.14 g/L, it was observed that SSC_{PC-ADP} is slightly higher than SSC_{OBS}. This overestimate can be explained by the acoustic backscattering strength which is a function of the size of particles (or flocs). In the early settling stage (i.e., SSC>0.14 g/L), the size of particles (or flocs) at the measured elevation is relatively larger than that in the later times. Thus, the larger size contributes to the increase in the PC-ADP's signal strength.

4.3. Uncertainty in acoustic inversion of PC-ADP

The inverting process from the acoustic signal to SSC using a simplified sonar equation has inherent limitations and uncertainty in measurement and data analysis, which were discussed as follows.

First, in the signal inversion algorithm, it was assumed that the size distribution of suspended sediments both temporally and spatially remains constant. For the practical application, a single value of particle size was used to calculate the sound attenuation coefficient and SSC for all profiling cells. This calculation, however, may produce a biased result when applying to the field site where sediment grain size distribution is known to continuously change in time and space. Therefore, it is necessary to know the spatial and temporal variations of particle size to interpret correctly, if they vary significantly. In addition, the single frequency of PC-ADP cannot differentiate between the changes in SSC and those in particle size distribution, such that a change in grain size

71

can be interpreted as a change in SSC. The above uncertainty related the particle size

may restrict the accuracy of PC-ADP and other acoustic devices with a single frequency.

This problem, however, can be partly solved by employing the multiple frequencies (Hay

and Sheng, 1992; Smerdon, 1996).

Second, unlike the non-cohesive sediment behavior, the flocculation or

deflocculation of cohesive sediments can change the size of flocs. To date, the question

on whether the acoustic response is mainly governed by the size and shape of floc as a

whole or those of its primary particles has not been clearly answered. Based on ADV

responses, Fugate and Friedrichs (2002) stated that the acoustic backscatter is relatively

insensitive to floc size changes, compared with optical device, and that the size and shape

of constituent grains are more important contributors rather than those of flocs. In the

context of acoustic backscatter, their findings are valid when the binding of flocs is loose

enough for acoustic signal to detect individual primary particles. If the flocs are

composed of the firmly-bound components, the acoustic signal may consider a floc as a

single grain. In this case, the backscattered signal is strongly dependent on the properties

of flocs. In general, the effective density (i.e., the difference between floc bulk density

and water density) of floc would decrease with the increase of floc size, because the

porosity of flocs will increase when higher order flocs are formed (van Leussen, 1988;

Manning and Dyer, 1999). Hence, a larger floc might have less chance to be detected as

a whole floc, if acoustic wavelength is short enough. To verify the acoustic response to

flocs, the coupling with other instrument (e.g., LISST) that can provide properties of

flocs is necessary, but this is beyond the scope of this study.

Third, the disadvantage of employed method is that the calibration constants and the knowledge of sediment grain size are required to determine SSC profile prior to the inversion procedure. Due to the positive feedback in the iteration algorithm, the results might be converged or diverged (Thorne and Hanes, 2002). Also, the solution is very sensitive to the sound attenuation coefficient (Eq. 3-7), because the equation includes an exponential term. Therefore, any error in this parameter may significantly influence on the accuracy of SSC profile.

Finally, there are several factors not present in the simplified sonar equation. Measurement errors may arise from the scattering of unwanted target such as air bubbles (Kinsler et al., 2000). As they have the high acoustic impedance, the strong scatter wave generated by air bubbles can be easily detected by the transducer. Unfortunately, it is impossible to quantitatively differentiate between suspended sediments and air bubbles in natural environments. Therefore, precaution should be taken to avoid the effect of air bubble when deploying this instrument.

5. Conclusions

The capability of 1.5-MHz PC-ADP to measure the SSC profile was assessed by comparing with SSCs measured by taking water samples. Within a limited SSC range, Clay Bank sediment with mixture of clay and very fine sand has the higher correlation coefficient (r^2=0.92) between SSC_v and PC-ADP signal level. On the other hand, the pure kaolinite clay shows a much smaller range of SSC within which the echo level is linearly proportional to SSC_v. These different responses might be attributed to the difference in the insonified grain size and the signal saturation level of selected sediments. It is noted

that the calibration result of Clay Bank sediment is based on the bed sediment sample, not the suspended sediment which may be much smaller.

The profiling performance in laboratory for Clay Bank sediment showed that SSC_{PC-ADP} has a good agreement with both SSC_{SAM} and SSC_{OBS} outcomes. This suggests that PC-ADP is a potential instrument to reveal the evolution of near-bed suspension, if sediment grain size is sufficiently large enough to be sensed, by visualizing the suspension event with comparable spatial resolution (down to 1.6 cm).

References

Admiraal, D.M., Garcia, M.H., 2000. Laboratory measurement of suspended sediment concentration using an Acoustic Concentration Profiler (ACP). Experiments in Fluids 28, 116-127.

Betteridge, K.F.E., Thorne, P.D., Cooke, R.D., 2008. Calibrating multi-frequency acoustic backscatter systems for studying near-bed suspended sediment transport processes. Continental Shelf Research 28(2), 227-235.

Deines, K.L., 1999. Backscatter estimation using broadband acoustic Doppler current profilers, IEEE 6th Working Conference on Current Measurement, San Diego, pp. 249-253.

Downing, J., 2006. Twenty-five years with OBS sensors: the good, the bad, and the ugly. Continental Shelf Research 26, 2299-2318.

Downing, J.P., Beach, R.A., 1989. Laboratory apparatus for calibrating optical suspended solids sensors. Marine Geology 86, 243-249.

Fisher, F.H., Simmons, V.P., 1977. Sound absorption in sea water. J. Acous. Soc. Am. 62(3), 558-564.

Fugate, D.C., Friedrichs, C.T., 2002. Determining concentration and fall velocity of estuarine particle populations using ADV, OBS and LISST. Continental Shelf Research 22, 1867-1886.

Gartner, J.W., Cheng, R.T., 2001. The promises and pitfalls of estimating total suspended solids based on backscatter intensity from acoustic Doppler current profiler, The

7th Federal Interagency Sedimentation Conference, Reno, Nevada, pp. III 119-126.

Hanes, D.H., Vincent, C.E., Huntley, D.A., Clarke, T.L., 1988. Acoustic measurements of suspended sand concentration in the C2S2 experiment at Stanhope Lane, Prince Edward Island. Marine Geology 81, 185-196.

Hay, A.E., Sheng, J., 1992. Vertical profiles of suspended sand concentration and size from multifrequency acoustic backscatter. J. Geophysical Research 97(C10),15661-15677.

Hill, D.C., Jones, S.E., Prandle, D., 2003. Derivation of sediment resuspension rates from acoustic backscatter time-series in tidal waters. Continental Shelf Research 23, 19-40.

Holdaway, G.P., Thorne, P.D., Flatt, D., Jones, S.E., Prandle, D., 1999. Comparison between ADCP and transmissometer measurements of suspended sediment concentration. Continental Shelf Research 19, 421-441.

Kim, Y.H., Voulgaris, G., 2003. Estimation of suspended sediment concentration in estuarine environments using acoustic backscatter from an ADCP, Coastal Sediments '03, CD-ROM published by World Scientific Corporation and East Meat West Production, Clearwater Beach, Florida.

Kineke, G.C., Sternberg, R.W., 1992. Measurements of high concentration suspended sediments using the optical backscatterance sensor. Marine Geology 108, 253-258.

Kinsler, L.E., Frey, A.R., Coppens, A.B., Sanders, J.V., 2000. Fundamentals of Acoustics. John Wiley & Sons, 548 pp.

Land, J.M., Kirby, R., Massey, J.B., 1997. Developments in the combined use of acoustic Doppler current profiler and profiling siltmeters for suspended solids monitoring. In: N. Burt, R. Parker and J. Watts (Editors), Cohesive Sediments, pp. 187-196.

Lee, T.H., Hanes, D.H., 1995. Direct inversion method to measure the concentration profile of suspended particles using backscattered sound. J. of Geophysical Research 100(C2), 2649-2657.

Maa, J.P.-Y., Kim, S.-C., 2002. A constant erosion rate model for fine sediment in the York River, Virginia. Environmental Fluid Mechanics 1, 345-360.

Manning, A.J., Dyer, K.R., 1999. A laboratory examination of floc characteristics with regard to turbulent shearing. Marine Geology 160(1-2), 147-170.

Mouraenko, O.A., 2004. Acoustic measurement techniques for suspended sediment and bedforms, Ph.D. dissertation, Univ. of Florida, 150 pp.

Richards, S.D., Heathershaw, A.D., Thorne, P.D., 1996. The effect of suspended particulate matter on sound attenuation in seawater. J. of Acoust. Soc. Am. 100(3), 1447-1450.

Shi, Z., Ren, L.F., Hamilton, L.J., 1999. Acoustic profiling of fine suspension concentration in the Changjiang Estuary. Estuaries 22(3A), 648-656.

Smerdon, A.M., 1996. Aquatec: AQ59:C-ABS System User manual, Aquatec Electronics LTD, Hartley Wintney, Hampshire, UK.

SonTek, 1997. SonTek Doppler current meters-using signal strength data to monitor suspended sediment concentration, 7 pp.

SonTek, 2001. PC-ADP Principles of Operation, San Diego, 12 pp.

Sternberg, R.W., Johnson, R.V., Cacchione, D.A., Drake, D.E., 1986. An instrument system for monitoring and sampling suspended sediment in the benthic boundary layer. Marine Geology 71,187-199.

Sutherland, T.F., Lane, P.M., Amos, C.L., Downing, J., 2000. The calibration of optical backscatter sensors for suspended sediment of varying darkness levels. Marine Geology 162, 587-597.

Thorne, P.D., Vincent, C.E., Hardcastle, P.J., Rehman, S., Pearson, N., 1991. Measuring suspended sediment concentrations using acoustic backscatter devices. Marine Geology 98(1), 7-16.

Thorne, P.D., Hanes, D.M., 2002. A review of acoustic measurement of small-scale sediment processes. Continental Shelf Research 22(4), 603-632.

Traykovski, P., Wiberg, P.L., Geyer, W.R., 2007. Observations and modeling of wave-supported sediment gravity flows on the Po prodelta and comparison to prior observations from the Eel shelf. Continental Shelf Research 27(3-4), 375-399.

van Leussen, W., 1988. Aggregation of particles, settling velocity of mud flocs: a review. In: J. Dronker and W. van Leussen (Editors), Physical Processes in Estuaries. Spriner-Verlag, pp. 347-403.

Vincent, C.E., Hanes, D.M., Bowen, A.J., 1991. Acoustic measurements of suspended sand on the shoreface and the control of concentration by bed roughness. Marine Geology 96(1-2), 1-18.

Wren, D.G., Barkdoll, B.D., Kuhnle, R.A., Derrow, R.W., 2000. Field techniques for suspended-sediment measurement. J. of Hydraulic Engineering 126, 97-104.
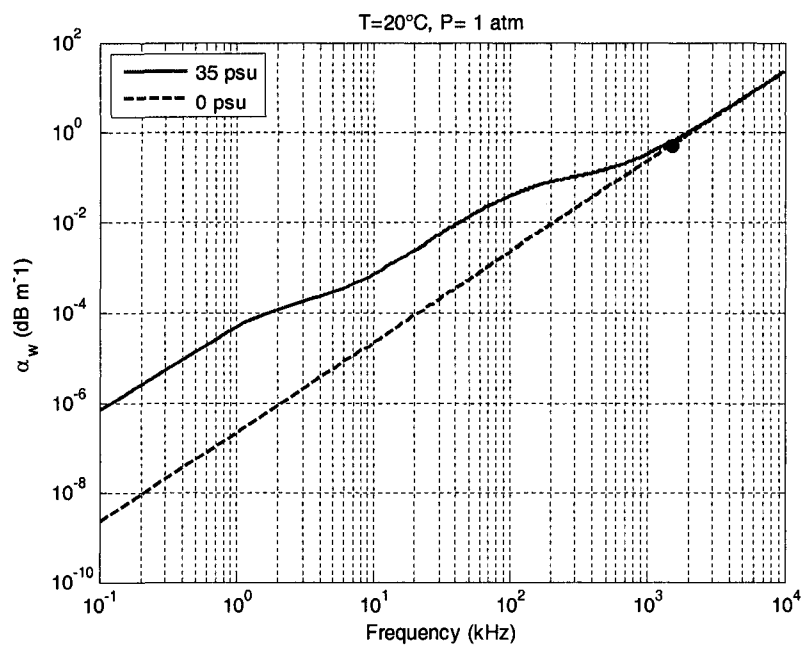
Fig. 3-1. Sound attenuation coefficient by seawater and freshwater under T= 20°C, P= 1 atm. The black dot represents the coefficient at 1.5 MHz (Fisher and Simmons, 1977).
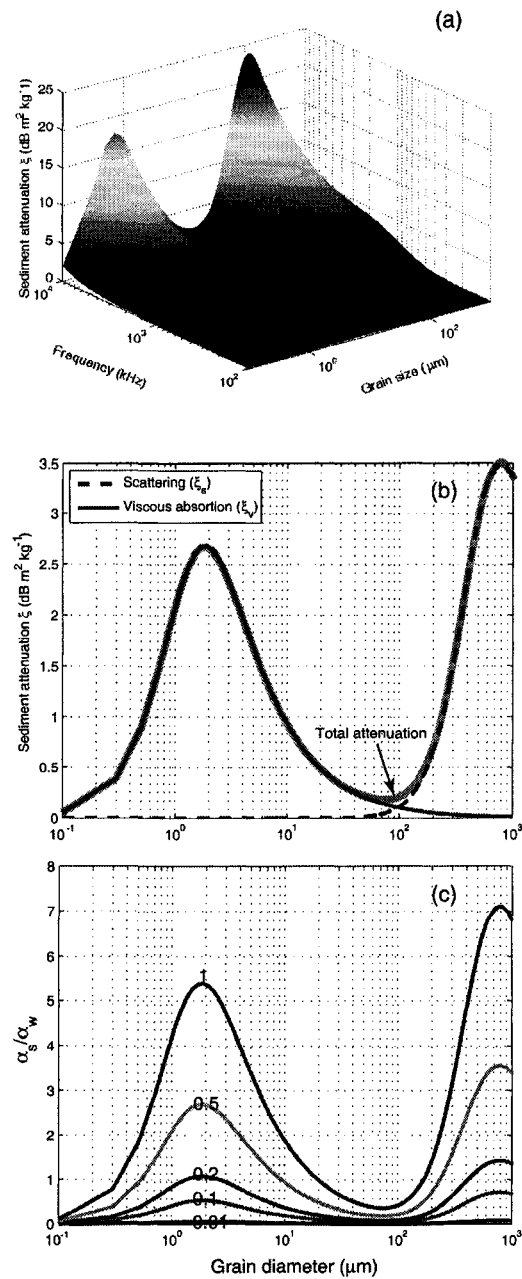
Fig. 3-2. (a) Total sound attenuation by viscous absorption and scattering of the suspended materials. The sound attenuation (in dB m^{-1}) can be calculated by multiplying the concentration and path length. (b) Partition of sound attenuation by sediment at 1.5 MHz: scattering and viscous absorption. (c) Ratio of sound attenuation by sediment to that by water at the various concentrations and grain sizes. Numbers indicate the suspended sediment concentration (in g/L).

80
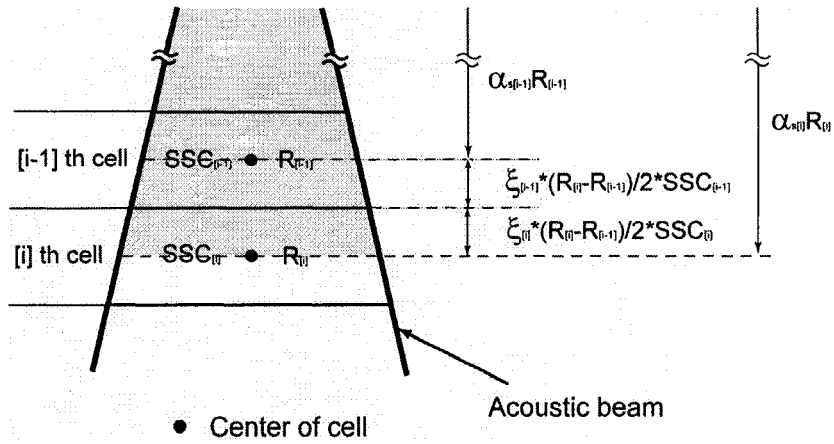
Fig. 3-3. Conceptual diagram for calculating the sound attenuation coefficient by sediment and SSC for individual cell using an iteration method.
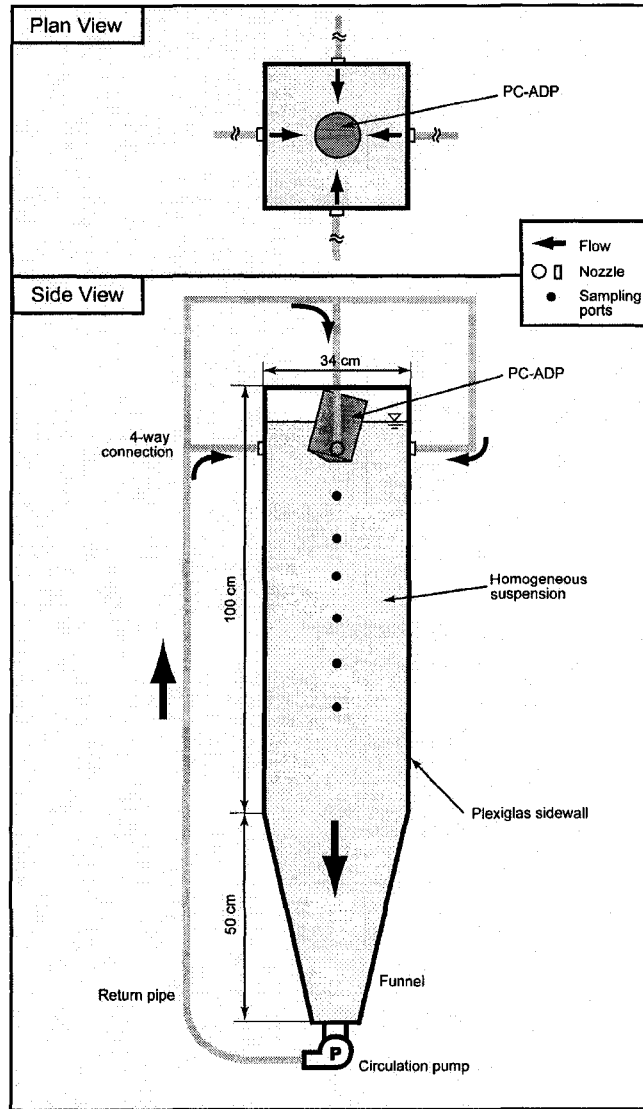
Fig. 3-4. Mixing chamber used for calibration. P represents the circulation pump for homogenous mixing.
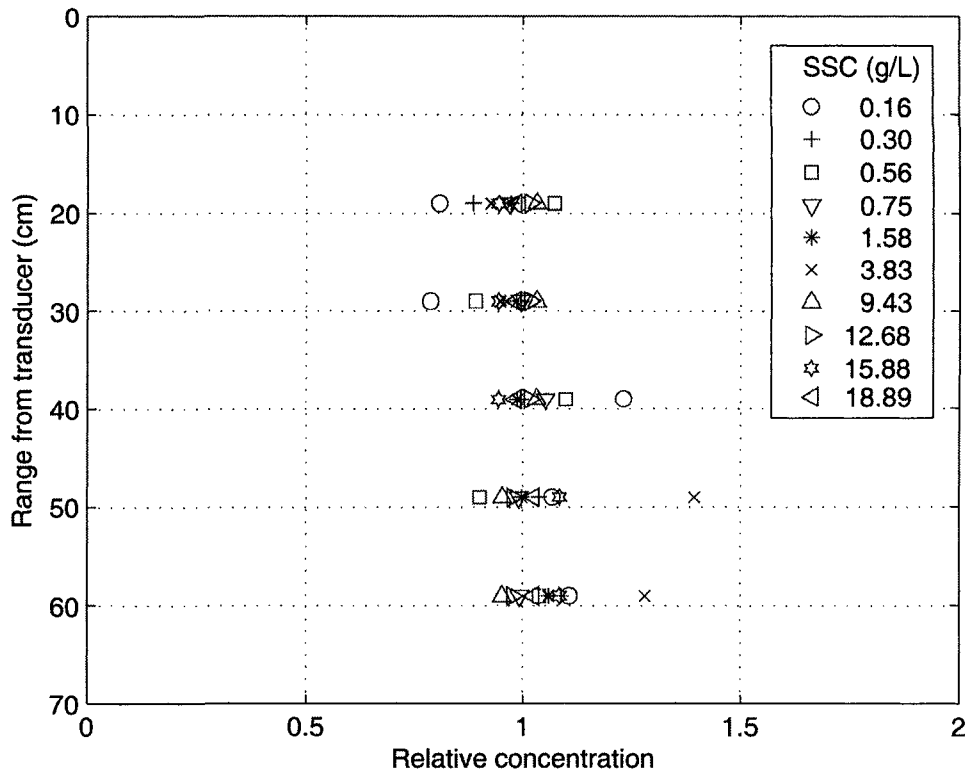
Fig. 3-5. Homogeneity in used mixing chamber. Relative concentration is the ratio of measured SSC to range-averaged SSC.
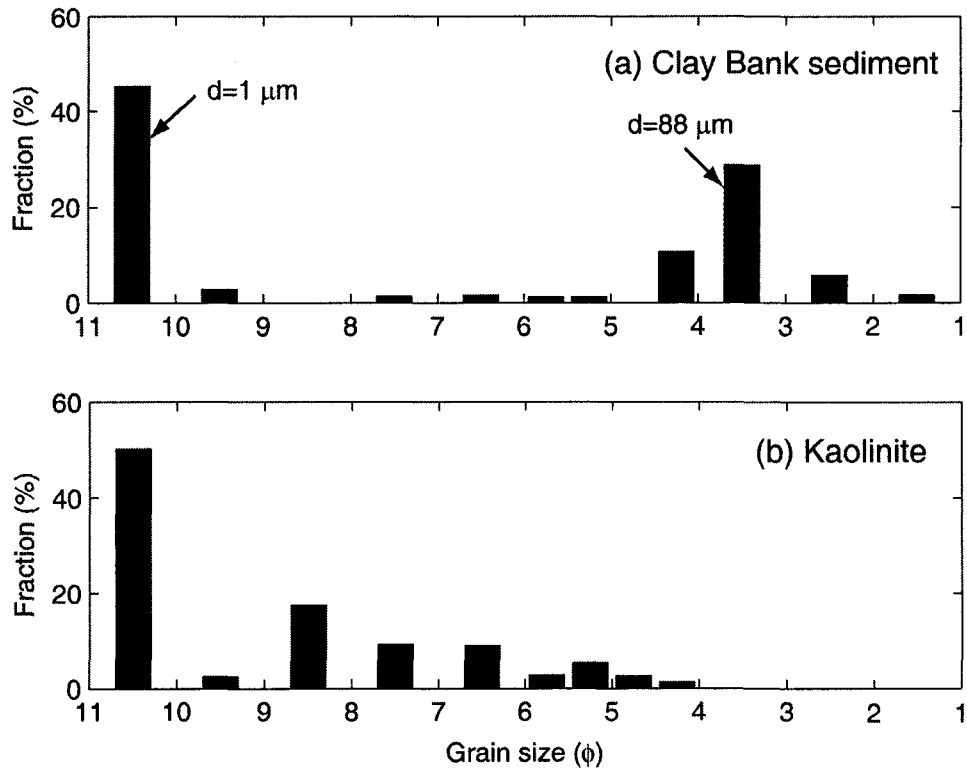
Fig. 3-6. Grain size distribution of used sediments: (a) Clay Bank sediment and (b) kaolinite.
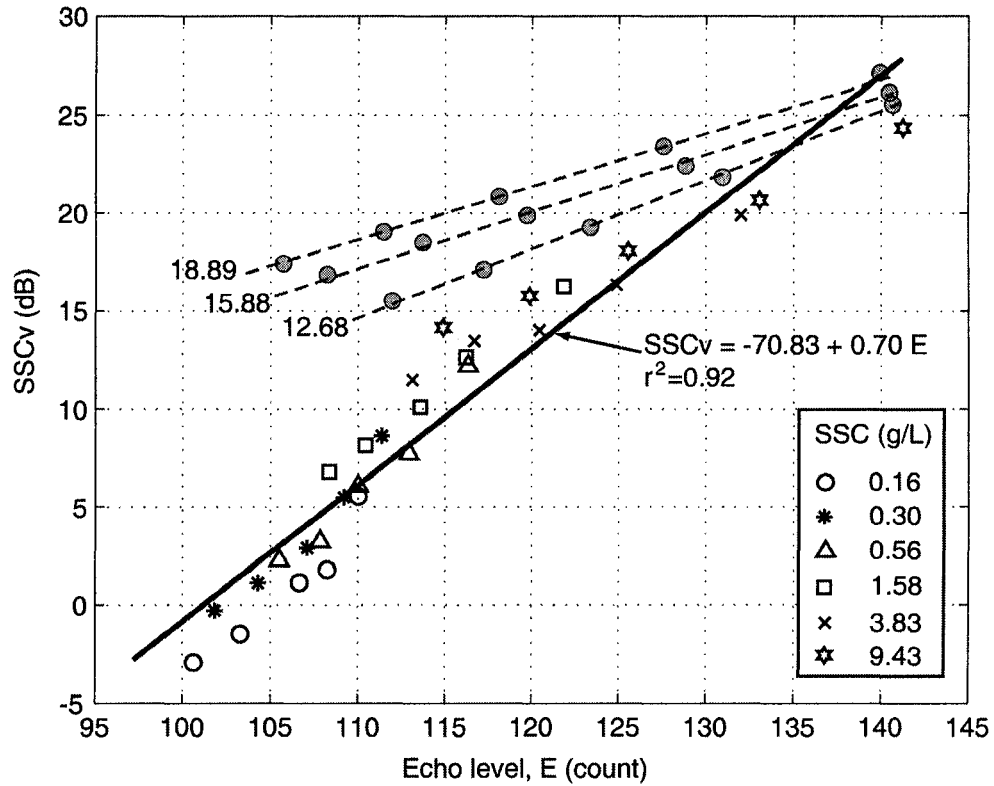
Fig. 3-7. Calibration results for Clay Bank sediment. Numbers indicate the suspended
    sediment concentration (in g/L). The lowest and highest echo levels at each
    concentration indicate the signals from the range of 59 and 19 cm, respectively.
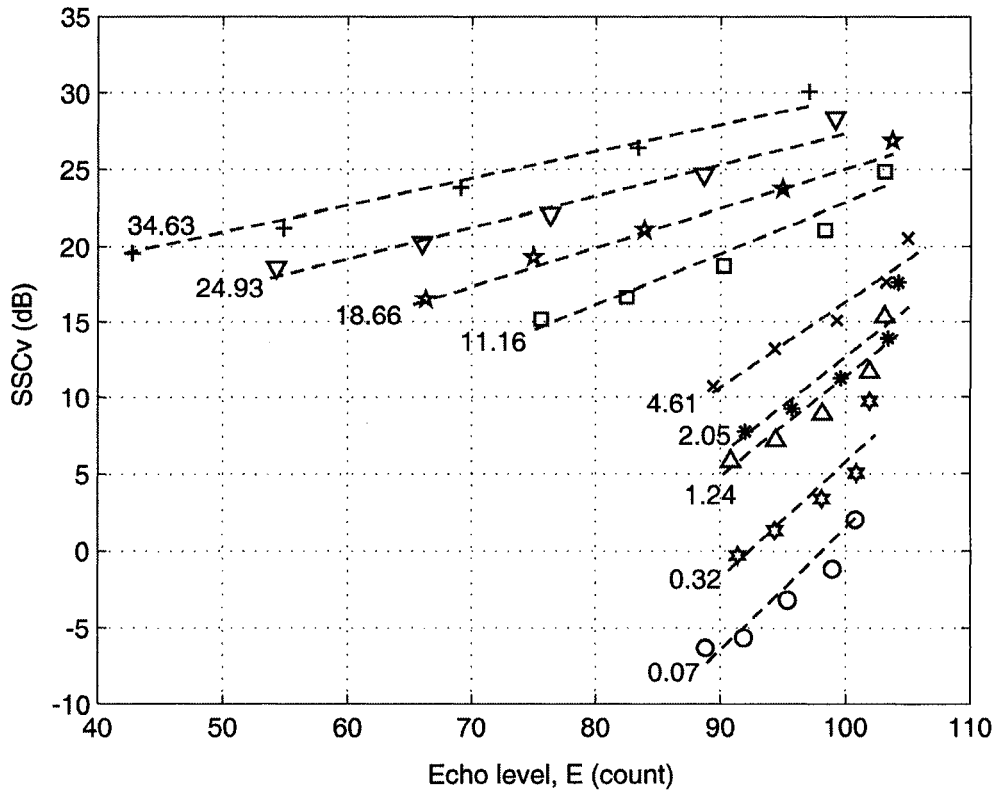
Fig. 3-8. Calibration results for kaolinite. Numbers indicate the suspended sediment concentration (in g/L). The lowest and highest echo levels at each concentration indicate the signals from the range of 59 and 19 cm, respectively.
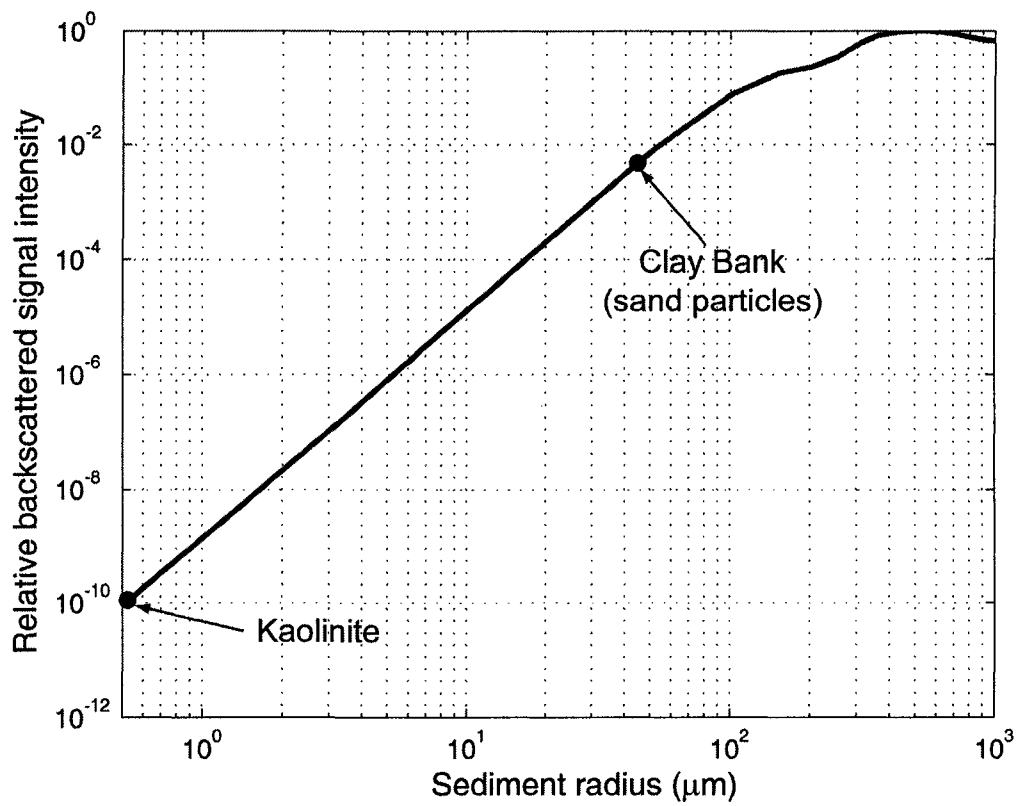
Fig. 3-9. Relative backscattered acoustic intensity expected at the frequency of 1.5 MHz, assuming that the particle is a rigid sphere.
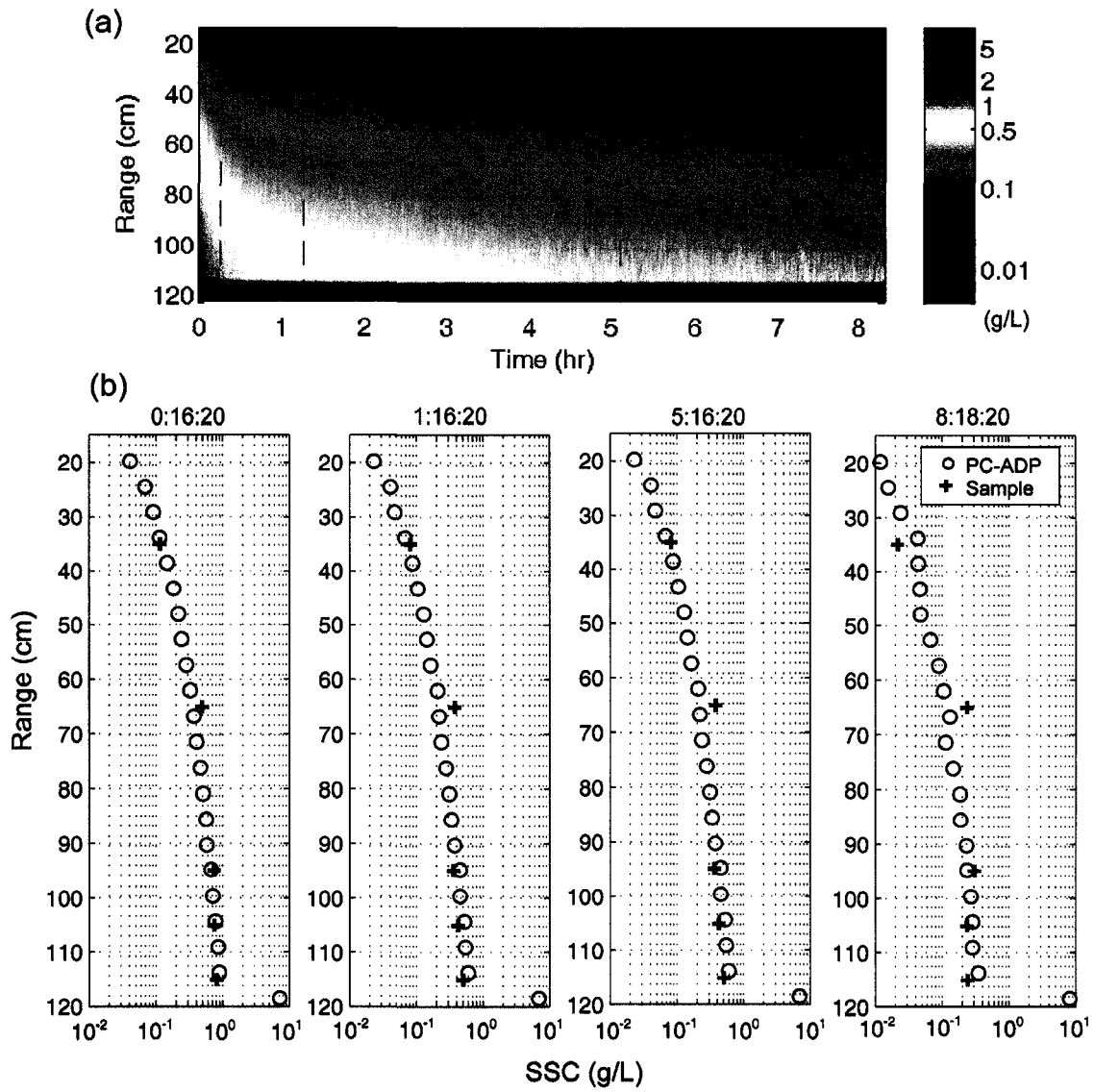
Fig. 3-10. (a) The time series of SSC profiles derived by PC-ADP. The strong echo around the range of 120 cm represents the tank bottom. (b) Comparison with sample-derived SSC (see the dashed lines in (a) for corresponding profiles). The numbers above the panel denote the elapsed time (hh:mm:ss).
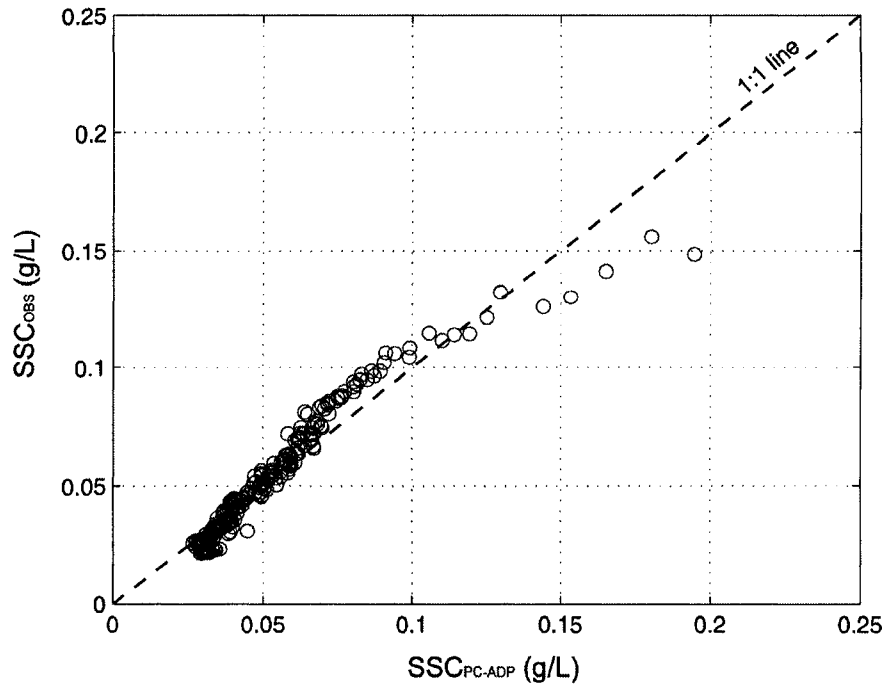
Fig. 3-11. Comparison between PC-ADP-derived SSC ($SSC_{PC\text{-}ADP}$) and OBS-derived SSC (SSC_{OBS}) at the range of 38.5 cm.

CHAPTER IV. CRITICAL SHEAR STRESS FOR COHESIVE SEDIMENT DEPOSITION: LABORATORY EXPERIMENTS

Abstract

Under the steady and unsteady flow, three laboratory experiments were conducted to answer the question, "does a critical bed shear stress for deposition (τ_{cd}) exist?" In these experiments, the direct observation of deposit stemmed from the inner corner of the laboratory flume bottom suggests that τ_{cd} does exist and that deposition only occurs when the local bed shear stress (τ_b) is less than τ_{cd}. The change of deposit length and suspended sediment concentration under simulated tidal cycles demonstrates that deposition can happen only at tidal decelerating phases with a recognizable τ_{cd}. This study further proves that both τ_b (a hydrodynamic parameter) and τ_{cd} (a sediment parameter) are the main controlling parameters for determining cohesive sediment deposition.

Keywords: cohesive sediment; deposition; critical bed shear stress; flume experiment

1. Introduction

Understanding erosion and deposition processes of cohesive sediments is important for better management of marine and estuarine environments. These processes are primarily controlled by the variation in hydrodynamic and sedimentary conditions (Umita et al., 1984; McAnally, 1999). It is generally accepted that the bottom sediment will be eroded when the local bed shear stress, τ_b, is above a critical value, i.e., critical bed shear stress for erosion (τ_{ce}) (Krone, 1962, 1993; Sanford and Halka, 1993; Winterwerp and van Kesteren, 2004). But the existence of a critical bed shear stress for deposition (τ_{cd}) is still debatable. To date, two opposite paradigms – "exclusive" or "simultaneous" erosion and deposition – have been used to describe the exchange of cohesive sediments at the sediment-water interface (Table 4-1).

The exclusive paradigm (Fig. 4-1a) suggests that erosion and deposition are not occurring at the same time (Krone, 1962; Partheniades et al., 1968; Parchure and Mehta, 1985; Lau and Krishnappan, 1994). In other words, erosion from the sediment bed occurs only when τ_b is larger than τ_{ce} and deposition to the bed occurs only when τ_b drops below τ_{cd}. In general, τ_{ce} is slightly greater than τ_{cd} such that an intermediate range ($\tau_{cd} < \tau_b < \tau_{ce}$) can exist for which neither erosion nor deposition occurs (Dyer, 1986; Sanford and Halka, 1993). This paradigm was derived based on a series of laboratory experiments (e.g., Krone, 1962; Partheniades et al., 1968; Parchure and Mehta, 1985; Lau and Krishnappan, 1994). All the above conclusions were drawn by interpreting the time series of the best-estimated depth-averaged suspended sediment concentration (SSC). It is noted, however, that there is no direct observation of when "deposition" at the sediment-water interface starts.

In contrast, the simultaneous paradigm (Fig. 4-1b) allows erosion and deposition to occur at the same time (Sanford and Halka, 1993; Winterwerp, 2006). It also implies that deposition exists at all times regardless of τ_b. This paradigm was originally proposed to explain the behavior of non-cohesive sediments, but several researchers (e.g., Lavelle et al., 1984; Bedford et al., 1987) adopted this concept and successfully used it for modeling the cohesive sediment transport. Because this paradigm produced a modeling result that agreed with field data, the validity of the simultaneous paradigm for cohesive sediments has been claimed. For example, Sanford and Halka (1993) showed poor simulation results using the "exclusive paradigm". When changed to the "simultaneous paradigm", however, they were better able to simulate the field-observed SSC. They concluded, therefore, that the exclusive paradigm appears to be unable to validate the field data. As pointed out by Maa et al. (in press), Sanford and Halka's conclusion was based on the observation of SSC at and above a level of 25 cm above the sediment bed, not including the SSC below that level. In other words, what they observed was that the downward flux at 25 cm above the bed always exists and it is larger than the upward flux when the tidal current (i.e., τ_b) started to decrease. Maa et al. (in press) also stated that the conclusion given by Winterwerp (2006) is a purely deductive and there is no observation to physically support that sediment was depositing all the time.

The aforementioned discrepancies between two opposite paradigms should be clarified for true understanding of cohesive sediment behaviors. To resolve the dispute of these two paradigms, a direct observation as to when deposition actually occurs would be preferable. For this reason, Maa et al. (in press) conducted a preliminary laboratory experiment to directly observe deposition under steady flows. Their results generally

support the "exclusive paradigm", but more extensive experiments are necessary to elucidate the depositional behavior under the unsteady flows, because the sediment bed response under the unsteady flow (e.g., tide current) may be different from that obtained from steady flow. Although some early studies (e.g., Hayter, 1983; Umita et al., 1984; van Leussen and Winterwerp, 1990) used cyclic tidal forces, their objectives were different. In this study, therefore, experiments with more realistic tidal forces were included to evaluate these two opposite paradigms.

2. Materials and methods

2.1. Experimental setup

Laboratory experiments were conducted using the annular flume housed in the Virginia Institute of Marine Science (VIMS). The flume has a circular channel with an outer diameter of 2.3 m and a channel width of 0.15 m (Fig. 4-2). The top ring driven by an electric motor generates the turbulent flow for eroding bottom sediments. Maa (1993) and Maa et al. (1995) formulated the spatially-averaged bed shear stress, $\langle \tau_b \rangle$, as

$$\langle \tau_b \rangle = 0.0114 \Omega^{1.693} \tag{4-1}$$

where $\langle \tau_b \rangle$ is in Pascal and Ω is the ring speed in rpm. An Optical Backscatter Sensor (OBS) was mounted on the inner wall about 9 cm above the flume bottom to continuously measure the change of SSC. Because of the relatively strong secondary circulation, suspended sediments are quite uniformly mixed in the flume. Thus, the single OBS readings could represent the depth-averaged SSC. Water temperature in the channel was measured by using a thermal sensor. To reduce data noises, each record represents the average of 100 measurements in 7 seconds.

94

Because of the presence of secondary flow induced by the centrifugal force, the distribution of τ_b is not uniform across the channel width (Maa, 1993; Maa et al., 1995). Fig. 4-3 shows the different pattern of τ_b distributions (τ_{b1}, τ_{b2} and τ_{b3}). Due to the side-wall effect, τ_b at $r = 1.0$ m (and 1.15 m) is zero. Owing to the eccentric force, τ_b is relatively larger on the outer half of the flume. Notice that two small areas near both corners where $\tau_b < \tau_{cd}$ provide space for sediments to deposit, and that the deposition area near the inner wall is much larger than that near the outer wall due to the skewed distribution of τ_b (Fig. 4-3). Because the flow is axially symmetrical for this kind of flume, the deposition area can be represented by the deposit length, ("DL" marked in Fig. 4-3). When $\langle \tau_b \rangle$ is large, DL is small, whereas when $\langle \tau_b \rangle$ becomes small, DL may rapidly increase, if $\langle \tau_b \rangle$ is smaller than a certain value (see τ_{b3} in Fig. 4-3).

Sediments collected from the Mai Po wetland, Hong Kong, were used in all experiments. The median grain size, d_{50}, is 2.6 µm. Clay minerals consist of Kaolinite (51%), Smectite (25%) and Muscovite (24%).

2.2. Experimental procedure

Prior to the commencement of an experiment, the flume was filled with a sediment-water mixture with a known concentration. Sea salt was added to reach the desired salinity (10 psu). The top ring was lowered into the flume to have a water depth of 10 cm. The sediment-water mixture was fully mixed again under a large $\langle \tau_b \rangle$ of approximately 1.1 Pa for 24 hrs. Then, the ring was stopped to allow suspended sediments to deposit and consolidate for 24 hrs.

Two types of tests (stepwise steady $\langle \tau_b \rangle$ and simulated tides) were carried out to reveal the depositional behavior (Table 4-2). The first type was a repeated experiment with the similar application of $\langle \tau_b \rangle$ to verify what was observed by Maa et al. (in press). A large $\langle \tau_b \rangle$ was applied for 1 hr, and then, the ring rotation speed was sequentially reduced to observe the depositional behavior and the growth of DL (Fig. 4-4). In the second type, $\langle \tau_b \rangle$ started from zero and linearly increased to a predetermined maximum (0.32 Pa), and then, $\langle \tau_b \rangle$ linearly decreased to zero (Figs. 4-5 and 4-6). This cycle was repeated three times to monitor the bed response induced by the artificial tides.

During the experiment, water samples were taken several times through the drainage cocks at three different elevations for calibrating OBS (Fig. 4-2). The withdrawn samples were filtered through 0.7-μm glass fiber filters. The residue on the filter was oven dried at 103–105°C for 24 hrs and then weighted for determining the SSC. During the experiment, through the transparent Plexiglas bottom, the growth and decay of DL in the radial direction were observed.

3. Results

3.1. Experiment with the stepwise steady bed shear stress

In this experiment, after $\langle \tau_b \rangle$ reduced to 0.13 Pa, the duration for each step changed to 2 hr (Fig. 4-4a). During the entire period of $\langle \tau_b \rangle = 0.13$ Pa and 0.09 Pa, the SSC decreased gently but the DL remained the same (Figs. 4-4b and c). This may be interpreted by the continuous deposition in the vertical direction at the confined space near the inner corner. In other words, the decrease of SSC contributed to the increase in mud thickness at the deposition area. For the next $\langle \tau_b \rangle$ (i.e., 0.06 Pa), the SSC showed a

small drop, and then continued the same decreasing trend. The DL increased to 1.5 cm

after about 0.5 hr, and remained about the same thereafter. In the transition period

between 0.06 and 0.03 Pa, the SSC dropped and further decreased from approximately

1.05 to 0.95 g/L (see the arrow in Fig. 4-4b), whereas the DL sharply increased from 1.5

to 3.3 cm (see the shaded area in Fig. 4-4c). This sharp increase of DL implies that $\langle \tau_b \rangle$ is

close to τ_{cd}, and thus τ_{cd} for the selected sediment is around 0.03 Pa. This result confirms

the observation of τ_{cd} claimed by Maa et al. (in press).

3.2. Experiment with the simulated tidal cycles

For the second experiment, the measurement focused on the changes of SSC. The

selected maximum $\langle \tau_b \rangle$ was approximately 0.32 Pa (Fig. 4-5a). In the first tidal cycle,

within an elapsed time of about 1 hr until $\langle \tau_b \rangle$ approached 0.1 Pa, there was no noticeable

increase of the SSC, which indicates that τ_{ce} at the mud surface was about 0.1 Pa for this

self-weight consolidated bed. The SSC accordingly increased with $\langle \tau_b \rangle$ until it reached

0.25 Pa. Because the OBS was saturated at that time (i.e., indicated by the flattened

output of OBS that is close to 5 volts), the SSC only increased slightly until $\langle \tau_b \rangle$ reached

0.32 Pa. When saturated, the OBS response was out of the linear range (Downing, 2006).

While $\langle \tau_b \rangle$ decreased from 0.32 to 0.15 Pa, the SSC only decreased slightly with a nearly

constant reading of 0.87 g/L. This response was also caused by the non-linear OBS

response, not the true SSC. Even with this condition, the small decrease of SSC suggests

that there was minor deposition at the small deposition zone near the inner corner and the

majority of suspended sediments were maintained in suspension. When $\langle \tau_b \rangle$ < 0.15 Pa,

the SSC began to decrease quickly, because the deposition zone became sufficiently large.

At the slack tide ($\langle \tau_b \rangle = 0$), there was a clear drop of SSC at the elapsed time of 6.6 hr and later at 13.25 hr after another tidal cycle (see the vertical arrows in Fig. 4-5c and d).

At the beginning of the second and the third tidal acceleration phases, it is remarkable that even though the tidal current was in the accelerating phase, the SSC was still gently decreasing (see Fig. 4-5c and d). There is a time lag of approximately 0.9 hr between the minimum $\langle \tau_b \rangle$ (at 6.6 hr) and the minimum SSC (at 7.5 hr). This lag is caused by the continuous deposition during the early stage of the acceleration phase. During this lag period, the DL was still large because $\langle \tau_b \rangle$ was small. The SSC showed a small increase at the onset of acceleration (6.7−6.8 hr and 13.3−13.4 hr) but it immediately decreased again. This response can be explained by the process that the small amount of sediments which were newly deposited near the center of the channel during the previous slack tide were easily re-dispersed, and immediately re-deposited at the corner where $\tau_b < \tau_{cd}$. When $\langle \tau_b \rangle$ was sufficiently large (> 0.1 Pa), the deposition zone became small and the newly erodible amount became large enough to produce an increasing SSC again after 7.5 hr (or 14.6 hr in the third cycle). In order to confirm the OBS-derived SSC, water samples were taken at three different elevations during the early stage of acceleration in the second and third cycles. The sample-derived SSC matches well with the corresponding OBS-derived SSC (Fig. 4-5c and d). Deposition at the corner, therefore, is still a dominant process even in the early stage of accelerating phases.

As the tidal cycle proceeded, the maximum SSC at each cycle gradually decreased (Fig. 4-5b). This may be associated with the secondary circulation as well as the uneven distribution of τ_b (see Fig. 4-3). Before running the experiment, the initial thickness of the bed deposit can be considered uniform across and along the channel,

since the sediment-water mixture was naturally settled and consolidated. After one tidal

cycle, however, the deposit near the inner wall would be thicker than that near the middle

of channel where local τ_b is the highest. Once suspended particles were accumulated

within the deposition zone (where $\tau_b < \tau_{cd}$) under the maximum $\langle \tau_b \rangle$, it is difficult for

those particles and flocs to escape from this zone over the successive tidal cycles. Also,

the relatively strong secondary circulation in the flume continuously brought sediments

from the high-τ_b area to low-τ_b area near the inner wall. Therefore, the erodible

sediments on the bed diminished, resulting in a decrease of the maximum SSC over the

cycles (Fig. 4-5b). The water samples withdrawn during the experiment may also

contribute a little, but this was proven not to be significant by carrying out a control test

without any water sample under the same hydrodynamic conditions. Consequently, the

main reason for the decrease in the maximum SSC after repeated cycles is attributed to

the secondary flows and the continuous deposition near the inner corner where $\tau_b < \tau_{cd}$.

The third experiment was conducted using the same τ_b for the second experiment,

but with less sediments for bed preparation (Fig. 4-6). The SSC generally followed the

similar trend shown in Fig. 4-5, but the maximum SSC was reduced to 0.38 g/L because

of less sediment supply from the bed. Thus, the OBS was not saturated and the SSC

continued to increase until $\langle \tau_b \rangle$ reached the maximum (= 0.32 Pa). While $\langle \tau_b \rangle$ reduced

from 0.32 to 0.15 Pa at the early time of deceleration phase, the DL remained at 2 cm and

SSC continued to slowly decrease (Fig. 4-6b and c), which implies that only bed

thickness increased during this time period. There was a slight decrease of SSC with

nearly constant DL between $0.06 < \langle \tau_b \rangle < 0.15$ Pa in the decelerating phase at every cycle.

This suggests that a small amount of deposition contributes to the continuous growth of

deposit thickness near the corner. The sharp increase of the deposit zone at approximately 5.8 hr in the first tidal cycle (or 12.6 hr in the second cycle) suggests that $\langle \tau_b \rangle$ is close to τ_{cd} (≈ 0.06 Pa) (Fig. 4-6c).

4. Discussions

4.1. Deposition rate vs. downward flux

By definition, deposition is a process that sediment particles or flocs come to the bed and, mostly importantly, stick to it (Krone, 1993; McAnally, 1999). According to the deposition formula given by Krone (1993), deposition is a function of τ_b, settling velocity and concentration of depositing aggregates. On the other hand, downward flux is defined as the gravity-induced downward movement of sediment particles or flocs (McAnally, 1999). The SSC at a practical observation level above the bed can be determined by the competition between downward flux caused by gravity and upward flux caused by turbulent diffusion. The advective vertical transport (wC, where w is the vertical component of tidal current and C is the SSC) also contributes to the change of SSC, but its role is not significant because the decrease of SSC happens both in flood (w is positive) and ebb (w is negative) tides (Maa et al., in press). When there is a sufficient sediment supply by bed erosion (e.g., at tidal acceleration phases) and the eddy diffusivity is also strong, the upward diffusion flux would be larger than the downward settling flux. As a result, the SSC at the observation elevation would increase with time. In contrast, if there is no sediment supply when erosion stops, the upward flux may be smaller than the downward flux, so that the SSC would decrease at the observation level. The above description suggests that the decrease of SSC at a specified distance above the

bed may not always cause deposition. This is because the net downward flux may form a relatively high-concentration layer right above the bed but the sediments still remain in suspension (Maa et al., in press). In this study, the relative high-concentration layer cannot exist because of strong secondary circulation. In the flume without secondary circulation, however, this layer will be moved by the mean current, such that this layer cannot be treated as an outcome of deposition. Consequently, the question as to whether deposition actually occurs or not should be dealt with directly at the bed, not in the water column, if possible. The only valid alternative would be using the total SSC or the depth-averaged SSC with the condition that the near-bed SSC can be measured accurately.

4.2. Secondary circulation effect

Results from the previous laboratory studies (e.g., Hayter, 1983; Umita et al., 1984; van Leussen and Winterwerp, 1990) that also used the simulated tides (T≈ 12 hr) were compared with the results of this study to understand the secondary circulation effect (Table 4-3 and Fig. 4-7). Although the SSC responses are different due to the differences in flume dimension, experimental conditions and selected sediment, this comparison is valuable for understanding cohesive sediment behaviors with a strong or a weak secondary circulation. All previous studies used annular flumes have the channel and the ring rotating in opposite directions. However, this does not mean the absence of secondary circulation, even if it may be weak.

Interestingly, all the previous study results show that the maximum SSC slightly increased with the number of tidal cycles even though they used a constant maximum bed shear stress (τ_{max}) for their experiments. The increasing trend is not clearly shown in Fig.

4-7 because only two tidal cycles were displayed, but it was reported in these studies. This outcome is likely when the secondary flow was minimized by rotating the channel and the ring in opposite directions.

After the first tidal cycle, the newly deposited top layer which is relatively uniformly distributed across the channel (because of a weak secondary circulation) would be easily agitated and eroded. The bed right below this new layer will be exposed to the fluid shear earlier than it would be, such that a little more sediments can be eroded even if the duration of erosion and the τ_{max} remains the same. This is possible because of the nature of turbulent flow. Under turbulent flow, even if the time-averaged τ_{max} is the same, there are always short bursts with instantaneous τ_b that is larger than the time-averaged τ_{max}. The repetition of tidal cycles, therefore, can gradually increase the SSC. The above is another reason for increase in SSC besides the explanation given by van Leussen and Winterwerp (1990). They explained that this is a kind of "weakening process" in the top layer of bed which causes a little more sediments to be eroded over tidal cycles.

On the other hand, our experimental results showed that the maximum SSC is decreasing with tidal cycles (Fig. 4-7d), due to the reason explained in the previous section. Once deposited near the inner wall, the chance for resuspension would be small, so that the decreasing trend was observed.

In order to explain these two kinds of SSC-response patterns under the simulated tidal cycles, the conceptual diagram given by Umita et al. (1984) was modified based on the strength of secondary circulation in the annular flume (Fig. 4-8). It is assumed that (1) flood and ebb tidal flows are symmetrical; and (2) the gradient of horizontal advection is zero.

102

In the case of a weak secondary circulation, the maximum SSC has an increasing trend over tidal cycles (Fig. 4-8a). During the accelerating phase of the first cycle, the SSC starts to increase when $\tau_b > \tau_{ce}$ and continues to increase until it reaches τ_{max}. After that, the variation in SSC is small until τ_b approaches τ_{cd}. This small decrease is caused by deposition at the corner areas. A rapid drop of SSC occurs when τ_b approaches τ_{cd}, and then a new deposition layer is uniformly developed above the old bed. When $0 < \tau_b < \tau_{cd}$ in the next tidal acceleration phase, deposition still continues but the re-dispersion of newly deposited materials which have a negligibly small τ_{ce}, also starts. As a result, the SSC may increase immediately and a rapid increase of SSC will be observed before τ_b reaches τ_{ce}.

For the case with a strong secondary circulation like the VIMS carousel (Fig. 4-8b), the first tidal cycle produced the similar SSC response when compared with the former case. While $0 < \tau_b < \tau_{cd}$ in the first deceleration phase, however, the amount of sediments deposited near the corner area would be larger than that for the previous case because the secondary circulation continues to bring sediments to the deposition area. When $0 < \tau_b < \tau_{cd}$ in the next acceleration phase, the deposition is still dominant because the re-dispersible material at the high-τ_b area is less than that for the previous case. Thus, the decreasing period of the SSC at the early stage of the second tidal acceleration is relatively longer, and the SSC may remain low until τ_b reaches τ_{ce}. At that time, a sharp increase of SSC can be generally found. During the ensuing cycles, secondary flows would be a major contributor to drive the sediments to the inner wall and deposit there. Therefore, the second maximum SSC is lower than the first one, and the following tidal cycles show a similar response pattern.

4.3. Paradigm evaluation

Hayter (1983) showed that the measured SSC is nearly in phase with flow velocity (Fig. 4-7a), i.e., the SSC decreased immediately after the flow velocity (i.e., τ_b) started to decrease and kept the decreasing trend until the next acceleration phase. His result is similar to other field-observed data showing that the SSC increases and decreases in phase with flow velocity (i.e., τ_b) (e.g., Nichols, 1986; Sanford and Halka, 1993; Maa and Kim, 2002). It is noteworthy, however, that there was no slack period due to the difficulty in flume control. The given minimum velocity was approximately 0.1 m/s which is still strong enough to sustain some sediment particles (or flocs) in suspension. Because there was little secondary circulation to make the SSC uniform in his flume, the observed SSC's were local SSC, not the depth-averaged SSC. That is, the phenomena observed during the decelerating phase can be explained by the fact that the downward flux exceeded the upward flux at the sampling elevation. This net downward flux may induce to either (1) develop a near-bed layer with a relatively high SSC when τ_b is still large and then deposit to bed when τ_b become small or (2) directly deposit to the bed at all times, depending on the existence of a high-concentration layer near the bed. Unfortunately, there was no evidence to support any of these two possibilities.

In contrast, the latter three data sets (Figs. 4-7b, c and d) are not in phase between τ_b and SSC. Umita et al. (1984) and van Leussen and Winterwerp (1990) applied the same τ_{max} to simulate the artificial tidal cycles, and the SSC response shows the similar pattern (see Figs. 4-7b and c). After τ_{max}, the SSC remained constant or slightly decreased, and the rapid decrease of SSC was commonly found prior to the slack tides.

Umita et al. (1984) observed that floc size was the minimum (d_{50} = 12 μm) at τ_{max} and became the maximum (d_{50} = 31 μm) immediately before τ_{cd} ($\approx$ 0.025 Pa). Thus, they claimed that significant deposition with flocculation occurred while τ_b was approaching to τ_{cd}, so that the rapid decrease of SSC can be found.

At present, it is not clear what causes the discrepancy between the SSC response given by Hayter's experiment (Fig. 4-7a) and those presented by Umita et al. (1984) and van Leussen and Winterwerp (1990)'s experiments (Figs. 4-7b and c), although all these three experiments had rotated the channel and the ring in opposite directions to minimize the secondary flow. One possible explanation is that the secondary circulation in Umita et al. (1984) and van Leussen and Winterwerp (1990)'s flume might not be as small as that in Hayter's flume. Thus, some degrees of mixing were still available so that the suspended sediment near the measuring level might be close to that observed in this study (Fig. 4-7d).

When there is no secondary circulation, as what happened in most cases in the field, re-dispersion can be considered an important process at the sediment-water interface at the beginning of tidal acceleration phases (Maa and Kim, 2002; Kwon, 2005). The SSC starts to increase at that time because re-dispersion of newly deposited materials becomes more dominant than deposition in a short time (Fig. 4-9). After the freshly deposited materials are dispersed, the underlying old bed is subject to erosion. During this transition, the re-dispersion process is gradually shifted to the erosion process as the tidal acceleration proceeds. Because of the difficulty in accurately estimating the sediment amount by re-dispersion or erosion, Maa and Kim (2002) proposed a simplification on this complicated process using a constant erosion rate (see the dot-

105

dashed line in Fig. 4-9). They suggested that erosion occurs only when the tidal current is in the acceleration phase. This is a practical approach because the total amount of erodible sediments using the constant erosion rate model may not be significantly different with that using a traditional erosion model.

In the decelerating phase, because the mixing capacity is decreasing, a relatively high-concentration layer can be formed right above the sediment bed. This can cause the collapse of turbulence, resulting in the super-saturated conditions in terms of carrying capacity (Toorman, 2002; Winterwerp, 2002). Even if the total amount of suspended sediments is still below the saturation concentration, the decelerating flow will not directly induce deposition because sediments that were already suspended can be maintained in suspension by the τ_b that is actually smaller than that required for bed erosion (Masselink and Hughes, 2003). Therefore, during the early stage of decelerating phases, sediment particles (or flocs) in suspension will be only re-distributed in the water column. In other words, the total mass of suspended sediment will not significantly change even though the density and size distribution of particles (or flocs) can be altered by the flocculation process. While $\tau_{cd} < \tau_b < \tau_{ce}$ in the deceleration, in particular, the downward flux continues to bring suspended sediments to the near-bed layer right above the bed but may not allow for deposition. Once τ_b falls below τ_{cd}, the suspended materials accumulated at the near-bed layer start deposition, resulting in a rapid decrease of the depth-averaged SSC (see the dashed line in Fig. 4-9).

Field-observed SSC (see the dotted line in Fig. 4-9) at a fixed level above the bed may show the immediate decrease after τ_{max} because it represents the net sediment flux. In summary, the deposition means that particles (or flocs) stay on the sediment bed

106

because the applied τ_b is weaker than the bonding force between the particles (or flocs) and the bed. The gap between the true depth-averaged SSC and the field-observed SSC is attributed to the lack of information for this relatively high-concentration layer near the bed, which may have a thickness on the order of several millimeters to centimeters. The existence of τ_{cd} and the velocity (or τ_b)-suspension lag observed in this laboratory study generally support the depositional behavior under the "exclusive paradigm".

5. Conclusions

The followings are summarized from this study:

(1) The duplicated steady flow experiment confirmed the results of a previous study given by Maa et al. (in press).

(2) Due to the uneven and skewed distribution of local τ_b, the change of the deposition length in a radial direction is direct observation on τ_b distribution in the annular flume. It also serves as a direct evidence to find "when the suspended sediment can be deposited?"

(3) Under the unsteady flow, τ_{cd} can be also identified by the rapid increase of DL and the sharp decrease of depth-averaged SSC. Even though the DL was measured and interpreted subjectively at discrete times, it can be reasonably concluded that τ_{cd} for the selected sediments is approximately 0.03−0.06 Pa.

(4) The artificial tidal cycling experiments also support the existence of τ_{cd}. The exclusive paradigm with the correct τ_{ce} profile and erosion behavior can explain the change of field-observed and depth-averaged SSC under all tidal regimes.

(5) Both τ_b (a hydrodynamic parameter) and τ_{cd} (a sediment parameter) are the main

controlling parameters for determining the deposition of cohesive sediment. Deposition occurs only when the local τ_b is less than τ_{cd}.

(6) Secondary flow in the VIMS carousel is a major contributor to cause the long-term decrease in maximum SSC over the tidal cycles.

References

Bedford, K.W., Wai, O., Libicki, C.M., van Evra, R., 1987. Sediment entrainment and deposition measurements in Long Island Sound. J. Hydr. Eng. 113, 1325-1343.

Downing, J., 2006. Twenty-five years with OBS sensors: The good, the bad, and the ugly. Cont. Shelf Res. 26, 2299-2318.

Dyer, K.R., 1986. Coastal estuarine sediment dynamics. John Wiley and Sons, New York, 342 pp.

Hayter, E.J., 1983. Prediction of cohesive sediment transport in estuarine waters. Ph.D. dissertation, University of Florida, 349 pp.

Krone, R.B., 1962. Flume studies of the transport of sediment in estuarial shoaling processes. Final Report, Hydraulic Engineering Laboratory and Sanitary Engineering Research Laboratory, University of California, Berkeley, 110 pp.

Krone, R.B., 1993. Sedimentation revisited. In: Mehta, A.J. (Ed.), Nearshore and Estuarine Cohesive Sediment Transport. AGU, Washington D.C., pp. 108-125.

Kwon, J.-I., 2005. Simulation of turbidity maximums in the York River, Virginia. Ph.D. dissertation, College of William and Mary, 127 pp.

Lau, Y.L., Krishnappan, B.G., 1994. Does reentrainment occur during cohesive sediment settling? J. Hydr. Eng. 120(2), 236-244.

Lavelle, J.W., Mofjeld, H.O., Baker, E.T., 1984. An in situ erosion rate for a fine-grained marine sediment. J. Geophys. Res. 89, 6543-6552.

Maa J.P.-Y., 1993. VIMS sea carousel: its hydrodynamic characteristics. In: Mehta, A.J. (Ed.), Nearshore and Estuarine Cohesive Sediment Transport. AGU, Washington D.C., pp. 265-280.

Maa, J.P.-Y., Lee, C.-H., Chen, F.J., 1995. Bed shear stress measurements for VIMS Sea

    Carousel. Mar. Geol. 129, 129-136.

Maa, J.P.-Y., Kim, S.-C., 2002. A constant erosion rate model for fine sediment in the

    York River, Virginia. Environ. Fluid Mech. 1, 345-360.

Maa, J.P.-Y, Kwon, J.-I., Hwang, K.-N., Ha, H.K., in press. Critical bed shear stress for

    cohesive sediment deposition under steady flows. J. Hydr. Eng. ASCE.

Masselink, G., Hughes, M.G., 2003. Introduction to coastal processes and

    geomorphology, Hodder Arnold, London, 354 pp.

McAnally, W.H., 1999. Aggregation and deposition of estuarial fine sediment. Ph.D.

    dissertation, University of Florida, 366 pp.

Nichols, M.M., 1986. Effects of fine sediment resuspension in estuaries, In: Mehta, A.J.

    (Ed.), Estuarine Cohesive Sediment Dynamics. Springer-Verlag, New York, pp.

    5-42.

Parchure, T.M., Mehta, A.J., 1985. Erosion of soft cohesive sediment deposits. J. Hydr.

    Eng. 111(10), 1308-1326.

Partheniades, E., Cross, R.H., Ayora, A., 1968. Further research on the deposition of

    cohesive sediments. Proceedings of 11th Conference on Coastal Engineering,

    723-772.

Sanford, L.P., Halka, J.P., 1993. Assessing the paradigm of mutually exclusive erosion

    and deposition of mud with examples from upper Chesapeake Bay. Mar. Geol.

    114, 37-57.

Toorman, E.A., 2002. Modelling of turbulent flow with suspended cohesive sediment. In:

    Winterwerp, J.C., Kranenburg, C. (Ed.), Fine Sediment Dynamics in the Marine

Environment. Elsevier, pp. 155-169.

Umita, T., Kusuda, T., Awaya, Y., Onuma, M., Futawatari, T., 1984. The behavior of suspended sediments and muds in an estuary. Water Sci. Tech. 17, 915-927.

van Leussen, W., Winterwerp, J.C., 1990. Laboratory experiments on sedimentation of fine-grained sediments: a state-of-the-art review in the light of experiments with the Delft tidal flume, In: Cheng, R.T. (Ed.), Residual Currents and Long-term Transport. Springer-Verlag, New York, pp. 241-259.

Winterwerp, J.C., 2002. Scaling parameters for high-concentrated mud suspensions in tidal flow. In: Winterwerp, J.C., Kranenburg, C. (Ed.), Fine Sediment Dynamics in the Marine Environment. Elsevier, pp. 171-186.

Winterwerp, J.C., 2006. On the sedimentation rate of cohesive sediment. In: Maa, J.P.-Y., Sanford, L.P., Schoellhamer, D.H. (Eds.), Estuarine and Coastal Fine Sediment Dynamics, Elsevier, Amsterdam, pp. 209-226.

Winterwerp, J.C., van Kesteren, W.G.M., 2004. Introduction to the physics of cohesive sediment in the marine environment. Elsevier, Amsterdam, 466 pp.

Table 4-1. Two opposite paradigms for erosion and deposition of cohesive sediments.

Characteristics	Exclusive paradigm	Simultaneous paradigm
Definition	Erosion and deposition will not occur at the same time.	Erosion and deposition will occur simultaneously.
Boundary condition[*]	$\dfrac{\partial C}{\partial t} = E$ for $\tau_b > \tau_{ce}$ $\dfrac{\partial C}{\partial t} = D$ for $\tau_b < \tau_{cd}$	$\dfrac{\partial C}{\partial t} = E - D$
Existence of τ_{ce}	Yes	Yes
Existence of τ_{cd}	Yes ($\tau_{cd} < \tau_{ce}$)	No (continuous deposition)
Deposition rate	$D = w_s C_b \left(1 - \dfrac{\tau_b}{\tau_{cd}} \right)$ for $\tau_b < \tau_{cd}$ $D = 0$ for $\tau_b > \tau_{cd}$	$D = w_s C_b$
References	Krone (1962); Partheniades et al. (1968); Parchure and Mehta (1985); Lau and Krishnappan (1994)	Sanford and Halka (1993); Winterwerp and van Kesteren (2004); Winterwerp (2006)

[*]Assuming a horizontally uniform flow and C is the depth-averaged suspended sediment concentration; E: Erosion rate; D: deposition rate; w_s: settling velocity; C_b: near-bed concentration

112

Table 4-2. Summary of experimental conditions and results.

Test	Case 1	Case 2	Case 3
Shear stress type	Stepwise	Tidal cycle	Tidal cycle
Maximum $\langle \tau_b \rangle$ (Pa)	1.14	0.32	0.32
τ_{cd} (Pa)*	0.03	n/a	0.06
Water temperature (°C)	26.5	25.9	27.3
Salinity (psu)	10	10	10
Sediment	Mai Po mud	Mai Po mud	Mai Po mud

*Determined by the DL near the inner wall

Table 4-3. Comparison of tidal cycle experimental results by using annular flume.

References	Hayter (1983)	Umita et al. (1984)	van Leussen and Winterwerp (1990)	This study
τ_{max} (or max. velocity)	0.5 m/s	0.4 Pa	0.4 Pa	0.32 Pa
Flume outer diameter (m)	1.73	2.2	2.1	2.3
Water depth (m)	0.3	0.2	0.3	0.1
Channel width (m)	0.21	0.2	0.2	0.15
Ratio of width/depth	0.7	1.0	0.67	1.5
Salinity (psu)	10	n/a	n/a (salt water)	10
Water temperature (°C)	n/a	20	n/a	26.6
In phase of τ_b and SSC	Yes	No	No	No
d_{50} of sediment (μm)	n/a	6	n/a	2.6
Sediment source	Clay from Lake Francis	Clay and silt from River Chikugo	Commercial kaolinite	Clay from Mai Po wetland
Consolidation time (hr)	40	24	n/a	24
Channel and ring rotation	Opposite rotation	Opposite rotation	Opposite rotation	Only ring rotation

114

(a) Exclusive paradigm

(b) Simultaneous paradigm
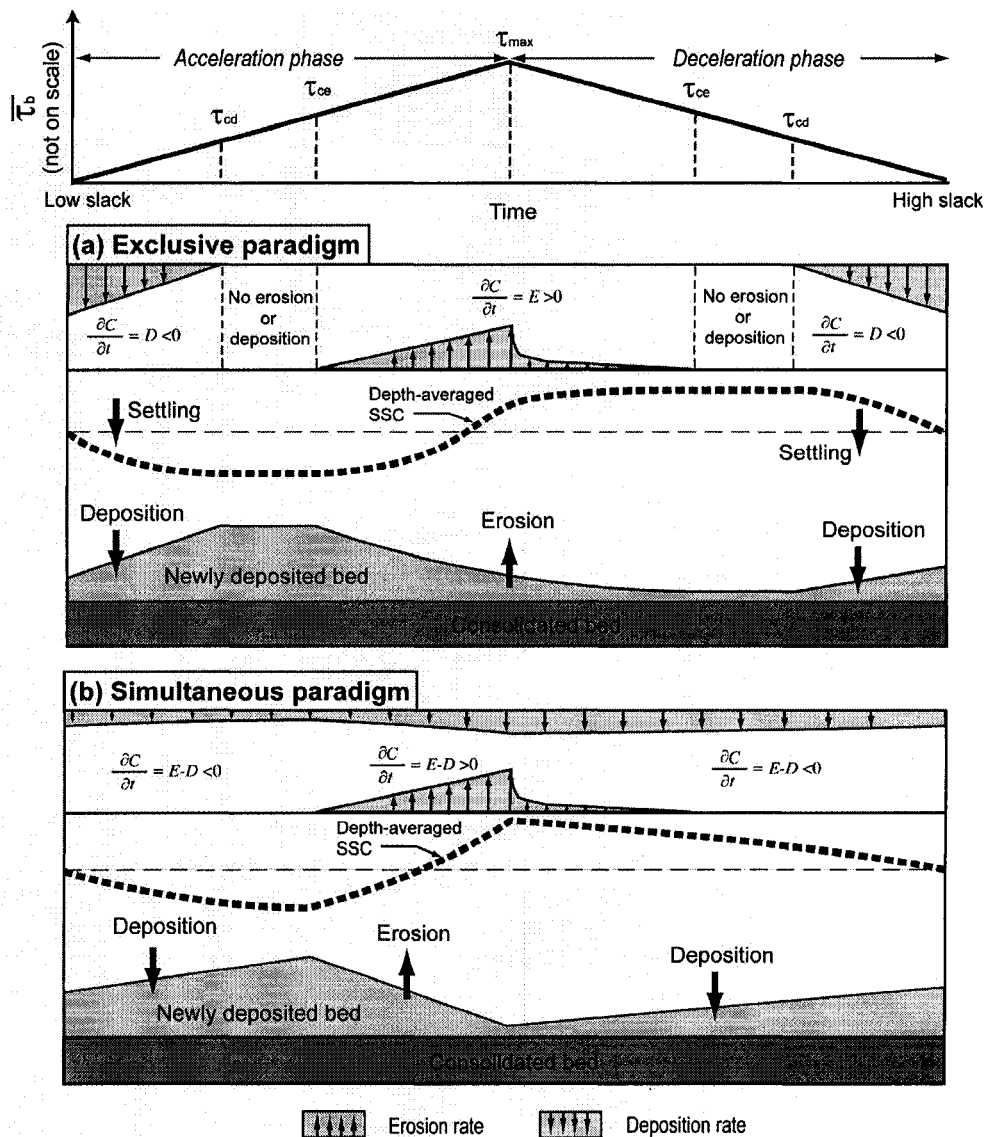
Fig. 4-1. Conceptual differences between exclusive and simultaneous paradigms for cohesive sediments under tidal forces. (a) Exclusive paradigm: erosion from the sediment bed occurs only when $\tau_b > \tau_{ce}$, and deposition to the bed occurs only when $\tau_b < \tau_{cd}$. It is assumed that the new deposit will immediately develop the same τ_{ce}, and τ_{ce} is not varying in the vertical direction. The depth-averaged SSC increases whenever $\tau_b > \tau_{ce}$. E and D represent erosion and deposition rate, respectively. (b) Simultaneous paradigm: deposition always exists due to the non-existence of τ_{cd}. Due to the continuous deposition regardless of τ_b, the depth-averaged SSC decreases immediately after τ_b starts to decrease.

(a)

2.3 m

M

(b)

Inner wall

Outer wall

Rotating ring

9 cmab   OBS

Drainage cock   8.8 cmab

10 cm

6.5 cmab

15 cm   4.5 cmab

Sediments

Plexiglass bottom
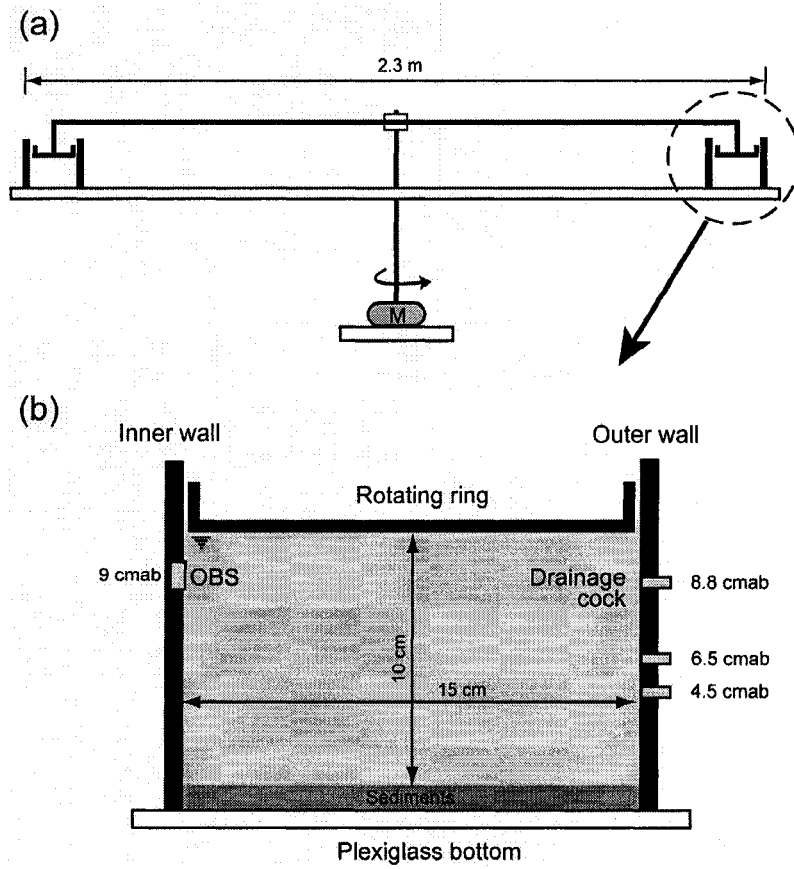
Fig. 4-2. (a) Schematic diagram of the annular flume housed in the VIMS. M represents a motor. (b) Cross-section view of the flume channel.
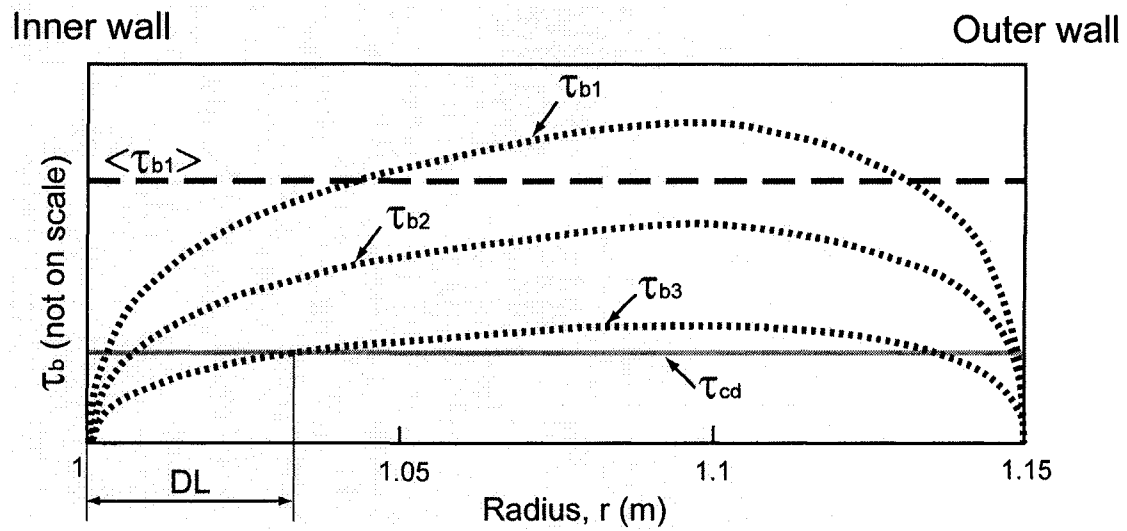
Fig. 4-3. Distribution of bed shear stress in the annular flume (after Maa, 1993). $\langle \tau_{b1} \rangle$ is the spatially-averaged bed shear stress for the τ_{b1} distribution. τ_{b2} and τ_{b3} show the distribution of two smaller bed shear stresses. DL represents the deposit length near the inner wall.
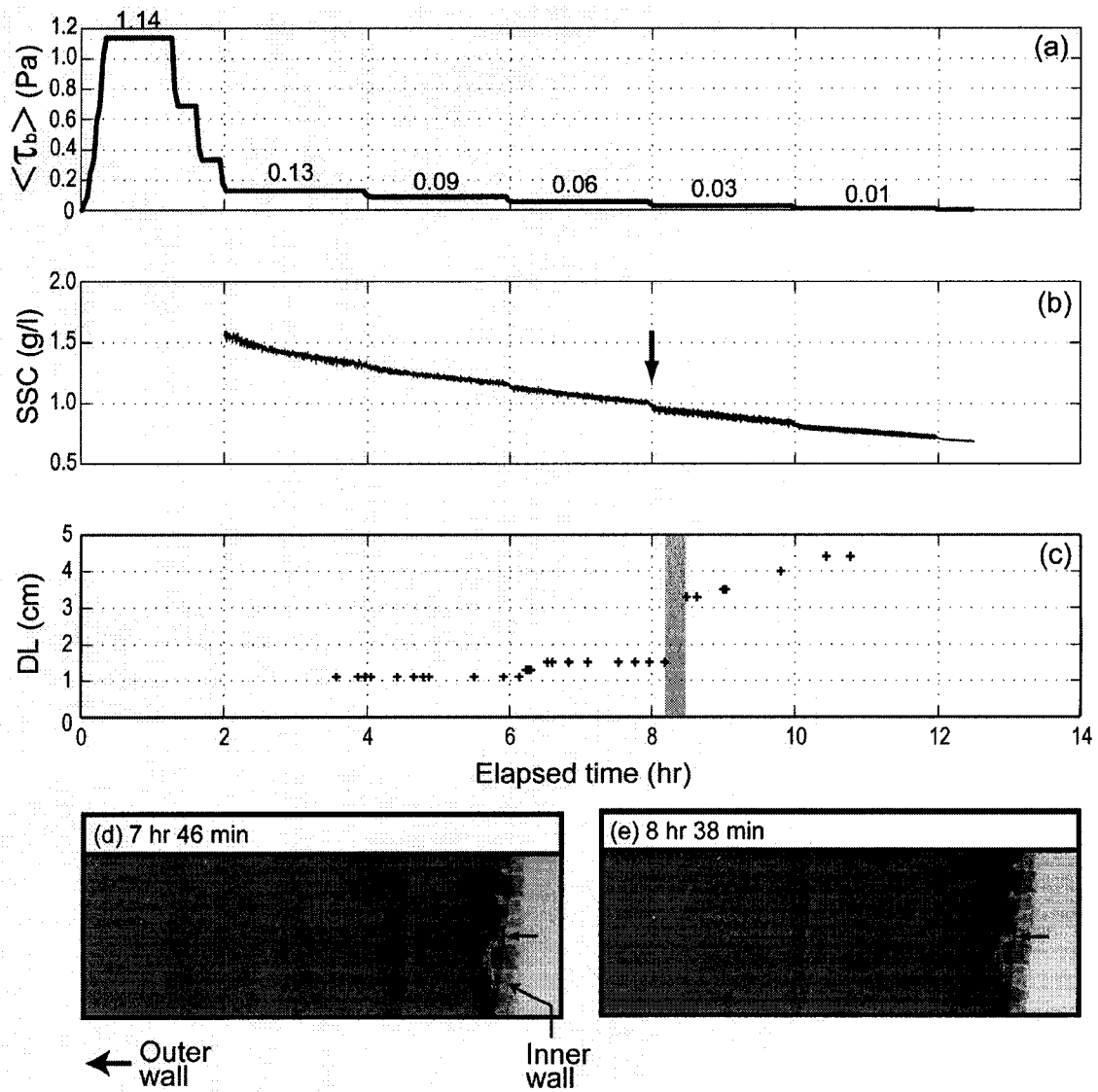
Fig. 4-4. Experiment results from the stepwise steady bed shear stresses. (a) $\langle \tau_b \rangle$; (b) OBS-derived SSC; and (c) Deposit length (DL) accreted near the inner wall. (d) and (e) are photo images taken from the flume bottom, facing upward, at an elapsed time of 7 hr 46 min and 8 hr 38 min.
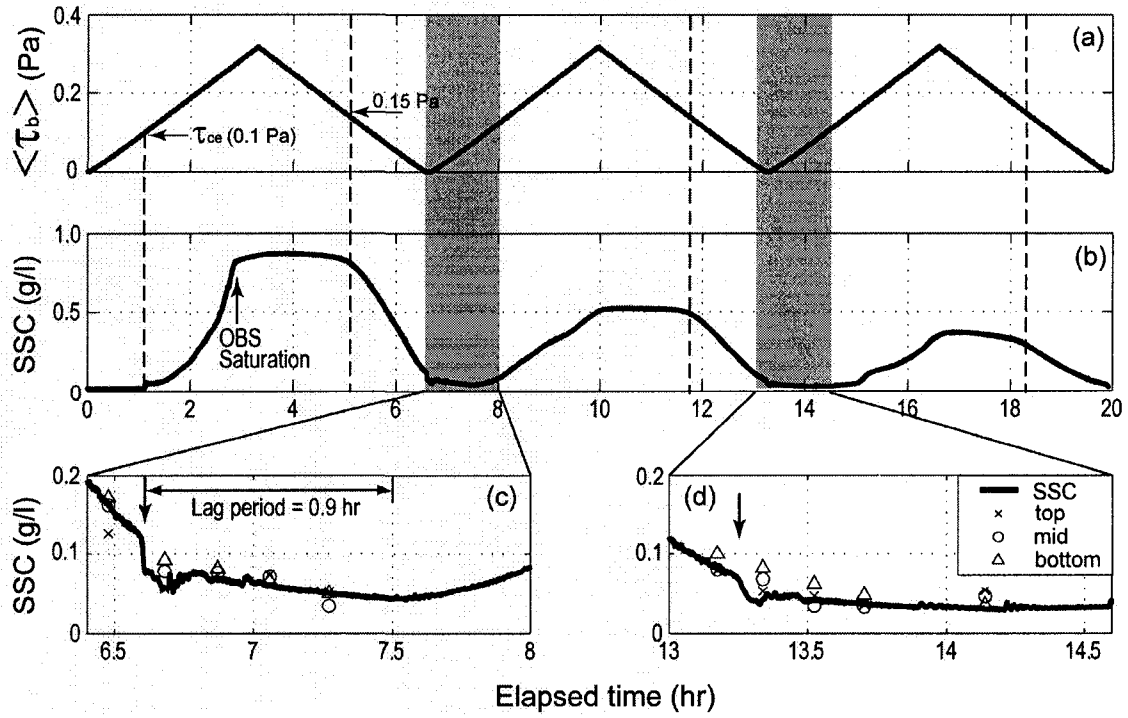
Fig. 4-5. Experiment results from the first simulated tidal cycles. (a) $\langle \tau_b \rangle$; and (b) OBS-derived SSC. (c) and (d) are details of the shaded areas in the second panel. The symbols represent the sample-derived SSC at three different levels.
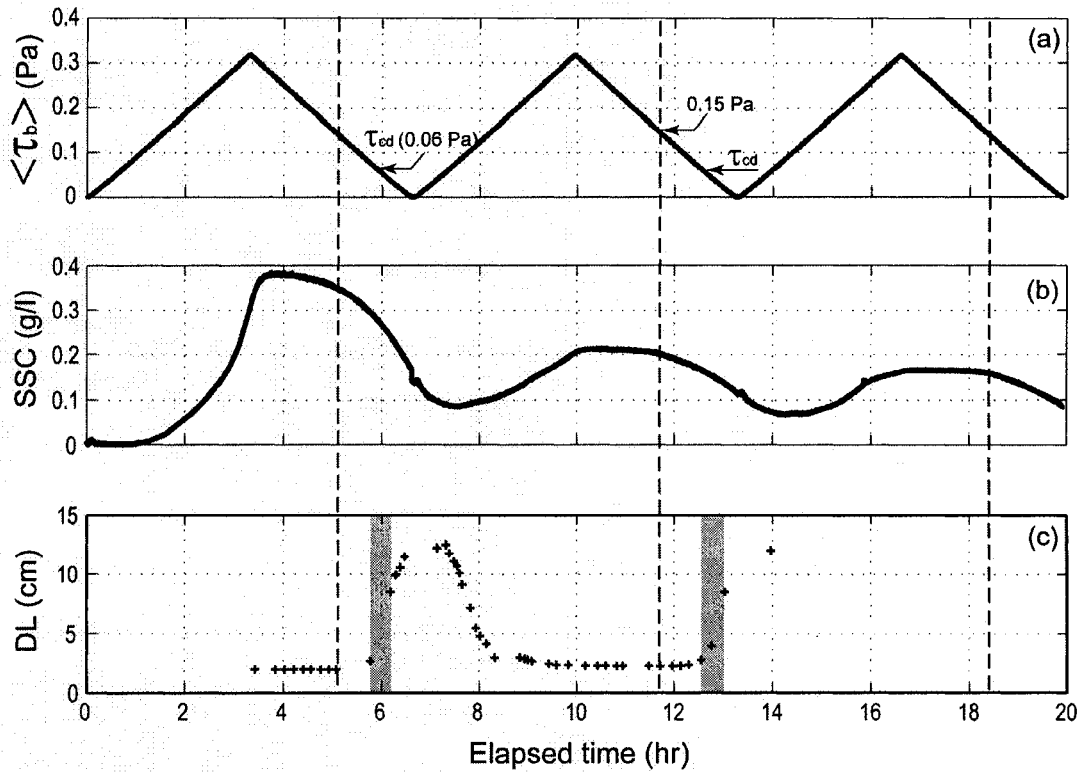
Fig. 4-6. Experiment results from the second simulated tidal cycles. (a) $\langle \tau_b \rangle$; (b) OBS-derived SSC; and (c) Deposit length (DL) accreted near the inner wall.
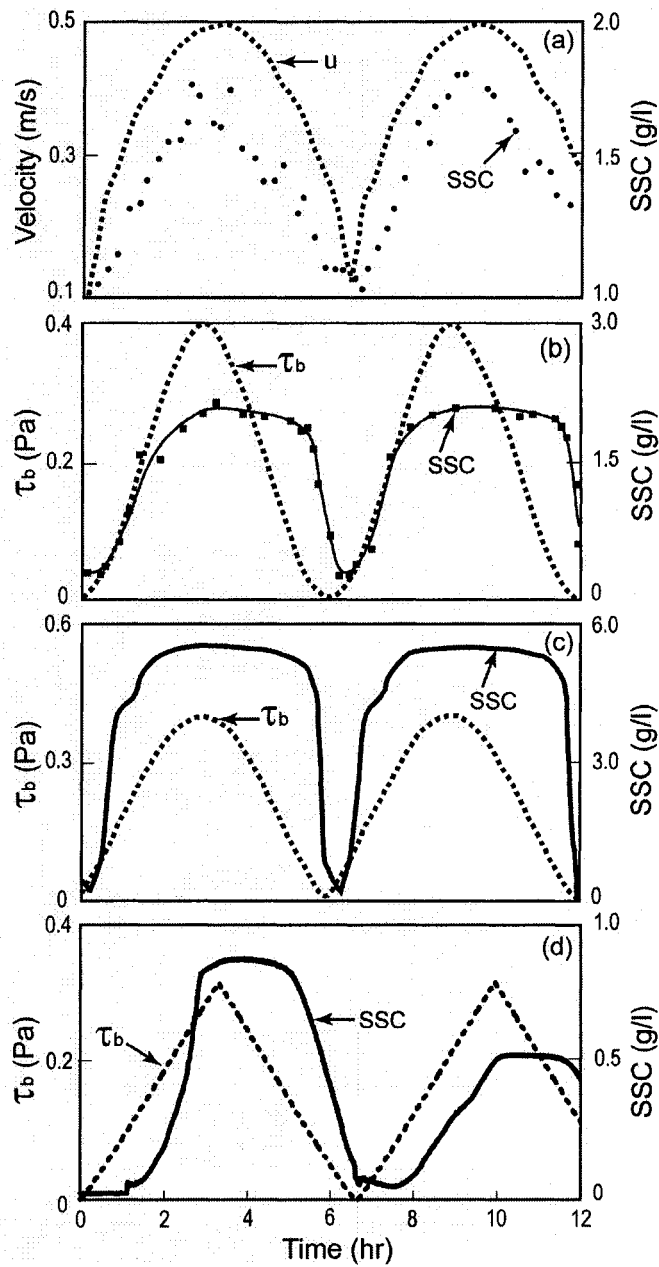
Fig. 4-7. Comparison of the SSC responses for different studies that use cyclic tidal forces. (a) Hayter (1983); (b) Umita et al. (1984); (c) van Leussen and Winterwerp (1990); and (d) This study. The first three studies all used an annular flume with both the ring and the channel rotating in opposite directions.
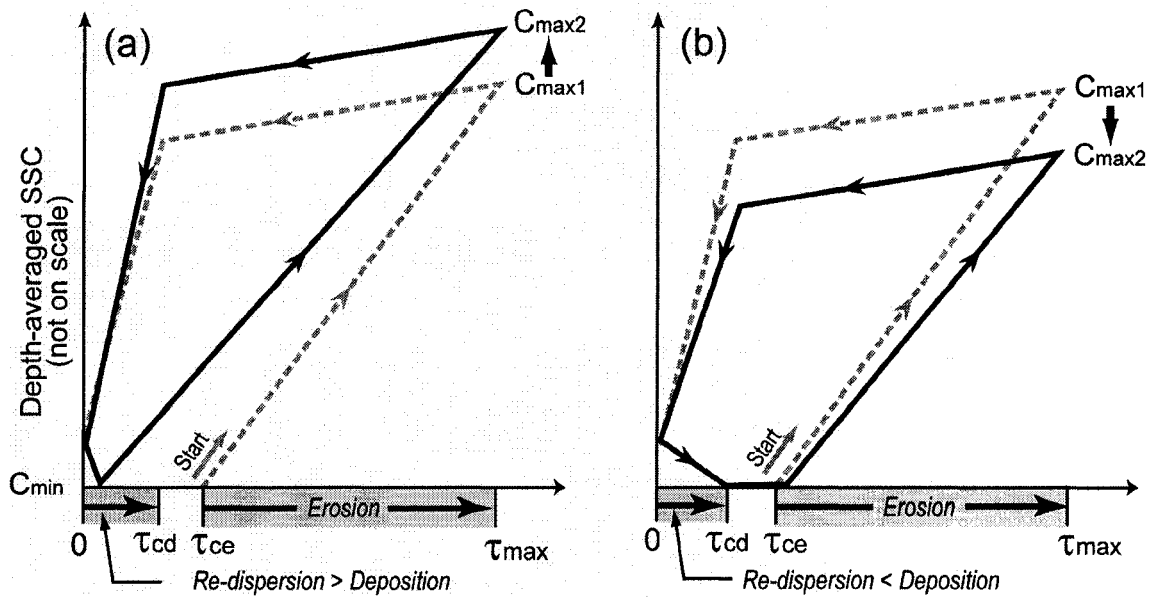
Fig. 4-8. Two kinds of SSC-response patterns generated by simulated tidal cycles (modified after Umita et al., 1984): (a) In the flume with a weak secondary circulation; and (b) In the VIMS laboratory carousel with a strong secondary circulation.
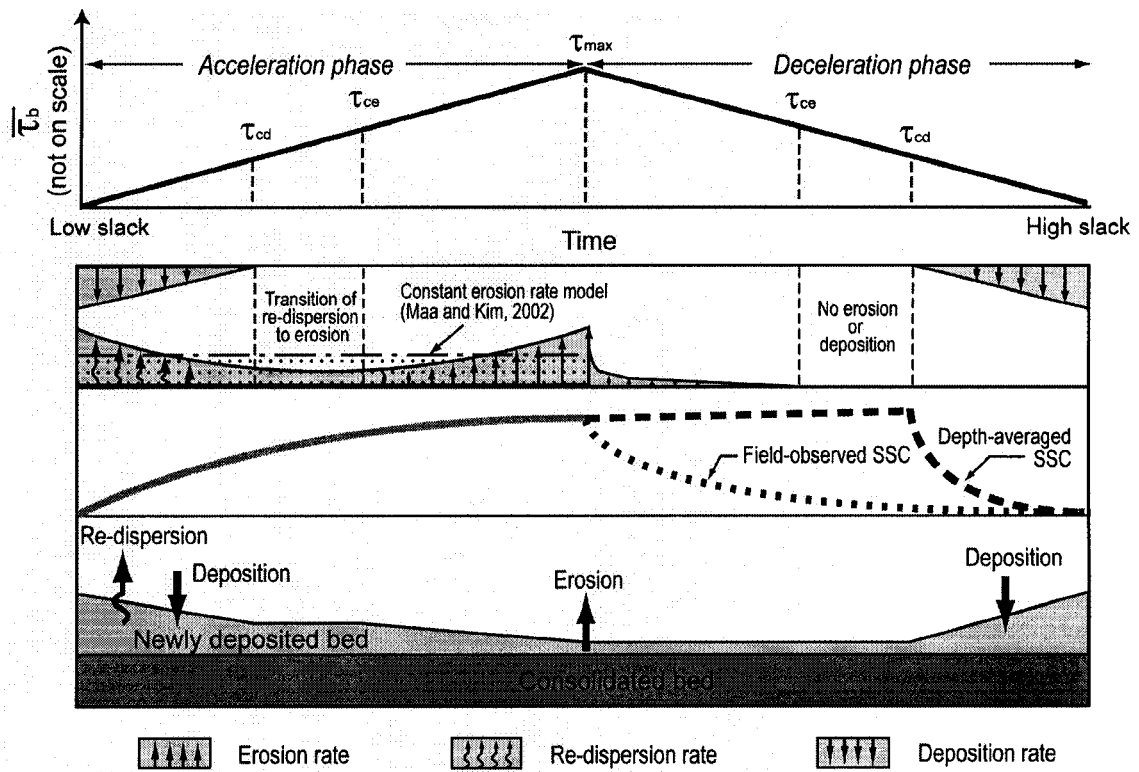
Fig. 4-9. Revised conceptual diagram to show the near-bed exchange processes of cohesive sediments under tidal cycles. The field-observed SSC at a fixed point in water column (i.e., local SSC and not close to the bottom) can decrease immediately after τ_{max} (because of the net downward flux), while the true depth-averaged SSC starts to decrease only when $\tau_b < \tau_{cd}$.

CHAPTER V. ACOUSTIC APPROACH FOR MEASURING BULK DENSITY OF COHESIVE SEDIMENT BEDS

Abstract

A non-intrusive acoustic technique and a signal-processing protocol were developed to estimate bulk density at consolidating sediment interface. Using high-frequency (300-700 KHz) Chirp acoustic waves, laboratory measurements were carried out in a consolidation tank filled with clay-water mixtures. Because the acoustic echo strength is proportional to the difference in acoustic impedance, and the sound speed in water is close to that in clay, the approximation of bulk density could be successfully presented. The acoustic wave reflectivity increased with increasing the bulk density at the water-sediment interface, which are well correlated with the consolidation status.

Keywords: acoustic, cohesive sediment, consolidation, bulk density, Chirp signal

1. Introduction

Cohesive sediments can be ubiquitously found in most coastal seas and estuaries. If present, they generally exhibit the largest gradient in sedimentary properties near the water-sediment interface (Mehta and Dyer, 1990; Winterwerp and van Kesteren, 2004; Holland et al., 2005). This gradient may be induced by the complexity of near-bed processes (e.g., erosion, deposition, consolidation and bioturbation) as a result of redistribution of near-bed sediments. In this aspect, understanding the uppermost layer (~10 cm) of sediment bed may provide the important clues for revealing sedimentary history and predicting future sediment behaviors.

A number of studies have been dedicated to address the characteristics of a top layer of consolidating or consolidated bed (e.g., Cutter and Diaz, 1996; Sills, 1998; Linterns et al., 2002). As yet, there are few reliable methods to adequately assess the bulk density of this layer because most previous methods are intrusive types which may severely disturb the target layers. At present, a direct coring which is considered as a standard against other methods requiring a calibration is widely being used to reveal internal bed features and to serve as the ground truth. This coring approach, however, is a time- and labor-consuming procedure. Additionally, it is impossible to meet the high spatial and temporal resolution required for most projects.

Other alternative techniques include using (1) the nuclear-ray (e.g., γ- and X-ray) attenuation, (2) electrical impedance change, (3) tuning fork and (4) acoustic wave attenuation. The principle of a nuclear device is based on the fact that sediments would absorb more nuclear radiations, as the bulk density increases (Hirst et al., 1975; Been and Sills, 1981; Sills, 1997, 1998). Thus, the attenuation of nuclear radiation passing through

126

a sediment layer can be the proxy for bulk density. The use of a nuclear probe, however, requires licenses and trainings for safe operation. The loss of a nuclear device at field may generate a serious nuclear contamination problem. The electrical method is based on the principle that the sediment itself is a poorer conductor when compared with water, and that the overall conductivity mainly depends on pore water content and its salinity (Libicki and Bedford, 1989; Dowling, 1990). It was concluded, however, that this method is not suitable in the brackish environments where the salinity frequently varies (Winterwerp and van Kesteren, 2004). The resolution for the electrical method is not high and it is still an intrusive approach (Ariathura and Arulananda, 1986). Most recently, a tuning fork is commercially available for in-situ density measurement (Fontein and van der Wal, 2006). Its measurement, however, is limited only for fluid mud, so that the integration with other methods (e.g., acoustic) is necessary to extend the sensing range to subsurface sediment layers. Using intrusive probes to measure the acoustic wave attenuation is possible (e.g., Hamilton, 1971; Maa et al., 1997) but the pace for identifying sediment properties would be slow.

These drawbacks described above consistently shed light on the non-intrusive acoustic method as an alternative because it has a capability to remotely measure the physical properties of sediment (Libicki and Bedford, 1989; Verbeek and Cornelisse, 1995; Maa et al., 1997; Holland et al., 2005). Acoustic approaches in the water column have already yielded a wealth of insight on the turbulence and related sediment transport using the acoustic backscattering theory (Thorne and Hanes, 2002). However, the application of acoustics with high-resolution to near-bed processes is still challenging.

Using the concept that the acoustic echo strength is proportional to the difference in acoustic impedance (i.e., a product of sound speed and density), the bulk density may be calculated by acoustic signals returned from the sediment bed (Maa and Lee, 2002; Ha et al., 2003). This approach is different with the analysis of backscattered signals to determine the suspended sediment concentration (SSC), which is beyond the scope of this study.

The aforementioned technique is not new, and the conventional low-frequency acoustic technique has been used for decades to address the geoacoustic properties of underlying sediment layer, but its resolution is not high enough to reveal the micro-scale changes (on the order of millimeters) within the top layer of a consolidating bed. In this study, therefore, we have explored the possibility of measuring bulk density and consolidation status using high-frequency acoustic Chirp waves. The main objective is to develop a non-intrusive method and a data-processing protocol for measuring bulk density without destruction of sediment structures.

2. Materials and methods

2.1. Experimental apparatus

Consolidation experiments were conducted at the Virginia Institute of Marine Science (VIMS) in a cylindrical consolidation tank (diameter: 0.75 m; height: 1.5 m). An immersion-type transducer (Panametrics-NDT, V389-SU) served as the transmitter and another (Panametrics-NDT, V301-SU) was used as the receiver. These two transducers were installed together with a horizontal distance of 5 cm. An arbitrary function generator (AFG) (Gage Applied, CG1100) generated the Chirp acoustic waves, which

128

were fed into a 25-watt power amplifier (Amplifier Research, 25A250A) for delivering the required power to excite the transmitter (Fig. 5-1). Since the acoustic return signal was weak, a 60-dB linear signal conditioner (Nsite LLC, SC60) was used to enhance its strength. For the purpose of producing comparable data, the gain settings in the power amplifier and signal conditioner were fixed for all measurements. With a sampling rate of 10 MHz, the conditioned signals were digitized by a 12-bit analog-to-digital converter (ADC) (Gage Applied, CS1250). The generation of source signal and the digitization of return signals were triggered at the same time. A home-made triggering device (555 timer circuit) synchronized these processes at a rate of 50 Hz. For every data set, 100 repeated measurements were ensemble-averaged to reduce noises. At the beginning of digitized echo signal, there is a short period of time (about 150 μs) within which data are contaminated by the large relic vibration, and thus, they were purposely replaced by 0 within that period.

A commercially available kaolinite (d_{50}=1 μm) was used in this experiment. For the sediment preparation, the dry kaolinite was mixed with tap water for about 30 days to reach a fully water-saturated condition. The kaolinite slurry was further diluted with tap water and mixed by using three submergible pumps with different vent directions to make a homogeneous mixture in the tank. The initial concentration was approximately 45 g/L and the initial height of water column was 1.40 m. After thoroughly mixing for 24 hrs, all pumps were stopped and removed from the tank to allow suspended sediments to settle and consolidate.

2.2. Experimental procedures

With a downward looking setup, two transducers were installed at 10 cm below the water surface, and air bubbles were carefully removed because their presence can exert a significant effect on the signal response (Mole et al., 1972; Skaropoulos et al., 2003). Acoustic signals were sequentially acquired at the elapsed times of 5, 24, 216, 338, 484 and 1034 hr. Through the translucent sidewall of the tank, the settlement of water-sediment interface height was recorded during the measurement. Using a syringe, water-sediment mixtures were taken through several sampling ports (0.1, 0.2, 0.4, 0.6, 0.8, 1.0, 1.15 and 1.3 m above the tank bottom) on the sidewall. Withdrawn samples were filtered through 0.7-μm glass fiber filters when the concentration of a sample is low. When a sample was collected below the water-sediment interface with a relatively high bulk density, a pre-weighted aluminum pan was used to hold the sample. The residue on filter (or the sample in aluminum pan) was oven dried at 103-105 °C for 24 hrs, cooled in a desiccator for 2 hr, and then weighted for determining the dry sediment weight, M_s. With the given volume of sediment sample, V_t, and the assumption of sediment density ($\rho_s = 2.65$ g/cm^3), the bulk density (ρ_b) was calculated by

$$\rho_b = \frac{M_s}{V_t} + \rho_w(1 - \phi_s) \qquad (5\text{-}1)$$

where $\phi_s = M_s / V_t / \rho_s$ is the sediment volume fraction in the unit volume of sample, ρ_w is the water density.

2.3. Chirp source signal

As a source signal, Chirp acoustic wave was employed to excite the transmitting transducer. This kind of signal, a frequency-modulated (FM) and amplitude-modulated

130

(AM) wave form (Fig. 5-2; Maa and Lee, 2002; Ha and Maa, 2004), has been widely

used in the sub-bottom profiling system (e.g., LeBlanc et al., 1992) for improving signal-

to-noise ratio (SNR). After the pre-determined signal duration ($\approx$ 37 μs), the signal

remains zero until the next triggering event. Details of advantages of the Chirp technique

over a traditional pulse-type signal were presented in Maa and Lee (2002).

The high-frequency (300-700 KHz) Chirp signal was generated by using the

following equation,

$$y(i) = \sin\left(\frac{i\pi}{n}\right)\sin\left(\frac{2(i-1)\pi}{T}\right) \tag{5-2}$$

where T is the wave period and it varies as $T=260-0.03(i-1)$, $i=1$ to n, and $n=3000$. The

first sine function on the right hand side of Eq. 5-2 plays a role in modulating the wave

amplitude, and the second is for modulating its frequency. Discrete data generated by Eq.

5-2 were loaded to the AFG by using its built-in waveform editor. With a conversion rate

of 80 MHz, the Chirp signal was generated with a center frequency of approximately 500

KHz (Fig. 5-2). The frequencies at the left and right wing of generated wave train are

approximately 300 and 700 KHz, respectively. It is noted that the waveform is different

with the original Chirp specification (LeBlanc et al., 1992) which used the Gaussian

distribution function to modulate the wave amplitude. Instead, we used a sinusoidal

waveform because it is as good as the Gaussian function in terms of the signal

modulation and SNR control (see Maa and Lee, 2002). The integrated system developed

in this study is named "Micro-Chirp system" after the Chirp acoustic wave.

2.4. Data processing

The digital signal processing (Fig. 5-3) mostly utilizes functions in Matlab® signal processing toolbox. The first step was filtering to improve SNR. For the purpose of filtering undesirable noises embedded in return acoustic waves, a digital band-pass filter was implemented to remove signals out of the given bandwidth (i.e., 300-700 KHz). As the second and more powerful de-noising technique, we used the cross correlation to significantly increase SNR and to determine the existence and location of any interface caused by the difference in acoustic impedance. Mathematically, the cross correlation of two signals, $f(t)$ and $g(t)$, can be defined by

$$r(\tau) = \int f(t) g(t + \tau) dt \qquad (5\text{-}3)$$

where $f(t)$ is the raw return signal, and $g(t)$ is the phase-shifted source signal, and τ has the effect of shifting $g(t)$ forward in time relative to $f(t)$ (Stearns, 2003). A correlation value, $r(\tau)$, will be high if the source is similar to the return signal. That is, it represents the degree of confidence that the true return signal is detected. When the discrete digital signals, $f(t)$ and $g(t)$, have the length of N, the element length of output, $r(\tau)$, is $2N$-1 and the zeroth lag is located in the middle of $r(\tau)$, Thus, only the second half of $r(\tau)$, starting at the zeroth lag, was taken for the next processes.

The value of acoustic impedance is always positive, but $r(\tau)$ has the positive and negative fluctuations. This fact allows us to simply look at the half (i.e., the positive side) of $r(\tau)$ by folding them at the middle. Mathematically, this is done by taking the absolute values of $r(\tau)$.

Limited by the carrying wave frequency (e.g., 500 KHz in this study), the fluctuation of $r(\tau)$ also has this frequency. Because of the nature of correlation, $r(\tau)$ will

not become zero when there is a small offset between $f(t)$ and $g(t+\tau)$. In other words, $r(\tau)$ has the maximum when $f(t)$ and $g(t+\tau)$ matches the best, whereas the value of $r(\tau)$ decreases when the match between $f(t)$ and $g(t+\tau)$ is less, and this decreasing rate is also limited by the frequency. Therefore, the envelope curve of $|r(\tau)|$ represents the measurement because the difference in acoustic impedance is proportional to that curve, not the fluctuations themselves (Eq. 5-4).

$$\frac{dZ(t)}{dt} \propto E\left[\,|r(t)|\,\right] \qquad\qquad (5\text{-}4)$$

where Z is the acoustic impedance, E stands for the envelope curve, and $|r(t)|$ is the processed signals after cross correlation. This envelope curve indicates the location of water-sediment interface and underlying substrata interface(s), if exists. The resolution of measurement is also primarily determined by the frequency of carrying waves and envelope of $|r(\tau)|$.

By integrating the envelope curve with time, a time series of acoustic impedance, $Z(\tau)$, can be calculated by

$$Z(\tau) = \rho_b(\tau)c = \int_0^\tau \frac{dZ(t)}{dt}\,dt \qquad\qquad (5\text{-}5)$$

where τ is the elapsed time, ρ_b is the bulk density, and c is the sound speed in medium. With the digitized envelope, the trapezoidal rule was applied for this integration.

Using $cd\tau = dz$ where z is a depth, the signal in time domain can be converted to the acoustic impedance, $Z(z)$, in spatial domain. Since the sound speed in water is close to that in clay (Maa et al., 1997; also see Fig. 5-7 in this study), it was assumed that all the variations of acoustic impedance are attributed to bulk density changes.

The processed signal strength cannot directly address the absolute value of acoustic impedance, so that a calibration step is needed to obtain the acoustically-derived ρ_b. Details will be described with an example in the next section.

3. Results and discussions

3.1. Withdrawn sample analysis

For the various consolidation stages, the locations of water-sediment interface were observed with the naked eyes through the tank wall. As time elapsed, the water-sediment interface gradually lowered, and bulk densities above and below that interface decreased and increased, respectively (Fig. 5-4). For example, at the elapsed time of 1034 hr, the bulk density at 0.1 m above the tank base increased to 1.25 g/cm^3, and the water above the interface became nearly clean ($\rho_b \approx 1.0$ g/cm^3). On the basis of the settlement rate of interface level, the settling and consolidation status can be divided into three stages (Fig. 5-5): (1) During the first few hours, the water-sediment interface was too crude to be recognized due to turbid conditions. At the elapsed time of 5 hr, the interface was finally identified at 1.13 m, and then it dropped rapidly to 0.44 m at 24 hr, leaving relatively clean overlying water. During this stage, the interface settlement rate was approximately 3.6 cm/hr; (2) Between 24 and 400 hr, the settling and consolidation continued with a moderate rate of approximately 0.06 cm/hr. The interface was located at 0.22 m in the end of this stage; and (3) After about 400 hr, the consolidation proceeded with a much slower rate, and the interface reduced to 0.2 m above tank bottom at the end of measurement. The consolidation status can be also explained by the acoustic wave reflectivity, which will be given later.

134

3.2. Acoustic signal analysis

Due to the difference in acoustic impedance, the first salient peak in return wave train was always encountered at the water-sediment interface, which is well correlated with the visually-observed interface (Fig. 5-4). The echo signal strength from the first acoustic interface tends to increase with the consolidation time. It is noticeable that 5-hr data showed a relatively weak voltage at the first peak. This might be explained by two possible reasons. One is due to a weak density gradient near the acoustic interface. At the early stage of consolidation, ρ_b would smoothly increase toward the sediment bed, such that the water-sediment interface is not sharp enough to generate the strong signal strength. The other is related to the beam pattern of source transducer. At 5 hr, the distance between source transducer and water-sediment interface was about 17 cm. Considering that the source-receiver separation is 5 cm, the angle of reflection should be approximately 8.4° (= $\tan^{-1}(2.5/17)$) in order to sense the return signal within the main lobe of receiver. However, the employed source transducer has a beam angle of 4.6°. That is, the reflected path for the first peak at 5 hr is out of main beam. As the water-sediment interface lowered, the return signal from the first interface moved into the main beam. The second spike commonly occurred at the tank bottom except for 5-hr data. At that time, the signal returned from the tank bottom was too weak to be detected. This indicates that transmitted acoustic waves were mostly attenuated during two-way travel time (TWTT) passing through high-concentration (ca. 40 g/L) sediment-laden layer with a thickness of 1.13 m.

135

As done with other acoustic instruments (e.g., acoustic Doppler current profiler (ADCP)), the acoustic signal returned from at least one measuring elevation was needed to calibrate against the sample-derived ρ_b. Since the wavelength (2-5 mm) of Chirp signal is much larger than the diameter (~1 µm) of kaolinite particles, the signals backscattered by suspended particles are negligibly small (see Fig. 5-4). Thus, the signals originated from water column were not included in calibration. Instead, all data of sample-derived ρ_b below the water-sediment interface were compared with the processed signal strengths at the corresponding sampling level (Fig. 5-6a). The processed signal strength generally exhibits a coherent relation with the true ρ_b. Due to the exponential relationship, the calibration equation can be expressed by

$$\rho_b(z) = a + be^{kS(z)} \tag{5-6}$$

where a, b and k are empirical coefficients calculated by using the least-squares curve fitting, and $S(z)$ is the processed signal strength at a distance (z). It was assumed that ρ_b will be 1 g/cm^3 at $S=0$, representing a clear water condition. With the calculated calibration coefficients, the comparison between sample-derived ρ_b and acoustically-derived ρ_b was shown in Fig. 5-6b. Acoustic method has a good agreement with the ground truth ($r^2=0.95$), showing the acoustic capability to remotely estimate ρ_b near the sediment bed.

When converting the processed signal strength in time domain to the bulk density in space domain, local sound speeds in both the water column and the consolidating mud layer are necessary. The TWTT between the transducer and the water-sediment interface (i.e., the first arrival peak in the envelope curve) and the corresponding propagation

length were used to determine the sound speed in water column. Similarly, TWTT between the water-sediment interface and the tank bottom (i.e., the time interval between the first and the second arrival peak) and the visually-observed sediment thickness were used to compute the sound speed in the clay layer. Because some sediment particles are still suspended in water column during the earlier stages (e.g., 5 and 24 hr), only data between 216 and 1034 hr were analyzed to avoid the sound attenuation effect by them.

Fig. 5-7 demonstrates that the sound speeds in the consolidating clay bed was always slightly lower than those in the overlying water column. On the average, the sound speed in water column remained around 1497 m/s over time. In consolidating clay bed, meanwhile, its average showed the slight decreasing trend after 338 hr even though the decreasing rate is still within the error range. The implication is that clay sediments exhibit greater density but a little less sound speed than those in water, and that the variations of sound speed are not significant within the range of ρ_b measured in this study. As a result, it is acceptable that a single value of sound speed can be practically used when converting the time series of signals to the space domain, because the maximum speed (1499.6 m/s) in water is only 2.3% higher than the minimum (1466.2 m/s) in the consolidating bed.

As another reference, the Wood's equation (Wood, 1964) that formulates the relationship between sound speed and ρ_b was used to verify the measured speeds.

$$c = \left(\frac{1}{[\phi / K_w + (1 - \phi) / K_s]\rho_b} \right)^{1/2} \tag{5-7}$$

where ϕ is fractional porosity, K_w and K_s are the bulk modulus of water and sediment, respectively. In Eq. 5-7, it was assumed that the rigidity introduced by the grain-to-grain

contact was negligibly small. It can be seen that the consolidating clay layer has the speeds higher than those predicted by Wood's equation (Fig. 5-7b). Jackson and Richardson (2007) stated that these higher values are related to the presence of rigidity in consolidating bed which was neglected in Eq. 5-7. Based on the Wood's curve, it is expected that the sound speed will decrease until ρ_b reaches 1.4 g/cm^3, and then it will gradually increase with the increase of ρ_b (or decrease of porosity).

3.3. Reflectivity coefficient and bulk density

In order to normalize the signal strength acquired at different ranges, the beam spreading and sound attenuation along the propagation path in water column should be compensated. The received pressure at the transducer (P) can be expressed as

$$P(z,t) = \frac{P_0 R(\theta,z,t)\sqrt{B(\theta)}}{d} e^{-\alpha d} \qquad (5\text{-}8a)$$

where P is the received signal pressure which is proportional to voltage, P_0 is the source level (reference to 1 m), R is the reflection coefficient, B is the beam pattern factor, θ is the beam angle, α is the sound attenuation coefficient, d is the total distance of acoustic propagation path, z is the height above the bed, and t is the consolidating geo-time. By rearranging Eq. 5-8a, R can be estimated by

$$R(\theta,z,t) = \frac{P(z,t)d}{P_0\sqrt{B(\theta)}} e^{\alpha d} \qquad (5\text{-}8b)$$

Since all parameters in right hand side of Eq. 5-8b are known, R for the water-sediment interface at the different geo-times can be determined. Provided that R is known, as

another approach, ρ_b of sediment bed can be explicitly estimated using Fresnel's reflection law

$$R = \frac{\rho_2 c_2 - \rho_1 c_1}{\rho_2 c_2 + \rho_1 c_1} \qquad (5\text{-}9)$$

where ρ is the density, c is the sound speed, and the subscripts 1 and 2 refer to the overlying water and the sediment layer, respectively. This is a simple and promising technique to estimate the near-bed ρ_b without depending on an empirical relation. The pre-determined sound speeds and R were required to calculate bulk density of sediment near the bed. With the same reason as Fig. 5-7, R and ρ_b only between 216 and 1034 hr were estimated (Fig. 5-8). Both were gradually intensified with consolidation time. As the difference in bulk density between the clay layer and the overlying water becomes larger with time, the difference in acoustic impedance increased accordingly. This increase implies that consolidation is still in progress even after 1034 hr, which is caused by the consolidation-induced outcomes (e.g., dewatering, decrease of porosity and increase of bed rigidity). Consequently, the maturity of consolidation status can be gauged by the change of R.

4. Conclusions

The conclusions drawn from this study can be summarized as follows:

(1) The developed acoustic technique and signal-processing protocol enable to remotely obtain the bulk density for consolidating clay bed. This technique is applicable for in-situ bulk density measurements for the top layer of sediment bed after a proper system calibration.

(2) Measured acoustic responses demonstrate that the consolidation results in increasing

the bulk density of sediment bed and the difference in acoustic impedance at the

water-sediment interface. Accordingly, the acoustic wave reflectivity at that interface

increased with consolidation time, but the sound speed only changed slightly so that

the changing rate can be considered as negligibly small and ignored for practical

applications.

References

Ariathurai, R., Arulanandan, K., 1986. An electrical method to measure in-situ sediment densities. In: A.J. Mehta (Ed.), Estuarine Cohesive Sediment Dynamics. Spring-Verlag, Berlin, pp. 206-218.

Been, K., Sills, G., 1981. Self-weight consolidation of soft soils: an experimental and theoretical study. Geotechnique 31(4), 519-535.

Cutter, G.R., Diaz, R.J., 1996. The Jefferson benthic sled and the burrow-cutter plowing profile camera: a viable new tool. Abstract of Marine Benthic Ecology Meeting, Columbia, South Carolina, USA.

Dowling, J.J., 1990. Estimating porosity of partially saturated sediment. Eng. Geol. 29, 139-147.

Fontein, W., van der Wal, J., 2006. Assessing nautical depth efficiently in terms of rheological characteristics. Proceedings of International Hydrographic Conference-Hyrdo'06, Antwerp, Belgium.

Ha, H.K., Maa, J.P.-Y., Park, K.-S., Lee, D.-Y., 2003. Acoustic approach for measuring near-bottom bed structures, Abstract of the 7th International Conference on Nearshore and Estuarine Cohesive Sediment Transport Processes, Virginia, USA, 85–86.

Ha, H.K., Maa, J.P.-Y., 2004. Micro-chirp technique for measuring near-bed sediment properties. Abstract of Atlantic Estuarine Research Society Fall Meeting, Lyndhurst, New Jersey.

Hamilton, E.L., 1971. Elastic properties of marine sediments. J. Geophy. Res. 76, 579-604.

Hirst, T.J., Rerlow, M., Richards, A.F., 1975. Improved in situ gamma-ray transmission densitometer for marine sediments. Ocean Eng. 3, 17-27.

Holland, C.W., Dettmer, J., Dosso, S.E., 2005. Remote sensing of sediment density and velocity gradients. J. Acoust. Soc. Am. 118(1), 163-177.

Jackson, D.R., Richardson, M.D., 2007. High-frequency seafloor acoustics. Springer, 616 pp.

LeBlanc, L.R., Mayer, L., Rufino, M., Schock, S.G., King, J., 1992. Marine sediment classification using the chirp sonar. J. Acoust. Soc. Am. 91(1), 107-115.

Libicki, C., Bedford, K.W., 1989. Remote and in situ methods for sub-bottom sediment characterization. J. Coastal Res. 5, 39-49.

Lintern, D.G., Sills, G.C., Feates, N., Roberts, W., 2002. Erosion properties of mud beds deposited in laboratory settling columns. In: J.C. Winterwerp and C. Kranenburg (Eds.), Fine-sediment Dynamics in the Marine Environment. Elsevier, 343-357.

Maa, J.P.-Y., Sun, K.-J., He, Q., 1997. Ultrasonic characterization of marine sediments: a preliminary study. Mar. Geol. 141, 183-192.

Maa, J.P.-Y., Lee, D.-Y., 2002. A preliminary study on using acoustic waves to measure high resolution marine sediment bed structure. In: J.C. Winterwerp, C. Kranenberg (Eds.), Fine-sediment Dynamics in the Marine Environment. Elsevier, pp. 469-481.

Mehta, A.J., Dyer, K.R., 1990. Cohesive sediment transport in estuarine and coastal waters, In: B. Le Mehaute and D.M. Hanes (Eds.), The Sea, Vol. 9, Part B, Ocean Engineering Science, John Wiley and Sons, New York, pp. 815-839.

Mole, L.A., Hunter, J.L., Davenport, J.M., 1972. Scattering of sound by air bubbles in water. J. Acoust. Soc. Am. 52, 837-842.

Sills, G.C., 1997. Consolidation of cohesive sediments in settling columns. In: N. Burt, R. Parker and J. Watts (Eds.), Cohesive Sediments. John Wiley and Sons, pp. 107-120.

Sills, G.C., 1998. Development of structure in sedimenting soils. Phil. Trans. R. Soc. Lond. 356, 2515-2534.

Skaropoulos, N.C., Yagridou, H.D., Chrissoulidis, D.P., 2003. Interactive resonant scattering by a cluster of air bubbles in water. J. Acoust. Soc. Am. 113(6), 3001-3011.

Stearns, S.D., 2003. Digital signal processing with examples in Matlab. CRC Press, 336 pp.

Thorne, P.D., Hanes, D.M., 2002. A review of acoustic measurement of small-scale sediment processes. Con. Shelf Res. 22(4), 603-632.

Verbeek, H., Cornelisse, J., 1995. Consolidation of dredged sludge, measured by an Acoustic Densitometer. Mar. Freshwater Res. 46, 179-188.

Winterwerp, J.C., van Kesteren, W.G.M., 2004. Introduction to the physics of cohesive sediment in the marine environment. Elsevier, Amsterdam, 466 pp.

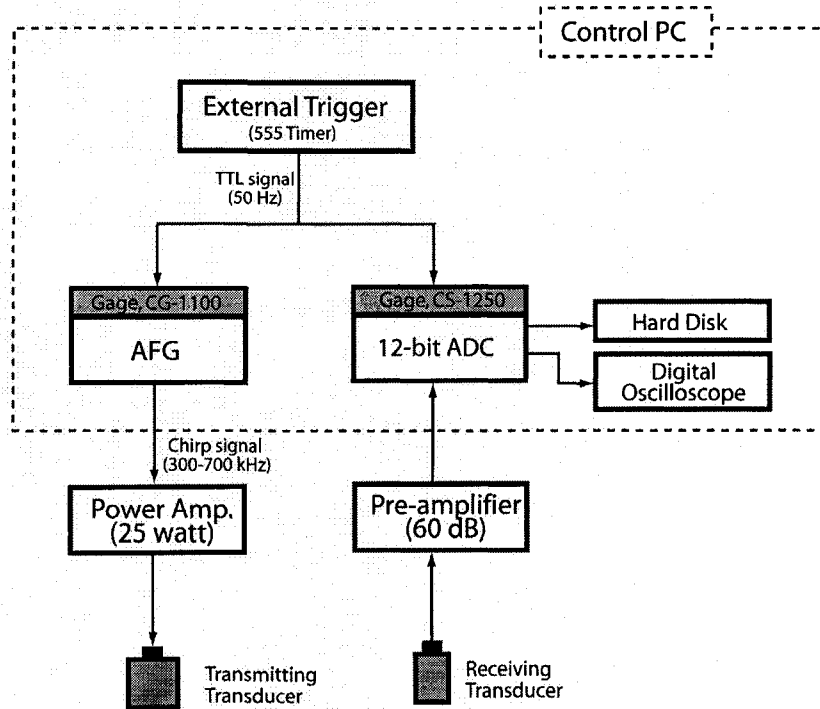Wood, A.B., 1964. A textbook of sound, Third edition, G. Bell and Sons, London.

Fig. 5-1. Block diagram of Micro-Chirp system developed in this study. An external
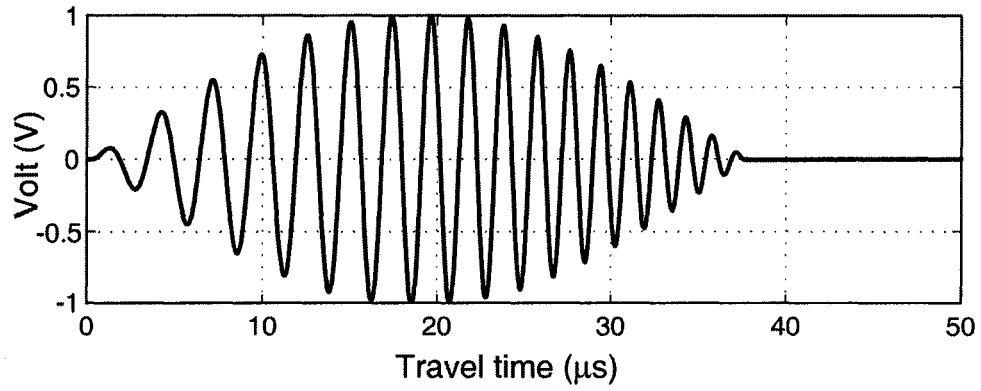trigger source, ADC and AFG were all integrated with the control PC.

Fig. 5-2. Waveform of Chirp signal used in this study. The central frequency is around 500 KHz and the frequency range is 300-700 KHz.
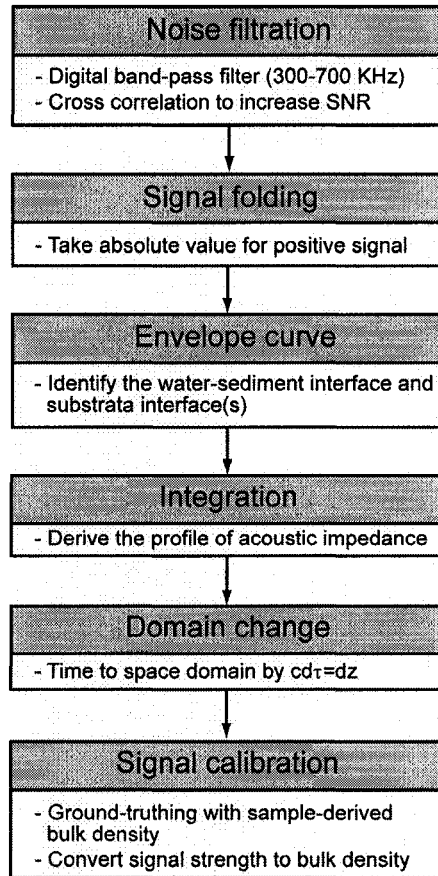
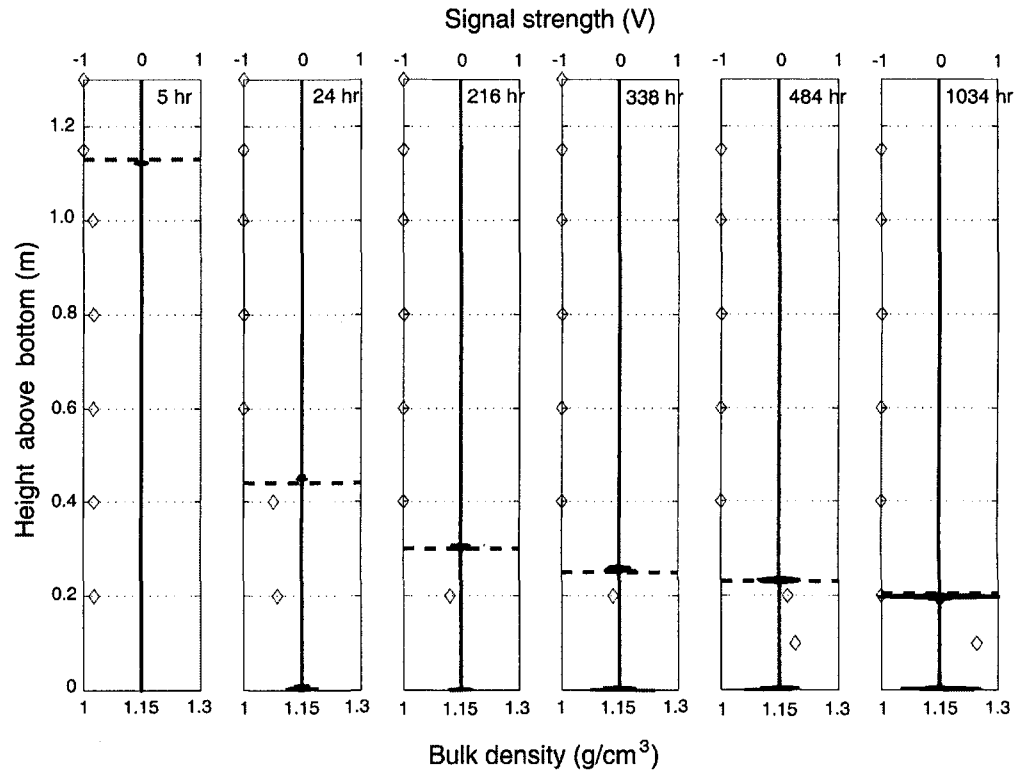Fig. 5-3. Flow chart for digital signal processing.

146

Fig. 5-4. Acoustic signals (solid lines at each subplot) at various consolidation stages. Bulk densities calculated from withdrawn samples were marked as diamond. Dashed lines indicate the water-sediment interfaces visually observed through the tank wall.
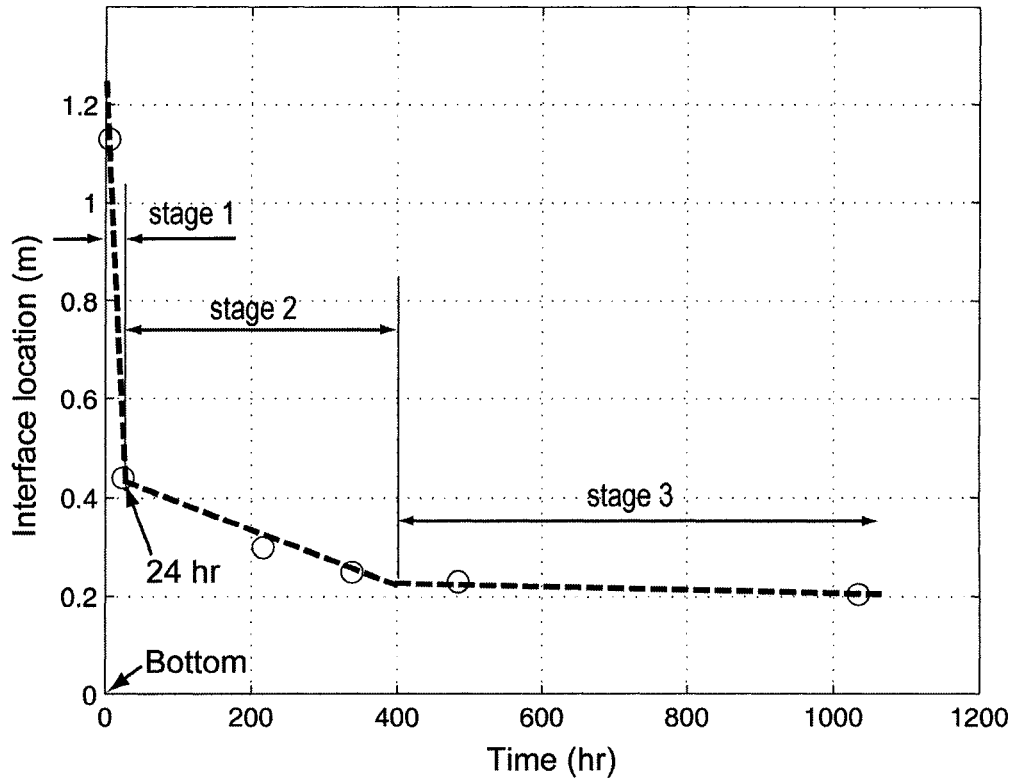
Fig. 5-5. Three stages of settling and consolidation based on the downward movement
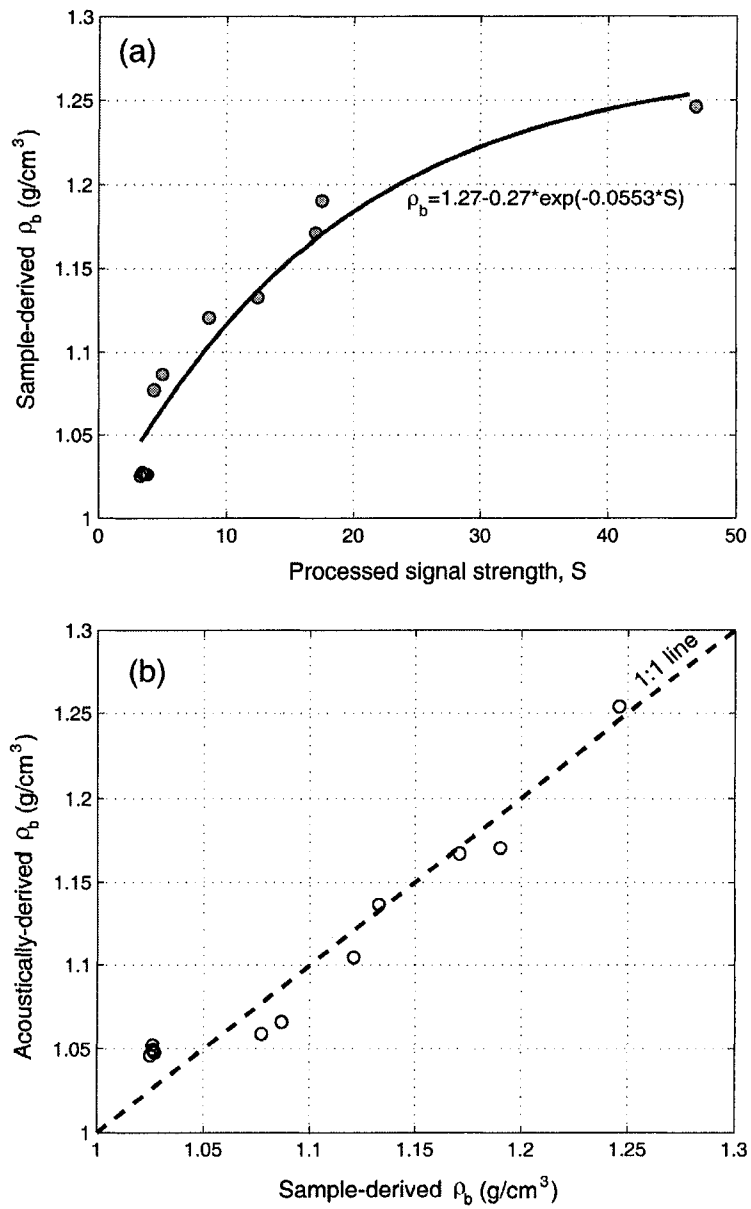rate of the water-sediment interface.

Fig. 5-6. (a) Relationship between processed signal strength and bulk density. (b)
Comparison between sample-derived bulk density and acoustically-derived bulk
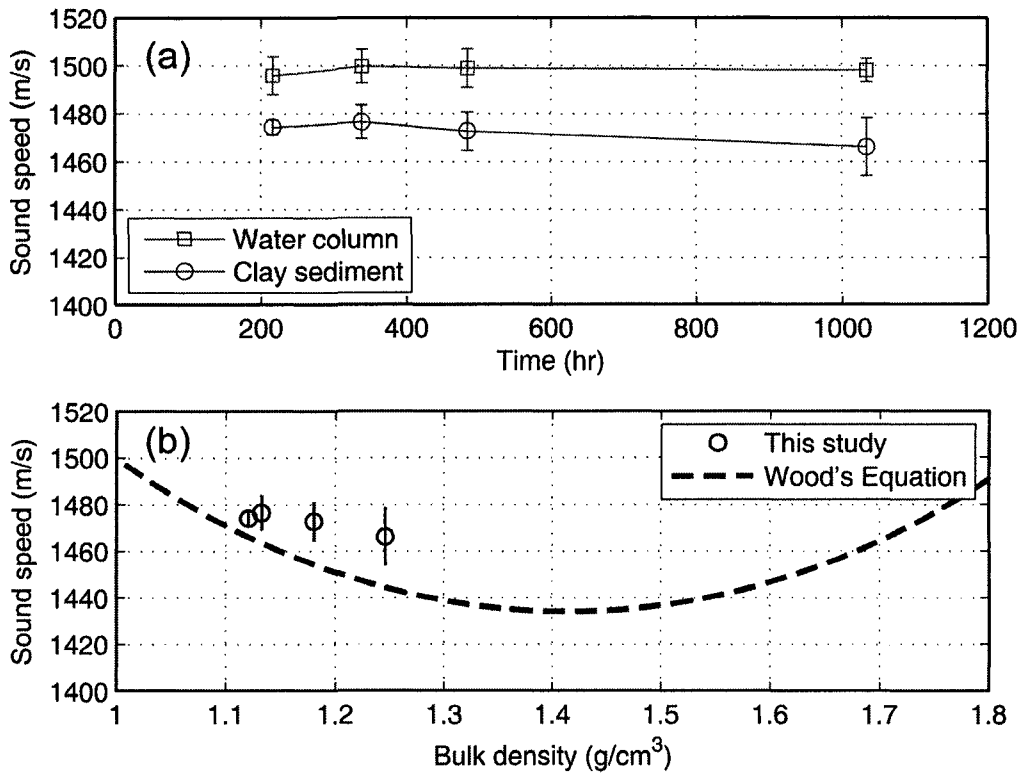density.

149

Fig. 5-7. (a) Sound speed in the consolidating clay bed and the overlying water; (b) bulk density versus sound speed in clay-water mixture.
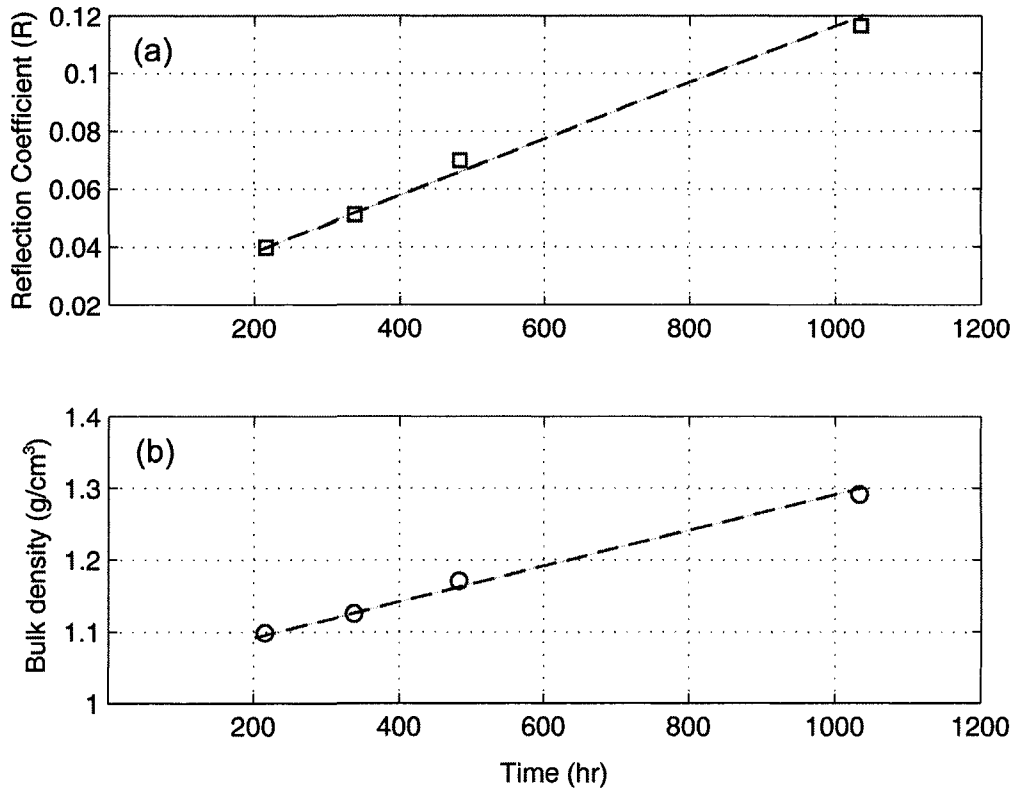
Fig. 5-8. (a) Reflectivity coefficient at the water-sediment interface. (b) Bulk density changes with consolidation time.

VITA

HO KYUNG HA

Born in Busan, Republic of Korea on February 5, 1974. He graduated in 1996 from Seoul National University with Bachelor of Science. He received his Master of Science degree from the Department of Oceanography of Seoul National University, 1998. After serving as an Air Force Officer, he entered Ph.D. program in the Virginia Institute of Marine Science, School of Marine Science, College of William and Mary, Virginia in fall of 2002.